Corso di dottorato di ricerca in Scienze della Terra

XXX ciclo

Geological contribution to tsunami hazard assessment along Italian coasts

Dottorando:
Dott. Simone Orefice

Tutor:
Dott. Paolo Marco De Martini

Co-tutor:
Dott.ssa Francesca Funiciello

Contents

Introduction

1. Introduction

This work aims to develop a contribution to the tsunami hazard in the NEAM region (North East Atlantic, Mediterranean and its connected seas region) with a particular emphasis on the Italian coasts.

A tsunami is a series of waves characterized by long wave lengths and high periods, triggered by a sudden bottom sea displacement (submarine fault, offshore earthquakes) or by other phenomena that cause a sudden change or disturbance in the water pressure such as a submarine/coastal volcanic eruption or landslides. According to the NOAA/WDC database (https://doi.org/10.7289/V5PN93H7) the most common tsunamigenic source type is related to offshore earthquakes, followed by volcanic activity (in terms of eruptions and collapses of the volcanic edifice) and landslides (subaereal and submarine). An offshore earthquake may produce a sudden bottom ocean displacement that transfers energy to the overhead water column, causing a sea level change in the source area. Tsunami waves propagate in all directions from the source area, but the main direction of the energy is controlled by the dimensions and orientation of the causative source (Papadopoulos et al., 2014). In the deep water the tsunami wave amplitude is very low and the velocity is related to the water depth, while in the near shore the wave amplitude increases and the wave velocity decreases. The leading wave of a tsunami may be negative or positive (leading trough or leading peak). A leading negative wave, approaching the coast, causes a retreat - rise pattern of the sea level, while a leading positive wave produces a sudden rise of sea level, followed by a retreat. From the near shore domain, tsunamis cause scouring, erosion, deposition, coastal morphological changes, damage and destruction in the coastal communities.

The Mediterranean Sea, due to its geodynamic setting, is characterized by several tsunamigenic sources (Papadopoulos et al., 2014). From a geological point of view the Mediterranean region is characterized by the presence of Neogene fold and thrust belts with associated foreland and back arc basin system (Cavazza et al., 2004). In this area, the Tethys oceanic lithosphere domains have been subducted (Cavazza et al., 2004). The result of this geological setting is represented by structures consisting of compressional zones and basins (fig.1).

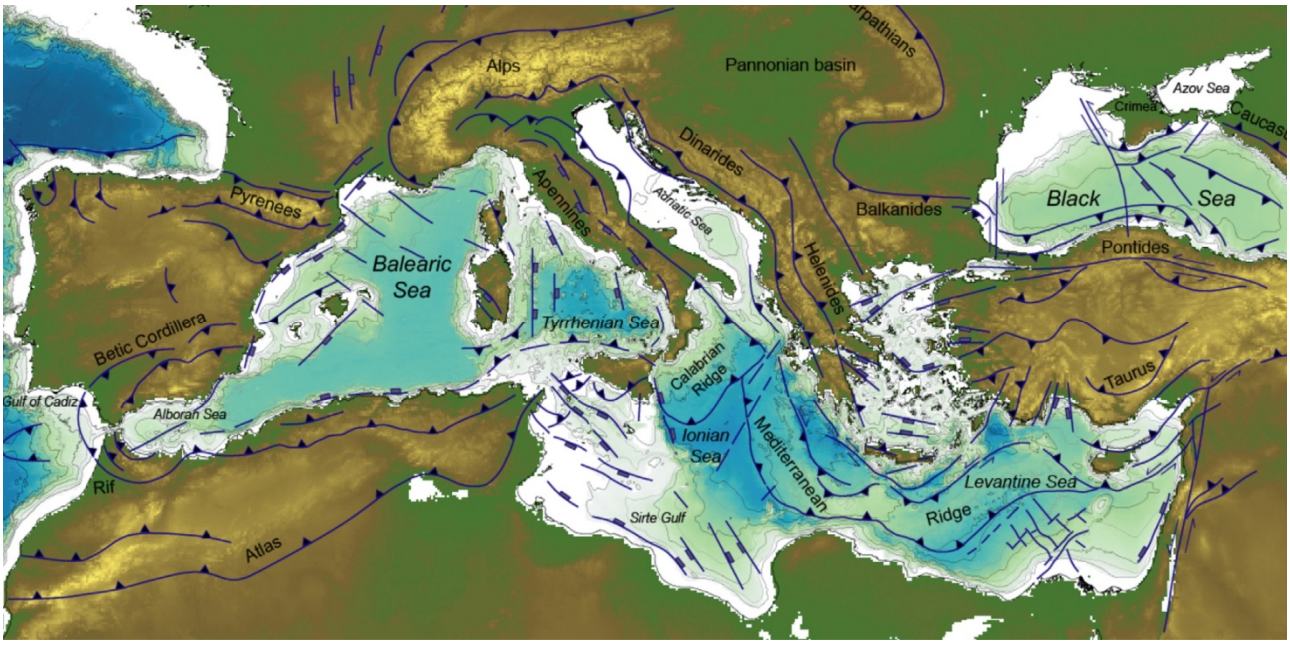

Fig. 1 – The map shows the main geological structures offshore and onshore of the Mediterranean region (after Papadopoulos et al., 2014).

The compressional structures such as the Hellenic Arc or the Calabrian Arc represent important sources of earthquakes and potential related tsunamis. At the same time, also the large number of active volcanoes may constitute potential tsunamigenic sources and thus a threat for the coastal populations. Most of the active volcanoes in the Mediterranean Sea are related to the subduction processes of the Calabrian and Hellenic Arc (Papadopoulos et al., 2014) and are located in the Ionian and Aegean seas.

According to the NOAA/WDS tsunami database some of the biggest Mediterranean tsunamis were produced by earthquakes originated in subduction zones (e.g. the events occurred in 365 AD, and 1303) (fig. 2) while the biggest example of a tsunami triggered by an eruption/caldera collapse is represented by the Thera volcano event (Santorini, Aegean Sea, Greece, fig. 3). The tsunami related Thera eruption/collapse was dated about 1620 BC (Friedrich et al., 2006), and probably caused the crisis of the Minoan civilization, destroying many settlements located in the northern side of Crete Island.

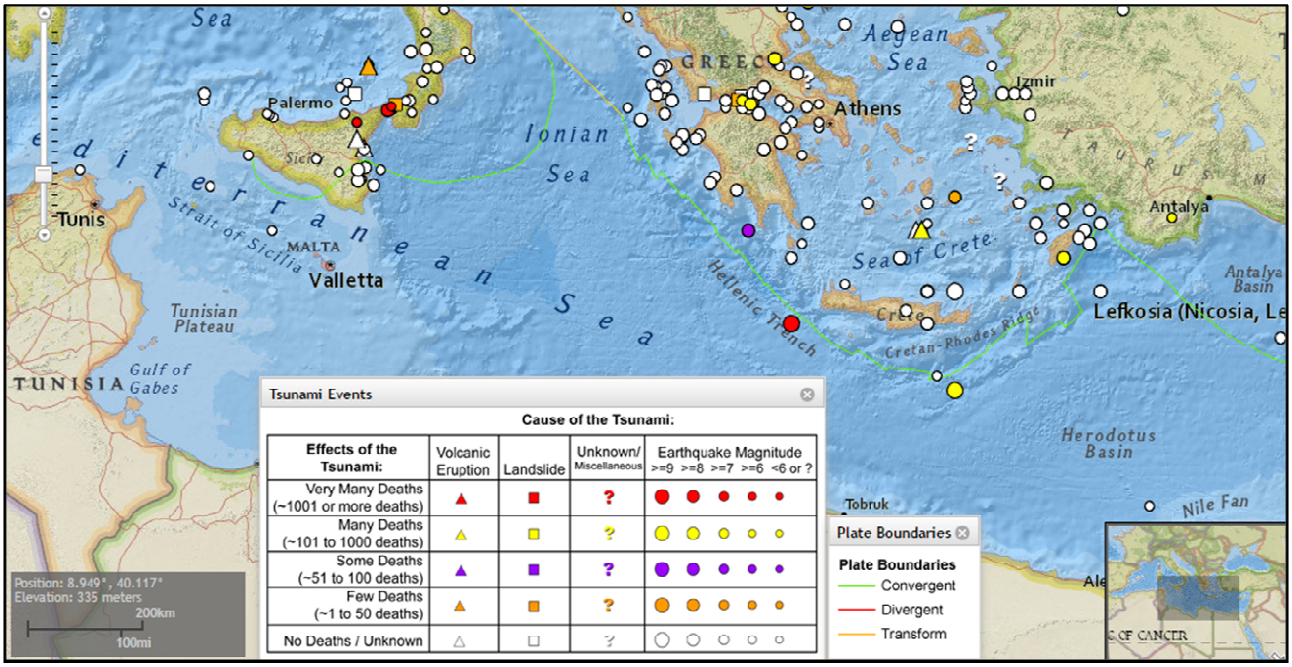

Fig. 2 – The figure shows a screen shot of the NOA/WDS Tsunami Database with the sources information of all tsunami events occurred and recorded from 2000 BC to the present. It is possible to observe the relation between the earthquake magnitude and their sources. The largest earthquake magnitudes are located at convergent margins (e.g. Hellenic arc).

Fig. 3 – The caldera of Santorini island (Greece). This eruption caused one of the largest known tsunami of the Medieterranean sea, dated about 1620 BC (image from Bing Maps).

At national level, in the last two decades, several studies demonstrated that Eastern Sicily coast (southern Italy) is the area most prone to tsunami hazard, in fact this portion of coast was hit by tsunami triggered by local sources as well as by distant sources (Table 1) (Tinti et al., 2003; Maramai et al., 2014). Scientists found inland the geological evidence of some ancient known tsunamis (both as loose sediments and transported boulders) like the 1169, 1693 and 1908 ones

caused by local earthquakes and like the 365 AD Crete event, caused by far field earthquake (De Martini et al., 2012 and references therein). The 365 AD Crete event, occurred along the Hellenic Arc subduction zone, represents the strongest known earthquake/tsunami of the Mediterranean area (estimated magnitude of 8, NOAA/WDS tsunami database). The 365 AD tsunami destroyed Alexandria (Egypt), killing about 50,000 people (Ammiano Marcellino, Res Gestae, 26.10.15–19). This seismic event produced a 9 meters maximum uplift in the southern sector of Crete (Tiberti et al., 2014 and references therein). In addition, the geological trace of the 365 AD tsunami was found at 1,2 km inland in a site located in the southernmost part of Sicily (Gerardi et al., 2012).

Moreover, at national level, also the Tyrrhenian Sea and the Adriatic Sea experienced destructive tsunami events. In the 1627 the coast of Gargano (Apulia region, southern Italy) was affected by a strong tsunami (Gianfreda et al., 2001; De Martini et al., 2003) whose source is still doubtful. Tinti and Piatanesi (1996) related the source to a fault located close to Lesina lake and Tortore river mouth (Gargano, Apulia region, southern Italy), while other authors attribute the source to the Tremiti Islands fault system or to some seismogenetic faults located in the eastern Adriatic margin (De Martini et al., 2003). Several tsunamis occurred also in the Tyrrhenian Sea, caused for example by the numerous landslides triggered on the Stromboli volcano flank (Eolie Island, southern Italy), (e.g. July 3, 1916, May 22, 1919, September 11, 1930, August 20, 1944 and December 22, 2002, Maramai et al., 2005; Maramai et al., 2014). Finally, based on historical documents a strong tsunami occurred on February 6, 1783, (Tinti and Guidoboni, 1988) strucking the western Calabria and the northern Sicily coasts, leaving a recognizable deposit (Pantosti et al., 2008).

Date	Source	Hit localities/areas
ca. 1600 BC	Santorini volcanic explosion	East Mediterranean
1st century (17 AD?)	unknown	Sicily
365 July 21	Crete-Gortyna quake	Sicily and other islands
1169 February 4	South-eastern Sicily quake	Messina, Catania, Sicily
1329 June 29	Etna eruption and quake	Mascali (eastern Sicily)
1542 December 12	South-eastern Sicily quake	Augusta
1693 January 11	South-eastern Sicily quake	Eastern Sicily and Malta
1783 February 5–6	Southern Calabria's quakes and landslide	Torre Faro, Messina, Scilla and Southern Calabria
1818 February 20	Eastern Sicily quake	Catania
1908 December 28	Messina Straits quake	Eastern Sicily and Southern Calabria, Malta
1990 December 13	South-eastern Sicily quake	Augusta

Table 1. Historical tsunamis along the coast of eastern Sicily (after Barbano et al., 2009).

Nowadays the Mediterranean coasts are densely populated, therefore it is necessary to define inundation scenarios together with their related emergency plans. The tsunami risk prevention is based on the knowledge of the potential tsunamigenic areas, of the tsunami consequences and of the

tsunami time frequency (Papadopoulos et al., 2014; De Martini et al., 2012). The tsunami hazard may be assessed through the study of past tsunamis with the identification and the characterization of their deposits and through approaches based on numerical simulations that model the generation, propagation and inundation of the tsunami waves (Butler et al., 2014). Today, the tsunami databases and catalogues (e.g. the NOAA/WDS tsunami database or the Euro-Mediterranean Tsunami Catalogue, Maramai et., 2014), that may extent back in time for at least 2000 years, provide important information and constraints on this kind of research.

Note that this research activity has been carried out within the European FP7 project ASTARTE, grant agreement: 603839 (Assessment, STrategy And Risk Reduction for Tsunamis in Europe, www.astarte-project.eu) and within the TSUMAPS-NEAM project, grant agreement: ECHO/SUB/2015/718568/PREV26 (www.tsumaps-neam.eu). EU project ASTARTE aims at developing a higher level of tsunami hazard assessment in the North East Atlantic and Mediterranean (NEAM) region by a combination of field work, experimental work, numerical modeling and technical development. TSUMAPS-NEAM represents a kind of spin-off of the ASTARTE project.

In this work I present a multidisciplinary approach that may contribute to the tsunami hazard assessment. In particular, my research activity analyzes this issue through two different points. The first one is based on the identification and characterization of paleotsunami deposits to define a minimum observed inundation extent and a minimum observed run - up height (for a site or for a specific coastal area), useful for establishing a potential reference for hazard estimations based on modeling of future events.
The run - up height represents the maximum topographic height reached by the wave, while the inundation distance is the maximum inland wave penetration with respect to the present shoreline (fig. 4).

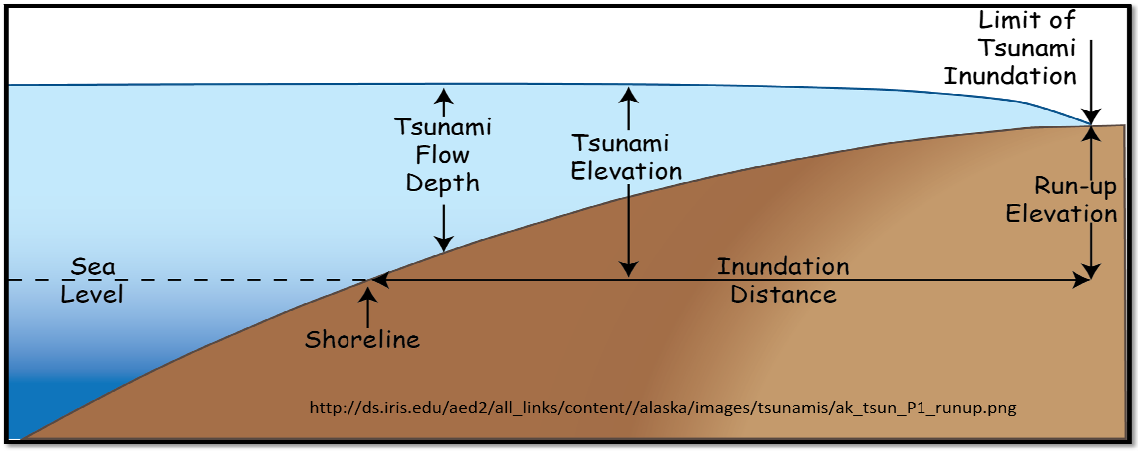

Fig. 4 - The figure shows the main tsunami wave parameters related to an inundation phase (after http://ds.iris.edu/). Tsunami flow depth: height of the wave with respect to the ground; tsunami elevation: height of the wave with respect to the sea level; run – up elevation: maximum topographic height reached by the wave; inundation distance: limit inland of the tsunami wave inundation.

This effort has been developed specifically along the eastern Sicilian coast at two sites, since the Siracusa Town was selected as the EC Astarte project test site in Italy and because along the coast of eastern Sicily we have:

- ✓ A long historical tsunami record (Maramai et al., 2014)
- ✓ 14 sites where paleotsunami deposits were recognized (De Martini et al., 2012)
- ✓ The 365 AD tsunami deposits evidence (Gerardi et al., 2012)

Moreover, these data will be included in the "ASTARTE Paleotsunami Deposits data base – NEAM region" (De Martini et al., 2017), a web-based database on Paleotsunami Deposits, created in order to be the future reference source for this kind of research in North East Atlantic, Mediterranean and its connected seas region, for which I am responsible for the Italian coast. The Astarte paleotsunami deposits database – NEAM provides important information about minimum run – up heights and minimum inundation distances, highlighting the coastal areas with more exposure to tsunami inundations and related hazard.

The second point of my research activity is based on the development and testing of an approximated method for the run-up estimation and inundation maps, both for scenarios related to past events and in the context of Probabilistic Tsunami Hazard Analysis (PTHA), in order to limit the computational burden associated to detailed numerical modeling of tsunami inundation.

All these topics are discussed in three different chapters. The first chapter is focused on the Astarte Paleotsunami Deposits database – NEAM in order to identify coasts affected by tsunamis in the past and to obtain minimum run-up and inundation distance values. The second chapter is focused on the paleotsunami deposits research activity carried out along the eastern Sicily coasts in order to

improve the knownledge about paleotsunami deposits and to obtain new data about minimum run-up heights and minimum inundation distances. The third chapter is based on the development and application of a modeling approach aimed to estimate the tsunami wave amplification from an offshore point to the shoreline to obtain run-ups and inundation maps.

1.1 Databases and Tsunami Deposits

Nowadays, there are several available tsunami databases (e.g. the NOAA/WDS tsunami database - https://doi.org/10.7289/V5PN93H7; the New Zealand tsunami database - http://data.gns.cri.nz/tsunami/index.html; the Japan Tsunami Trace Database - http://tsunami-db.irides.tohoku.ac.jp/ and the Australian tsunami database – Goff et al., 2014) providing information about the tsunami event as well as the source mechanism and the related onshore and offshore geological evidence. From a general point of view, tsunami databases can be divided into two categories: those that provide data at global level (e.g. the NOAA/WDS tsunami database) and those presenting data at regional level (e.g. the Japan Tsunami Trace Database).

At European level, the Euro-Mediterranean Paleotsunami Database, developed within the TRANSFER project (Tsunami Risk ANd Strategies For the European Region), represented the first attempt aimed to create a database focused only on tsunami deposits. This database was the starting point for the development of the Astarte Paleotsunami database – NEAM region that together with the north-east Atlantic (NEA) Paleotsunami Deposits database (Costa et al., 2016) provides an important dataset (derived from scientific literature) focused only on the geological evidence left by the sea wave (tsunami deposit). As previously mentioned, tsunami deposits provide information about inundation distances, run-up heights and the age of the events. The spatial distribution of tsunami deposits together with the events age can help us to understand where, and potentially with which recurrence a future inundation could take place. However, run-up and inundation distances data have to be considered as minimum values since during the Holocene the sea level was never higher than today (Fleming et al., 1998) and taking into account that a tsunami wave can reach sites located far inland but without leaving a ”signature” able to be preserved for long time (Szczuciński al., 2012).

On the base of these last considerations, in this thesis, I present the Astarte paleotsunami deposits database trying to provide all possible information that can be used within hazard estimations based on modeling of potential future events and on geological data. At the same time, the research inland of paleotsunami deposits along the coasts of eastern Sicily aims to enrich the database thus providing new data about run-up heights and inundation distances.

Geological evidence of paleotsunami is typically represented by deposits or by geomorphological features (De Martini et al., 2012, Gianfreda et al., 2001). Onshore paleotsunami deposits are the symbol of high energy events and can be represented by coarse clastic deposits (ranging from large pebbles to boulders; Terry and Goff, 2014) or by looses sediments (fig. 5) while the geomorphologic record is often recognized as dune modifications and other coastal peculiar features (Gianfreda et al., 2001).

Most of tsunami sediments is characterized by a single sandy layer or by few sandy layers separated by mud laminations often with an erosive contact at the bottom and a thickness ranging from few centimeters to a maximum of 20-30 cm (Tuttle et al., 2004; Morton et al., 2007). The structure can be massive or normal/inverse graded (Morton et al., 2007). A single structureless layer is the symbol of a rapid deposition, while several layers, often intercalated by mud laminations, represent two or more tsunami waves (Morton et al., 2007). The mud laminations are related to the sediment transport, in fact they can settle down between successive tsunami waves or can be introduced as soil eroded from surrounded slopes by the return flow (Morton et al., 2007). A tsunami layer may contain within it (usually in the lower part of the bed) rip-up clasts. Moreover, tsunami wave sediments may have also an important part of organic remnants and fossils from offshore, such as foraminifera, diatoms, fragments of corals and bivalves (Shiki et al., 2008).

A coastal site able to preserve paleotsunami sediments has to be characterized by a low – energy sedimentation coastal environment, as a coastal marsh or a coastal lagoon, where past high-energy marine inundations may have been recorded by the deposits left on the ground and preserved in the stratigraphical record (Morton et al., 2007; Papadopoulos et al., 2014). Moreover, sites of investigation have to be chosen with a distance from the present shoreline of at least 200 meters in order to exclude or to limit the influence of the storms (Nanayama et al., 2000; Goff et al., 2004; Tuttle et al., 2004). From a general point of view, tsunami deposits may differ from the storm deposits (Morton et al., 2007) in terms of thickness (larger for storms), grain size characteristics (storm deposits are better sorted) and internal structure (storm deposits are often laminated and may show foreset and cross – bedding sedimentary structures).

Through the analysis of several sediment cores and trenches, many paleotsunami sediment layers have been recognized along the eastern Sicily coasts (Pantosti et al., 2008; De Martini et al., 2010; Scicchitano et al., 2010; Gerardi et al., 2012), and on the north coast of Gargano promontory (Apulia, southern Italy) by De Martini et al. (2003). In addition, Smedile et al., (2010) presented an offshore evidence of 12 tsunami events occurred in the Augusta Bay (Eastern Sicily). This study was carried out on a 6.7 m long, fine sediment core sampled at a water depth of 72 m, 2.3 km

offshore. Most of sediment tsunami layers (onshore and offshore) was recognized through several kinds of analyses including X-ray imaging, high-resolution measurement of physical properties, grain-size analysis, micropaleontology, isotopic dating methods (210Pb, 137Cs and 14C) and tephrachronology.

Tsunami deposits represented by large boulders are often located on rocky platforms or terraces characterized by a height above the sea level of maximum 10 meters (for Italy see: Scicchitano et al., 2007; Barbano et al., 2010; Mastronuzzi et al., 2012). These blocks can reach several tons in weight (for example 75 tons, Scheffers and Scheffers, 2007) and are detached from the near shore and deposited inland by tsunami and also by storm waves. Today, it is still difficult to estimate if the emplacement of a block may be attributed to a storm or to a tsunami wave (Barbano et al., 2010). In this context, scientists adopt hydrodynamic equations taking into account the setting and the physical properties of the boulders, to understand their emplacement (Scicchitano et al., 2007; Barbano et al., 2010). For instance, Biolchi et al. (2015) on the base of the combination of results obtained from hydrodynamic equations and radiocarbon dating suggest that some boulder accumulations, detected along the coasts of Malta, are related to the action of intense storm waves and only some of them may have been caused by tsunami. The coasts of eastern Sicily from Augusta to Pachino have several boulders accumulation related to the strong tsunamis occurred in 1169, 1693 and 1908 (Scicchitano et al., 2007; Barbano et al., 2010). Also the Apulia region, due its geomorphological coastal setting, is characterized by boulders deposition tsunami-related. Along the coast of this region several localities such as “Torre Sant’Emiliano” or “Torre Santa Sabina” show evidence of transported blocks interpreted as paleotsunami deposits (Mastronuzzi et al., 2000, 2004, 2007).

Tsunami signatures, as previously mentioned, may also be represented by geomorphological evidences. Recently, it was observed that a strong tsunami can modify and change the coastal setting of a certain portion of coast (Paris et al., 2009; Koiwa et al., 2017). The Lesina lake (Apulia, southern Italy) is an example of how a past tsunami might have changed the coastal morphology. In detail, the sand barrier system, that separates the lake form the Adriatic sea, shows at least three washover fans interpreted as due to three distinct tsunamis respectively related to a pre-Roman event dated about 2430 yr BP, the 493 AD event and the 1627 local event. (Gianfreda et al., 2001). Moreover, Goff et al. (2007) developed a method based on LIDAR data combined with ground surveys in order to identify past tsunami from their geomorphic signatures. They identified several tsunami-related geomorphological features as:

- ✓ Pedestals: remnant sections of dune ridge separated by scoured areas

- ✓ Hummocky topography or sand sheets that form landward from pedestals (hummocky topography is the old, weathered equivalent of sand sheets)
- ✓ Parabolic dune fields, which are remobilized sand sheets landward of pedestals
- ✓ Low Profile Sequences: post-tsunami feature indicative of changes to coastal sediment budget.

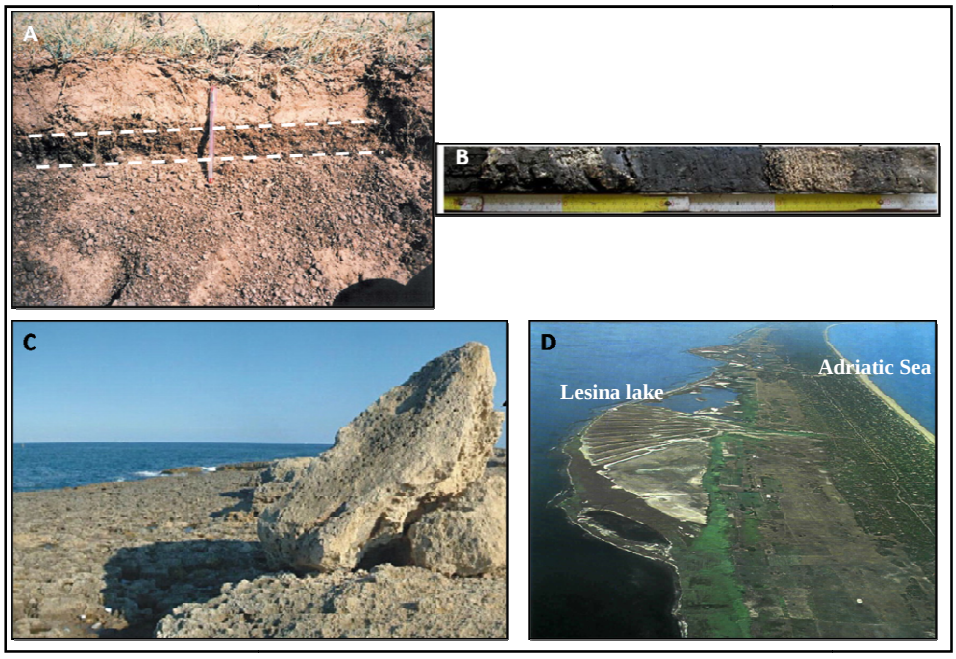

Fig. 5 – The figure shows the main paleotsunami deposit evidence. A) Paleotsunami sediment in a trench wall, Didim, Turkey (Papadopoulos et al, 2014); B) Paleotsunami sediment layers in a core dug in the eastern Sicily (De Martini et al., 2010); C) Boulders accumulation in the Ognina locality, eastern Sicily, (Scicchitano et al., 2007); D) Washover fan in the Lesina lake, Gargano, Apulia region (Gianfreda et al 2001).

1.2 The modeling approach

Today, tsunami simulations are often used to assess the hazard in a given area of interest (Lorito et al., 2008; Tonini et al., 2011). In fact, unfortunately the geological evidence of past tsunamis may not always be preserved along a stretch of coast. Tsunami deposits could have been eroded or the coastal settings were not suitable for the recording of a past tsunami. The modeling approach is able to estimate the generation, the propagation and the inundation phase due to an extreme event like a tsunami wave both at local level (e.g. Tonini et al., 2011) as well as at regional level (Løvholt et al., 2012). Tsunami hazard analysis follows two main approaches: the Scenario-Based Approach, SBTHA (Tinti and Armigliato, 2003; Løvholt et al., 2006; Lorito et al., 2008) and the Probabilistic Tsunami Hazard Assessment, PTHA (Geist and Parsons, 2006). The main goal of PTHA is to determine the probability of exceedance of a given tsunami metric (flow depth, run-up, current speed, etc.) over a given exposure time for a selected coastal area/site, quantifying both aleatory and

epistemic uncertainty. Differently, the SBTHA analyzes the worst scenario for a given area. Once the source areas have been identified, SBTHA foresees that for each type of tsunamigenic source identified in each area (earthquake, landslide, volcanic eruption) the “credible worst case” is selected.

Site – specific studies with detailed modeling of the run-up are computationally costly (Løvholt et al., 2012; Løvholt et al., 2014). Moreover, very detailed and accurate topo-bathymetric models (needed for local simulations) are often unavailable at certain localities. Therefore, approximated methods in order to estimate run-up heights and inundation distances are used.

In this thesis, I present a modeling approach based on a procedure called “the amplification factor method” proposed and validated by Løvholt et al., 2012. The amplification factor method is an approximated fast procedure to estimate, at regional level, the run-up value and the inundation distance along a stretch of coast. This procedure consists in relating the water surface elevation at a given isobath (e.g. 50 m depth) with the maximum surface elevation during inundation past the shoreline using a set of amplification factors. It is then assumed that the water level at the shoreline is a proxy for the maximum run-up except for very flat coastal morphologies. In this thesis, following the procedure adopted by Løvholt et al. (2012), the amplification factor method was updated and improved (Harbitz et al., 2016). More in detail, in order to compute the wave amplification from an offshore point to the shoreline, local bathymetries were used (previously idealized bathymetries were used), giving more accuracy to the results. Nevertheless, it is important to remember that this procedure gives only an overview of the wave amplification and therefore it cannot be used for local hazard assessment. Despite this, this work shows that a potential relation between the distribution of some tsunami deposits and the wave amplification exists.

References

Ammiano Marcellino, Res Gestae, 26.10.15–19

Barbano M.S., De Martini P.M., Pantosti D., Smedile A., Del Carlo P., Gerardi F., Guarnieri P., Pirrotta C., (2009). In Search of Tsunami Deposits Along the Eastern Coast of Sicily (Italy): The State of the Art. Recent Progress on Earthquake Geology, chapter 5. ISBN: 978-1-60876-147-0 Nova Science Publishers, Inc.

Biolchi S., Furlani S., Antonioli F., Baldassini N., Causon Deguara J., Devoto S., Di Stefano A., Evans J., Gambin T., Gauci R., Mastronuzzi G., Monaco C., and Scicchitano G., (2015). Boulder accumulations related to extreme wave events on the eastern coast of Malta. Nat. Hazards Earth Syst. Sci. Discuss., 3, 5977–6019.

Barbano M.S., Pirrotta C., Gerardi F., (2010). Large boulders along the south-eastern Ionian coast of Sicily: Storm or tsunami deposits?. Marine Geology, 275, 140 – 154.

Butler R., Burney D., Walsh D., (2014). Paleotsunami evidence on Kaua‘i and numerical modeling of a great Aleutian tsunami. Geophysical Research Letters, 41, 19, 6795 – 6802. DOI: 10.1002/2014GL061232.

Cavazza W., Roure F.M., Spakman W., Stampfli G.M., Ziegler P.A., (2004). The TRANSMED Atlas. The Mediterranean region from crust to mantle geological and geophysical framework. A Publication of the Mediterranean Consortium for the 32nd International Geological Congress 2004, XXIV, 141, p. 44 (illus., 37 in color. With CD-ROM).

Costa P.J.M., Dawson S., Quintela M., Andrade C., Milne F., Dourado F. and Dawson A. (2016). Tsunami Deposits Database – Retrieved from http://tsunami.campus.ciencias.ulisboa.pt/.

De Martini P.M., Barbano M.S., Pantosti D., Smedile A., Pirrotta C., Del Carlo P., and Pinzi S. (2012). Geological evidence for past-tsunamis along eastern Sicily (Italy): an overview. Nat. Hazards Earth Syst. Sci., 12, 2569-2580, doi:10.5194/nhess-12-1-2012.

De Martini, P.M., Barbano, M.S., Smedile, A., Gerardi, F., Pantosti, D., Del Carlo, P., Pirrotta, C, (2010). A unique 4000 year long geological record of multiple tsunami inundations in the Augusta Bay (eastern Sicily, Italy). Marine Geology, 276, 42-57, doi: 10.1016/j.margeo.2010.07.005

De Martini P.M., Burrato P., Pantosti D., Maramai A., Graziani L., Abramson H., (2003) Identification of tsunami deposits and liquefaction features in the Gargano area (Italy): paleoseismological implication. ANNALS OF GEOPHYSICS, VOL. 46, N. 5.

Fleming K., Johnston P., Zwartz D., Yokoyama Y., Lambeck K., Chappel J., (1998). Refining the eustatic sea-level curve since the Last Glacial Maximum using far and intermediate-fields sites. Earth and Planetary Science Letters 163, 327-342.

Friedrich W.L., Kromer B., Friedrich M., Heinemeier J., Pfeiffer T., Talamo S., (2006). Santorini eruption radiocarbon dated to 1627–1600 B.C. Science 312, 548

Gerardi F., Smedile A., Pirrotta C., Barbano M. S., De Martini P. M. ,Pinzi S. , Gueli A. M., Ristuccia G. M., Stella G., and Troja S. O., (2012). Geological record of tsunami inundations in Pantano Morghella (south-eastern Sicily) both from near and far-field sources. Nat. Hazards Earth Syst. Sci., 12, 1185–1200. doi: 10.5194/nhess-12-1185-2012.

Gianfreda F., Mastronuzzi G., Sansò P., (2001). Impact of historical tsunamis on a sandy coastal barrier: an example from the northern Gargano coast, southern Italy. Natural Hazards and Earth System Sciences (2001) 1: 213–219, ©European Geophysical Society 2001.

Geist E., Parsons T., (2006). Probabilistic analysis of tsunami hazards. Nat Hazard 37, 277–314.

Goff J., Chaguè – Goff C., (2014). The Australian tsunami database: A review. Progress in Physical Geography 2014 38: 218. DOI: 10.1177/0309133314522282.

Goff J.R., Hicks D. M., Hurren H. Tsunami geomorphology in New Zealand. A new method for exploring the evidence of past tsunamis. NIWA Technical Report 2007.

Goff J., McFadgen B.G., Chagué-Goff C., (2004). Sedimentary differences between the 2002 Easter storm and the 15th century Okoropunga tsunami, southeastern North Island, New Zealand. Marine Geology 204, 235–250. doi:10.1016/S0025-3227(03)00352-9.

Harbitz C.B., Glimsdal S., Løvholt F., Orefice S., Romano F., Brizuela B., Lorito S., Development of Local Amplification Factors in the NEAM Region for Production of Regional Tsunami Hazard Maps, AGU Fall Meeting, 12-16 December 2016

Japan Tsunami Trace database (Tsunami trace height information). Disaster Control Research Center (DCRC), Graduate School of Engineering, Tohoku University Japan Nuclear Energy Safety Organization (JNES). http://tsunami-db.irides.tohoku.ac.jp/

Koiwa N., Takahashi M., Sugisawa S., Ito A., Matsumoto H., Tanavud C., Goto K., (2017). Barrier spit recovery following the 2004 Indian Ocean tsunami at Pakarang Cape, southwest Thailand. Geomorphology (Accepted Manuscript), doi: 10.1016/j.geomorph.2017.05.003.

Lorito S., Tiberti M. M., Basili R., Piatanesi A., & Valensise, G., (2008). Earthquake-generated tsunamis in the Mediterranean Sea: Scenarios of potential threats to Southern Italy. J. Geophys. Res., 113, B01301, 10.1029/2007JB004943.

Løvholt F., Glimsdal S., Harbitz Carl B., Horspool N., Smebye H., De Bono A., Nadim F., (2014). Global tsunami hazard and exposure due to large co-seismic slip. International Journal of Disaster Risk Reduction.

Løvholt F., Glimsdal S., Harbitz Carl B., Zamora N., Nadim F., Peduzzi P., Dao H., Smebye H., (2012). Tsunami hazard and exposure on the global scale. Earth-Science Reviews, Volume 110, Issues 1–4, Pages 58-73.

Løvholt F, Pedersen G, Gisler G., (2006). Oceanic propagation of a potential tsunami from the La Palma Island. J. Geophys. Res., 113, C09026, http://dx.doi.org/10.1029/2007JC004603.

Maramai A., Brizuela B., Graziani L. The Euro-Mediterranean Tsunami Catalogue, 2014. Annals of Geophysics, 57,4. Doi: 10.4401/ag-6437

Maramai A., Graziani L., Tinti S., (2005). Tsunamis in the Aeolian Islands (southern Italy):a review. Marine Geology 215, 11–21.

Mastronuzzi G., Pignatelli C., (2012). The boulders berm of Punta Sa Guerra (Taranto, Italy): a morphological imprint of the Rossano Calabro tsunami of April 24, 1836? Earth Planets Space, 64, 10 829-842.

Mastronuzzi G., Pignatelli C., Sansò P., Selleri G., (2007). Boulder accumulations produced by the 20th of February, 1743tsunami along the coast of south eastern Salento (Apulia region, Italy). Marine Geology 242,191–205.

Mastronuzzi G., Sansò P., (2000). Boulders transport by catastrophic waves along the Ionian coast of Apulia (southern Italy). Marine Geology 170, 93-103.

Mastronuzzi G., Sansò P., (2004). Large boulder accumulations by extreme waves along the Adriatic coast of southern Apulia (Italy). Quaternary International, 120, 173 – 184.

Morton R.A., Gelfenbaum G., Jaffe B.E., (2007). Physical criteria for distinguishing sandy tsunami and storm deposits using modern examples. Sedimentary Geology, 200, 184 – 207.

Nanayama F., Shigeno K., Satake K., Shimokawa K., Koitabashi S., Miyasaka S., Ishii M., (2000). Sedimentary differences between the 1993 Hokkaido–Nansei–Oki tsunami and the 1959 Miyakojima typhoon at Taisei, southwestern Hokkaido, northern Japan. Sedimentary Geology 135, 255–264

NGDC/WDS Global Historical Tsunami Database, 2100 BC to present. doi:10.7289/V5PN93H7

Pantosti D., M.S. Barbano, A. Smedile, P.M. De Martini and G. Tigano, (2008). Geological evidence of paleotsunamis at Torre degli Inglesi (northeast Sicily). Geophysical Research Letter, 35, L05311, doi: 10.1029/2007GL032935.

Paris R., Wassmer P., Sartohadi J., Lavigne F., Barthomeuf B., Desgages E., Grancher D., Baumert, P., Vautier F., Brunstein D., Gomez C., (2009). Tsunamis as geomorphic crises: Lessons from the December 26, 2004 tsunami in Lhok Nga, West Banda Aceh (Sumatra, Indonesia). Geomorphology 104(1–2), 59-72.

Papadopoulos G.A., Gràcia E., Urgeles R., Sallares V., De Martini P.M., Pantosti D., González M, Yalciner A.C., Mascle J, Sakellariou D., Salamon A., Tinti S., Karastathis V., Fokaefs A., Camerlenghi A., Novikova T., Papageorgiou A., (2104). Historical and pre-historical tsunamis in the Mediterranean and its connected seas: Geological signatures, generation mechanisms and coastal impacts. Marine Geology, 354, 81–109. http://dx.doi.org/10.1016/j.margeo.2014.04.014.

Scheffers A., Scheffers S., (2007). Tsunami deposits on the coastline of west of Crete (Greece). Earth and Planetary Science Letters 259, 613–624

Scicchitano G., Costa B., Di Stefano A., Longhitano S.G., Monaco C., (2010). Tsunami and storm deposits preserved within a ria-type rocky coastal setting (Siracusa, SE Sicily). Zeitschrift für Geomorphologie Vol. 54, Suppl. 3, 051-077.

Scicchitano G., Monaco, C., and Tortorici, L., (2007). Large boulder deposits by tsunami waves along the Ionian coast of south-eastern Sicily (Italy). Mar. Geol., 238, 75–91.

Shiki T., Tachibana T., Fujiwara O., Goto K., Nanayama F., Yamazaki T., (2008). Characteristic features of tsunamiites. In: Shiki, T., Tsuji, Y., Yamazaki, T., Minoura, K. (Eds.), Tsunamiites — Features and Implications. Elsevier, Amsterdam, pp. 319–340.

Smedile A., De Martini P. M., Pantosti D., Bellucci L., Del Carlo P., Gasperini L., Pirrotta C., Polonia A., and Boschi E., (2011). Possible tsunamis signatures from an integrated study in the Augusta Bay offshore (Eastern Sicily–Italy). Mar. Geol., 281,1–13.

Szczuciński W., Kokociński M., Rzeszewski M., Goff C.C., Cachão M., Goto K., Sugawara D., (2012). Sediment sources and sedimentation processes of 2011 Tohoku-oki tsunami deposits on the Sendai Plain, Japan — Insights from diatoms, nannoliths and grain size distribution. Sedimentary Geology, 282, 40-56.

Terry J.P.; Goff J., (2014). Megaclasts: Proposed Revised Nomenclature At the Coarse End of the Udden-Wentworth Grain-Size Scale for Sedimentary Particles. Journal of Sedimentary Research, 84(3-4):192-197.

The Euro-Mediterranean Paleotsunami Database (http://paleotsunami.rm.ingv.it/). TRANSFER project (Tsunami Risk AN Strategies For the Europen Region.

The New Zealand Tsunami Database: Historical and Modern Records, Natural Hazards Databases, GNS Science, Lower Hutt [07/05/2017].

Tiberti M.M., Basili R., Vannoli P., (2004). Ups and downs in western Crete (Hellenic subduction zone). Nature, SCIENTIFIC REPORTS | 4 : 5677 | DOI: 10.1038/srep05677

Tinti S., Armigliato A., (2003). The use of scenarios to evaluate the tsunami impact in southern Italy. Marine Geology 199 (3-4), 221, 243.

Tinti, S., Guidoboni, E., (1988). Revision of the tsunamis occurred in 1783 in Calabria and Sicily (Italy). Science of Tsunami Hazards 6, 17–22.

Tinti S., Piatanesi A., (1996). Numerical simulations of the tsunami induced by the 1627 earthquake affecting Gargano, Southern Italy. J. Geodynamics, 21, 141 – 160.

Tonini R., Armigliato A., Pagnoni G., Zaniboni F. & Tinti S., (2011). Tsunami hazard for the city of Catania, eastern Sicily, Italy, assessed by means of Worst-case Credible Tsunami Scenario Analysis (WCTSA), Nat. Hazards Earth Syst. Sci., 11, 1217–1232.

Tuttle M.P., Ruffman A., Anderson T., Jeter H., (2004). Distinguishing tsunami from storm deposits in eastern North America: the 1929 Grand Banks tsunami versus the 1991 Halloween storm. Seismological Research Letters 75, 117–131.

Chapter 1

The ASTARTE Paleotsunami Deposits database – NEAM region

The Paleotsunami deposits database was funded by the European Union's Seventh Framework Programme (FP7/2007-2013) under grant agreement n_ 603839 (Project ASTARTE - Assessment, Strategy and Risk Reduction for Tsunamis in Europe).
The European Union project ASTARTE aims at developing a higher level of tsunami hazard assessment in the North East Atlantic and Mediterranean (NEAM) region by a combination of field work, experimental work, numerical modeling, and technical development. The project is a joint work of 26 institutes from 16 European countries and links together the description of past tsunamigenic events, the characterization of tsunami sources, the calculation of the impact of such events, and the development of adequate resilience strategies (www.astarte-project.eu).

I describe and present here the Astarte Paleotsunami Deposits Database – NEAM region. In this context, I was the compiler and the scientific manager for all Italian data and I was asked to manage and control at least half of all scientific data inserted in the database so far. I also performed a statistical analysis of some selected database data in order to highlight the potentialities of such database and to point out important information. Moreover, I contributed, although to a lesser extent, to the improvement of the structure and architecture of the database, in order to better organize the scientific paleotsunami data.

1. Introduction

In the last two decades, many scientific works about tsunami deposits have demonstrated the high tsunami hazard of several portions of coast worldwide (e.g. Mastronuzzi et al., 2007; De Martini et al., 2012; Sugawara et al., 2012; Fischer et al., 2016). The identification and the characterization of (paleo) tsunami deposits have improved the knowledge about these extreme events. Tsunami deposits can provide us information about the minimum inundation distance, the minimum topographic height reached by the sea wave (run-up) and the age of the event. These data are useful to understand the tsunami size, the related sources and their recurrence. Therefore, information derived from paleotsunami deposits can be considered essential for a possible local application in terms of prevention by highlighting the tsunami wave inundation area. Moreover, the geological approach together with numerical simulations can be considered a viable procedure to assess the hazard along a given stretch of coast in order to emphasize the importance of a prevention plan, especially in the light of the recent tsunamis of Indonesia 2004 and Japan 2011.
The spatial distribution and sedimentological features of the 869 A.D. Jogan tsunami deposit along the Pacific coast of Japan (Sugawara et al., 2012) represents an example of the importance of the information derived from paleotsunami deposits. This ancient tsunami is considered the paleo-event

of the 2011Tohoku-Oki earthquake/tsunami since, in the Sendai plain, the comparison of the inland limit inundation between the two tsunamis is approximately the same, but in the Sanriku and Joban coasts the Jogan deposit was identified only in few localities. This caused an underestimation in the prediction of the Tohoku-Oki tsunami wave size (Sugawara et al., 2012). In fact, the magnitude of the Jogan earthquake (Mw= 8.4), derived from the spatial distribution of deposits and from numerical modeling, was too small to predict the magnitude of the Tohoku-Oki earthquake (Mw= 9.0-9.1) (Sugawara et al., 2012).

Nowadays, the need to collect together the highest number of tsunami data in order to provide useful information both from a scientific point of view and in terms of prevention, has encouraged the development of several databases. At global level, one of the most known is the NGDC/WDS tsunami database (National Geophysical Data Center / World Data Service (NGDC/WDS): Global Historical Tsunami Database, National Geophysical Data Center, NOAA). The NGDC/WDS tsunami database reports a list of historical tsunami source events and run-up locations worldwide, taking into account an age range from 2000 B.C. to the present.

This database (fig.1) is based on two related files. The first one includes information on the tsunami source such as the date, time, and location of the source event; cause and validity of the source, tsunami magnitude and intensity; maximum water height; the total number of fatalities, injuries, houses destroyed, and houses damaged; and total damage estimate (in U.S. dollars). The second file contains information on the run-ups (the locations where tsunami waves were observed by eyewitnesses, reconnaissance surveys, tide gauges, and deep-ocean sensors) such as name, location, arrival time, maximum water height and inundation distance, and socio-economic data (deaths, injuries, damage) for the specific run-up location.

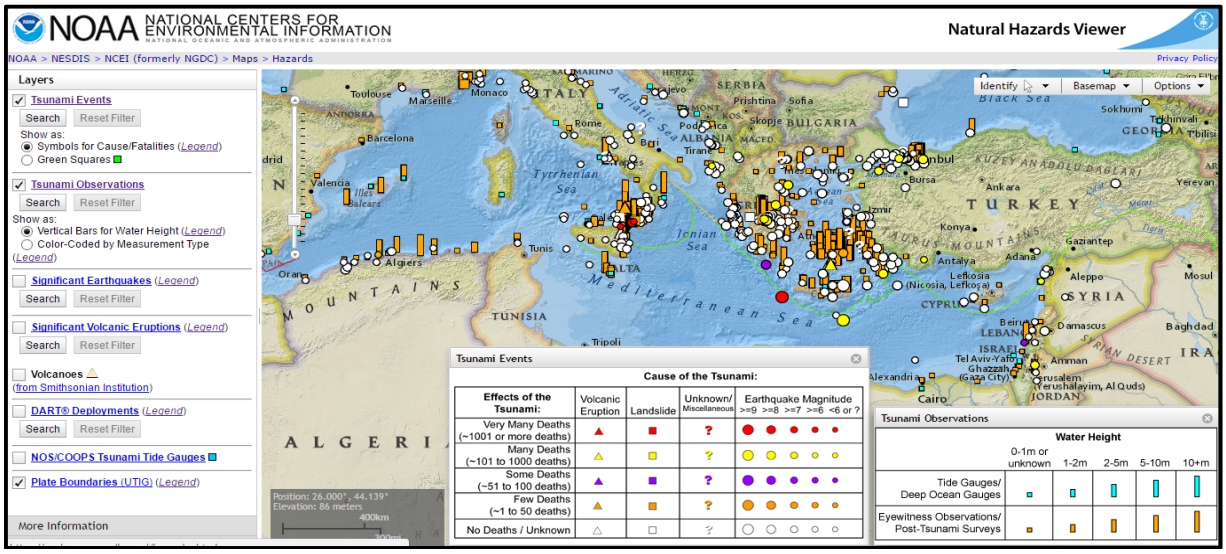

Fig. 1 – An overview of the NGDC/WDS tsunami database highlighting the two main files: the Tsunami Events (sources) and the Tsunami observations (run – up).

Moreover, NOAA provides a global tsunami deposits database, organized in one table showing the following fields (fig 2): Citation (Author, Year, Type), Event, Geologic Age, Earliest Year, Latest year, Latitude, Longitude, Location name, Country, Body of water (the interested sea during the event), Narrative description and Setting during the event.

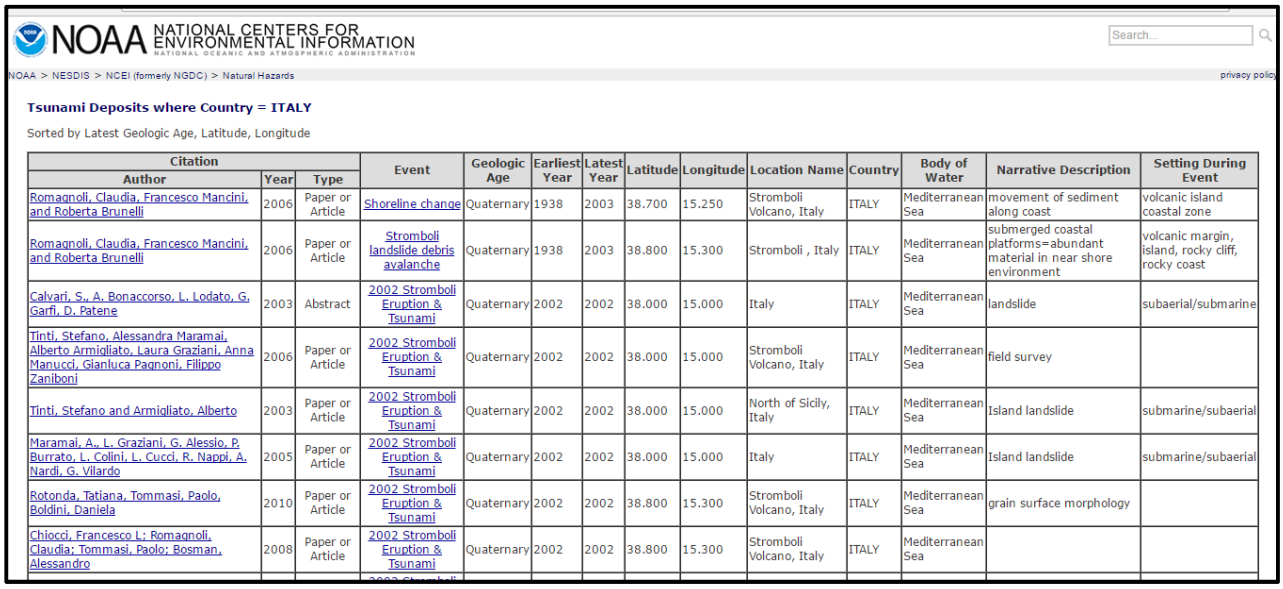

NOAA NATIONAL CENTERS FOR ENVIRONMENTAL INFORMATION

NOAA > NESDIS > NCEI (formerly NGDC) > Natural Hazards

Tsunami Deposits where Country = ITALY

Sorted by Latest Geologic Age, Latitude, Longitude

Citation			Event	Geologic Age	Earliest Year	Latest Year	Latitude	Longitude	Location Name	Country	Body of Water	Narrative Description	Setting During Event
Author	Year	Type											
Romagnoli, Claudia, Francesco Mancini, and Roberta Brunelli	2006	Paper or Article	Shoreline change	Quaternary	1938	2003	38.700	15.250	Stromboli Volcano, Italy	ITALY	Mediterranean Sea	movement of sediment along coast	volcanic island coastal zone
Romagnoli, Claudia, Francesco Mancini, and Roberta Brunelli	2006	Paper or Article	Stromboli landslide debris avalanche	Quaternary	1938	2003	38.800	15.300	Stromboli , Italy	ITALY	Mediterranean Sea	submerged coastal platforms=abundant material in near shore environment	volcanic margin, island, rocky cliff, rocky coast
Calvari, S., A. Bonaccorso, L. Lodato, G. Garfì, D. Patene	2003	Abstract	2002 Stromboli Eruption & Tsunami	Quaternary	2002	2002	38.000	15.000	Italy	ITALY	Mediterranean Sea	landslide	subaerial/submarine
Tinti, Stefano, Alessandra Maramai, Alberto Armigliato, Laura Graziani, Anna Manucci, Gianluca Pagnoni, Filippo Zaniboni	2006	Paper or Article	2002 Stromboli Eruption & Tsunami	Quaternary	2002	2002	38.000	15.000	Stromboli Volcano, Italy	ITALY	Mediterranean Sea	field survey	
Tinti, Stefano and Armigliato, Alberto	2003	Paper or Article	2002 Stromboli Eruption & Tsunami	Quaternary	2002	2002	38.000	15.000	North of Sicily, Italy	ITALY	Mediterranean Sea	Island landslide	submarine/subaerial
Maramai, A., L. Graziani, G. Alessio, P. Burrato, L. Colini, L. Cucci, R. Nappi, A. Nardi, G. Vilardo	2005	Paper or Article	2002 Stromboli Eruption & Tsunami	Quaternary	2002	2002	38.000	15.000	Italy	ITALY	Mediterranean Sea	Island landslide	submarine/subaerial
Rotonda, Tatiana, Tommasi, Paolo, Boldini, Daniela	2010	Paper or Article	2002 Stromboli Eruption & Tsunami	Quaternary	2002	2002	38.800	15.300	Stromboli Volcano, Italy	ITALY	Mediterranean Sea	grain surface morphology	
Chiocci, Francesco L; Romagnoli, Claudia; Tommasi, Paolo; Bosman, Alessandro	2008	Paper or Article	2002 Stromboli Eruption & Tsunami	Quaternary	2002	2002	38.800	15.300	Stromboli Volcano, Italy	ITALY	Mediterranean Sea		

Fig. 2 – The tsunami deposits fields available in the NOAA global tsunami deposits database. In this example the database was queried with all paleotsunami deposits data compiled for Italy. The figure shows a selection of some data about paleotsunami deposits found in Italy.

Another important and well known tsunami database is the Historical Tsunami Database World Ocean (HTDB/WLD) (http://tsun.sscc.ru/htdbwld/) managed and maintained by the Novosibirsk Tsunami Laboratory (NTL) of the Institute of Computational Mathematics and Mathematical Geophysics ICM&MG, Siberian Division of Russian Academy of Sciences since 1991. The database is characterized by two main sets of data: the event data (observational data and parametric source data) and the run-up heights data (observed or measured). The event dataset contains the source and some integrated tsunami parameters for 2270 historical tsunamigenic events occurred in the World Ocean from 1628 B.C up to the present time. In detail there are the full date and time of an event, position of its source, the source depth, the basic set of source magnitudes, tsunami intensity (on the Soloviev-Imamura scale), tsunami magnitude (on the Imamira-Iida scale), the maximum observed run-up value, the total number of available run-up and tide-gauge measurements, damage code, the number of reported fatalities due to an event, a cause of the tsunami, validity of an event, warning status (where available), tsunamigenic region code, the basic reference and a brief description of the source region data. The run-up dataset has about 9000 coastal run-up observations and tide-gauge measurements of wave heights. This part was imported from the NGDC Worldwide Tsunami Database. Improvements and corrections were made for the

Kuril-Kamchatka region and for the US Pacific coast, Alaska and Hawaii. In addition measurements of wave heights for the Pacific tsunamis of 1992-2006 obtained in the post-event field surveys were added. For each wave height record the following information is given: the name of the site (Region name, Area name and Site name), its geographical coordinates, the type of measurement (R - run-up, T - tide-gauge) and the observed run-up height or the double amplitude (in meters).

Goff et al. (2016) defined the latter two databases as the two major historical tsunami databases available now. In addition to these, in the literature we can find other databases, often focused only on tsunamis that struck the coasts of a single country, as the Japan Tsunami Trace Database, the Australian tsunami database or the New Zealand tsunami database.

The "Japan Tsunami Trace Database" (http://tsunami-db.irides.tohoku.ac.jp) has been developed by the School of Engineering of Tohoku University and by the Japan Nuclear Energy Safety Organization (JNES). The database provides information of the major tsunamis that occurred from 1596 AD to present. In detail, there are data about the "Tsunami Trace Data" of the Japan (data on locations with traces of past tsunamis) (fig. 3) focusing the attention on the event, on the source, and also on the tsunami deposit (where available).

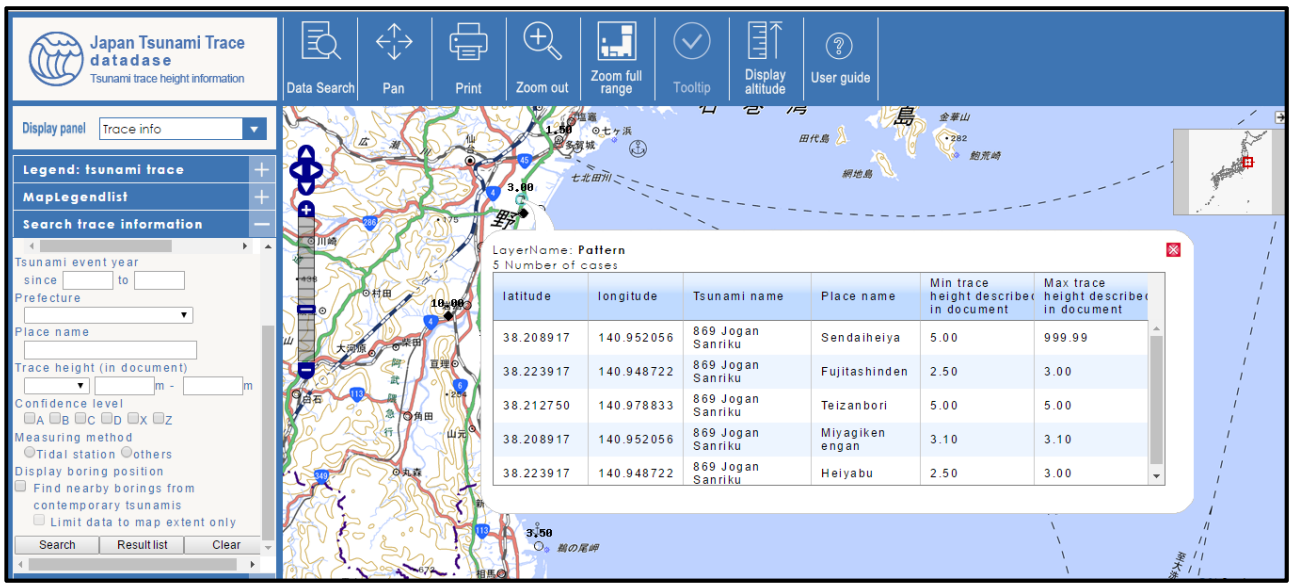

Fig. 3 – The web GIS map shows an example of run-up heights referred to the 869 AD Jogan Sanriku tsunami, recorded along the eastern coast of Japan.

The New Zealand Tsunami database (http://data.gns.cri.nz/tsunami/index.html) reports information about tsunamis that have affected the New Zealand coastline since the first human that lived this land to the present day. The purpose of the database is to increase awareness of New Zealand's tsunami hazard, in order to be a fundamental help for coastal planning, tsunami modeling, hazard

estimates and forecasting, and promote further research. The database architecture is based on a main file that contains all sites affected by tsunamis (listed in a table and represented in a georeferenced interactive map). From each location file it is possible to access to more information regarding an overview of the event, impact measurements, impact observations, source parameters, descriptive accounts and references. The database is the work of the historical seismologist Gaye Downes of GNS Science who collected reports of tsunamis around New Zealand and, in many cases, carried out research to determine parameters of the source, travel time and impact associated with each event. Reports of tsunamis that make up the core of this database come from tide gauges, newspaper articles, harbour masters, records from ships, personal diary entries and Māori oral records. Another database, the New Zealand paleotsunami database, is actually available at https://ptdb.niwa.co.nz/. It is based on the work of James Goff (Professor of the University of New South Wales, Australia) and is provided by the National Institute of Water & Atmospheric Research Ltd (NIWA) and the Ministry for Civil Defence and Emergency Management (MCDEM) (together, the Providers). The database contains paleotsunami evidence (for the New Zealand) related to each single site affected. Evidence may be defined as physical from geological and archaeological sources and as cultural information from anthropological and cross-disciplinary studies. The Database currently contains 429 line items describing more than 50 paleotsunami events. Data include: site information, nature of the evidence, chronology and dating techniques, maximum water heights, horizontal inundation distances, sources and supporting meta-data for specific locations.

The Australian tsunami database (reviewed by Goff et al., 2014) provides information on 145 individual tsunamis, although the total number, considering all events per state, is 195. The format adopted in the database provides information about the event, validity of the event, age of the event, site affected by the event, details about the site location, deposits, run-up, cause of the event, deaths and references. Furthermore, when physical evidence of a deposit is reported, a separate worksheet entitled Proxy data is added. The main dataset used in this database derives from NOAA/NGDC Tsunami Event Database (NGDC), from the digitized Australian and New Zealand newspapers of the National libraries of Australia and New Zealand, from two Australian reports (New South Wales: Beccari, 2009; Tasmania: Morris and Mazengarb, 2009) and from other numerous data sources.

At European level, the Euro-Mediterranean Paleotsunami Database, developed within the TRANSFER project (Tsunami Risk ANd Strategies For the European Region), was the first focused only on tsunami deposits. This database was the starting point for the development of the new Astarte Paleotsunami deposits database for the NEAM region.

Similarly to the Transfer Paleotsunami deposits database, Costa et al., (2016) developed a tsunami deposits database for the NE Atlantic (85 entries so far). Paleotsunami deposits data are organized in a GIS map view and in a table view. In a unique table view, locations and geomorphic setting of sites, paleotsunami deposits geometries (thickness, max extent inland, max height), analysis of interpretation, ages and references are reported.

The Astarte Paleotsunami Deposits database – NEAM region was created within the ASTARTE EU project that aims to develop a tsunami hazard assessment in the North East Atlantic and Mediterranean (NEAM) region by a combination of several methods. The database has the purpose to provide the official existing scientific data on tsunami deposits recognized in the NEAM area. Moreover, also the geomorphic signatures derived from a tsunami event are reported (Gianfreda et al., 2001, Goff et al., 2007). All data archived into the database are geo-referenced and derive from official scientific literature (e.g. a scientific work or an official report). To date, a total of 151 sites and 220 tsunami evidences were recorded within the database.

The database is a joint work at European level. The realization of the database as the entering of the scientific data involved several European institutes and compilers. In detail:

- *Paolo Marco De Martini, Simone Orefice, Alessandra Smedile, Antonio Patera and Daniela Pantosti* from Istituto Nazionale di Geofisica e Vulcanologia, Roma, Italy.
- *Raphael Paris* from Université Clermont Auvergne, Laboratoire Magmas et Volcans, F-63000 Clermont-Ferrand, France.
- *Pedro Terrinha* and *João Noiva* from Instituto Português do Mar e da Atmosfera, Lisboa, Portugal.
- *James Hunt* from National Oceanography Centre, Southampton, United Kingdom.
- *Gerassimos Papadopoulos* and *Ioanna Triantafyllou* from National Observatory of Athens, Greece.
- *Ahmet C. Yalciner* from Middle East Technical University, Ankara, Turkey.

Most of existing databases exhibit a level of confidence of the shown data. The validity of each tsunami event as well as that of each kind of data may be only defined by the reviewer. In this way the decision to include or to exclude a given event or data, even though discussed and debated in the scientific community, may be subject to personal interpretation. In order to avoid this approach, in the absence of a guideline, the Astarte Paleotsunami Deposits database – NEAM region data are not subject to interpretation and are inserted exactly as published in the official scientific literature. Therefore, the user will not find any reference to the validity of the data shown but he will be free to evaluate the reliability of the data in the light of the their knowledge.

2. ASTARTE Paleotsunami Deposits database

The Paleotsunami Deposit geographic database is a relational database managed by ArcGIS for Desktop 10.5 software by Esri Inc. This geographical information system (GIS) allows all partners to collaborate through a common platform for archiving data. The internet interactive map service is hosted by the ArcGIS Online portal (www.arcgis.com).

2.1 The database architecture

The database structure is characterized by the presence of two main tables: the Site table and the Event table. Each Site is related to one or more Event record (tsunami). At the same time, both the Site table and the Event table are related to other tables, as shown in the database scheme represented below (fig.4).

Fig. 4 - The architecture of the database. Note the type of relationship between the two main tables (Site and Event) and the other tables (Reference, Compiler, Geomorphic setting, Type of site, Type of evidence, Type of analysis and Dating).

2.2 Site table

The site information is organized in one main table (table 1) and in other four related tables (Compiler, Reference, Geomorphic setting and Type of Site). The Site table contains the following fields:

Site	
Field Name	**Description**
Site name	Provide name quoted in literature or, if none, provide a reasonable name from a nearby locality
Year of investigation (from; to)	The age range of investigation of the site
Country	Country of the site location.
Region	Region of the site location.
Province	Province of the site location.
Site Geometry	Point if are reported results obtained from an individual point (e.g. a core), Area if are reported results from different observational points (e.g. several cores). When "Area" is selected the maximum extension of the area (radius in meters) is also reported.
Latitude	Provide Latitude in degrees expressed as a decimal fraction (i.e., 00.0000°); north is positive value.
Longitude	Provide Longitude in degrees expressed as a decimal fraction (i.e., 00.0000°); east is positive value.
Datum	Provide the kind of datum: ED50, ETRF89, Roma40 or WGS84
Elevation	Elevation in meters of the site above (positive value) or below (negative value) the present sea level.
Elevation type	GPS or Topographic map.
Distance	Maximum distance in meters of the site from the present shoreline.
Time all	Maximum age of the observed sequence (Yr BP).
Number of Events	The number of tsunami events recognized in the site.
Site description	The field provides a narrative on the site.
Site Notes	The field provides necessary data for the site description.

Table 1: List and description of all fields contained in the Site Table.

The Compiler table (table 2) archives the contact information of each compiler (Name, Surname, Affiliation, Acronym and Email). The Reference table (table 3) archives the full reference of the published paper or official report, and includes the following fields: Authors, Title, Publication, Volume, Issue, Total number of pages, Year of publication, DOI, URL, Contact Name, Contact email. The Geomorphic settings table (table 4) contains the information on the geomorphic settings

of each site (Area protected by coastal dunes, Coastal lake, Coastal marsh, Estuary, Fluvial plain, Offshore, Rocky coast and Other). The Type of site table (table 5) defines the type of investigation adopted at the site (Artificial cut, Coast, Engine core, Exploratory trench, Hand core, Natural exposure and Other).

Compiler

Name
Surname
Affiliation
Acronym
Contact Email

Table 2: The "compiler" table archives the contact information of database compiler.

References

Authors
Title
Publication
Volume
Issue
Pages
Year
Doi
URL
Abstract
Contact
Contact Email

Table 3: The "reference" table provides the full references of the published paper or official report.

Geomorphic setting

Area protected by coastal dunes
Coastal lake
Coastal marsh
Estuary
Fluvial plain
Offshore
Year
Doi
Rocky coast
Other

Table 4: The "Geomorphic setting "table provides the geomorphic setting of the site where a paleotsunami deposit was recognized.

Type of Site

Artificial cut
Coast
Engine core
Exploratory trench
Hand core
Natural exposure
Other

Table 5: The "Type of site" table provides the type of investigation adopted to explore the site.

2.3 Event table

The events information, as for the site description, is organized in one main table (table 6), and in other three related tables (Type of evidence, Type of analysis, and Dating). The Event table contains the following fields:

Event	
Field Name	**Description**
Depth	The depth of the tsunami deposit in meters with respect to the present ground surface / sea bottom.
Thickness or dimension	The max value in meters of a tsunami layer or the max axis for blocks.
Evidence description	Free narrative on the process followed for the recognition of the tsunami deposit.
Lab Youngest Age (LYA)	Numeric value of the youngest laboratory age as yr BP (before present).
LYA standard deviation	Error of the laboratory radiocarbon age.
Youngest calendar age (Min and Max)	The youngest age as yr AD/BC (yr AD positive values and yr BC negative values). The field reports the dendrochronologically corrected age for Radiocarbon, historical/archaeological estimates.
Lab Oldest Age (LOA)	The numeric value of the oldest laboratory age as yr BP (before present).
LOA standard deviation	Error of the laboratory radiocarbon age.
Oldest calendar age (Min and Max)	The oldest age as yr AD/BC (yr AD positive values and yr BC negative values). The field reports the dendrochronologically corrected age for Radiocarbon, historical/archaeological estimates.
Preferred Age (Min and Max)	The minimum and maximum preferred ages for the tsunami (yr AD positive values and yr BC negative values).
Historical Age	Year of a potential tsunamigenic earthquake/landslide/eruption occurred within the interval of the time defined for the tsunami (yr AD positive values and yr BC negative values).
Event description	Short discussion about the type of dated materials (if marine, it is should be specify the Delta R), the position with respect to the tsunami deposit to be dated, pertinent problems and any information that is considered as relevant.
Event notes	This field reports necessary data for the event description.

Table 6: Fields and their relative description contained in the Event table.

The data archived in the other related tables provide information about the type of evidence of the tsunami (table 7), the type and number of analyses supporting the interpretation (table 8) and the dating method adopted to constrain the tsunami deposit age (table 9).

Type of evidence	
Geomorphology	
Sediment	
Transported Blocks	
Other	

Table 7: The “Type of evidence” table provides the type of tsunami deposit recognized

Type of Analysis	
Environmental	
Geochemical	
Magnetic	
Micromorphological	
Paleontological	
Sedimentological	
X-ray	
Other	

Table 8: The “Type of Analysis” table provides the type of analysis that supported the tsunami origin of the deposit

Dating	
Archaeological	
Cs137	
OSL	
Paleontology	
Palynology	
Pb210	
Radiocarbon	
Sedimentation rate	
Tephrachronology	
Thermoluminiscence	
Other	

Table 9: The “Dating” table provides the type dating method adopted in order to obtain a tsunami deposit age range.

3. The ArcGIS Online portal

ArcGIS Online by ESRI Inc. is a portal built to create and to share maps on the web. This collaborative web GIS hosts the Astarte Paleotsunami Deposits database – NEAM region at the URL http://arcg.is/00jWTv, which can be freely queried and explored by any ArcGIS Online user. The GIS can be accessed also from the ArcGIS Online site www.arcis.com, tab Gallery, using the keywords Astarte and Paleotsunami in the Search box.

The display area (fig. 5) of the Astarte paleotsunami deposits web map shows a world basemap powered by ESRI, where each feature represents the site where at least one paleotsunami deposit was recognized. The map can be easily zoomed and navigated using the navigation tools on the interface.

The area on the left of the web map, the table of contents, contains three tabs: About, Content and Legend.

The Content tab shows all the objects stored in the database. The first occurrence is the Site layer, symbolized with a yellow star. The other objects are the related tables (Compiler, Event, Geomorphic setting, Reference, Type of analysis, Type of evidence, Type of site and Dating).
The About tab shows the metadata of the web map, like the technical details of the database, a brief description, the type of license, the authors, etc.
The Legend tab shows only the feature layers included in the web map.

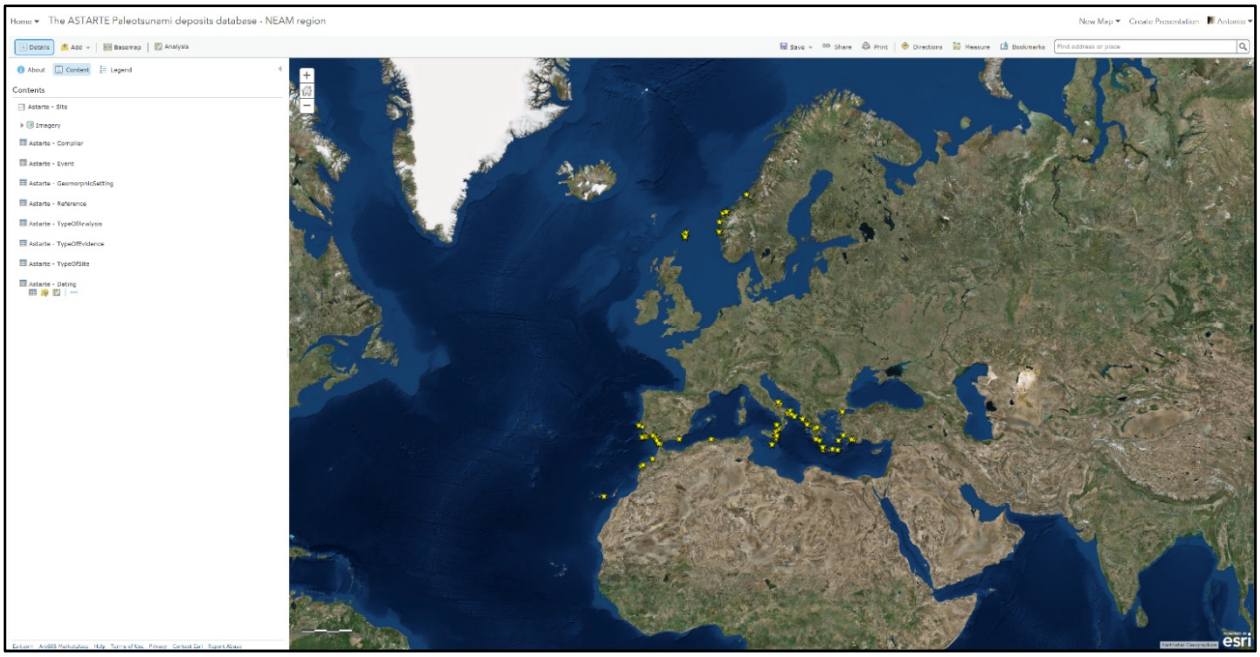

Fig 5 - The ArcGIS Online web map of the Astarte Paleotsunami deposits database – NEAM region. The yellow stars, plotted on a world imagery basemap, represent the site where at least one paleotsunami deposit was recognized. In the table of contents all the tables that make up the database scheme are shown.

The user can also display the information of each site by clicking directly on each yellow star symbol. The attribute table of the selected site opens and from this pop-up window it is possible to navigate to all the other related tables (fig. 6).

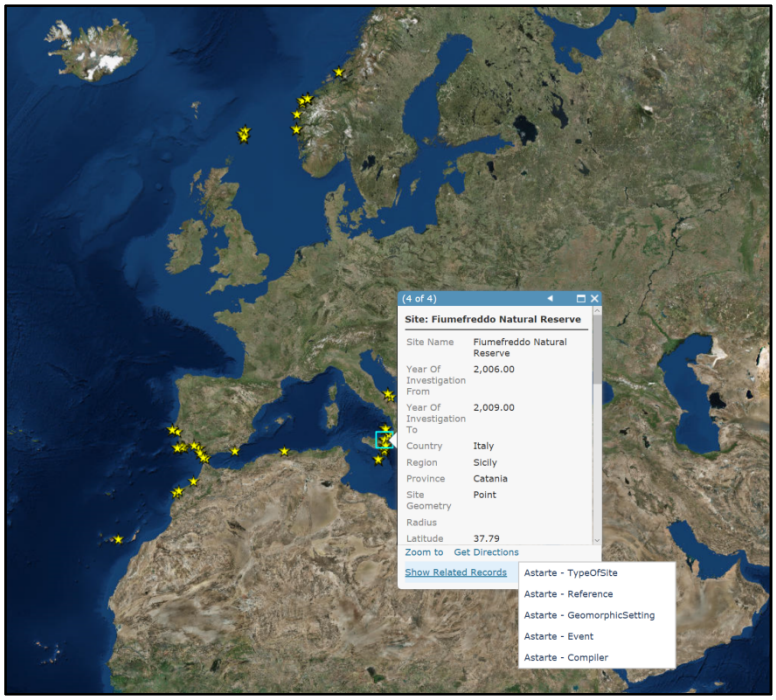

Fig. 6 – The attribute table of the Site layer with the option to navigate to the other related tables.

ArcGIS Online allows also the applying of a filter on a table in order to view only the information that satisfies one or more conditions. If the user applies a filter on the feature layer Site (fig. 7), the map will display only the sites that satisfy the query (fig. 8). If the user applies a filter on a related table, the table will show only the records that satisfy the expressions applied.

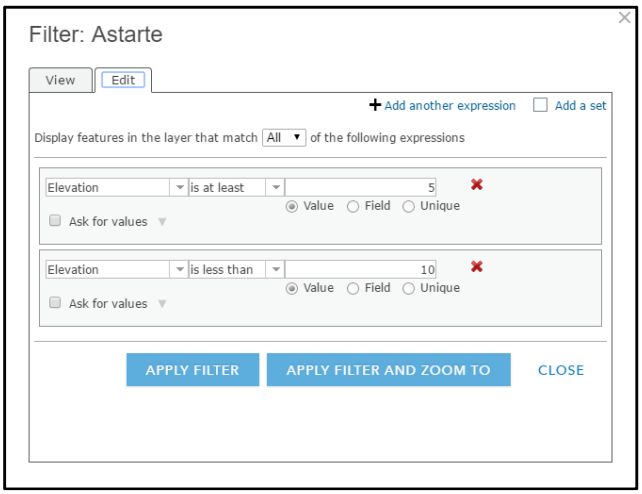

Fig. 7 – Example of a filter with two expressions applied to the Site layer.

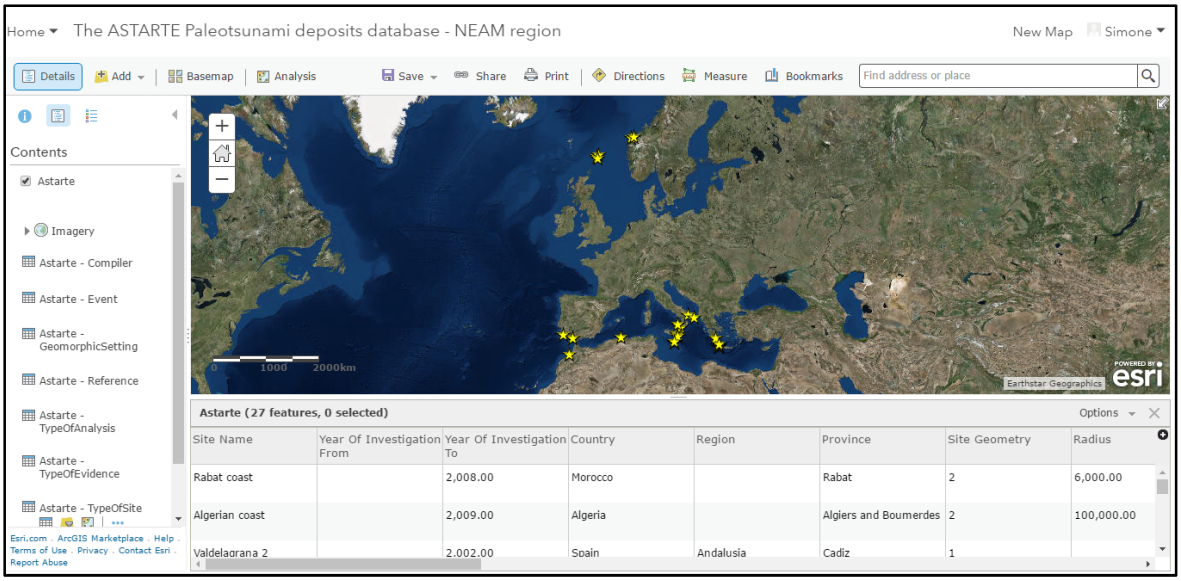

Fig. 8 – Result of the filter shown in Fig. 7 and applied to the Site table. The map shows only the sites with an elevation between 5 and 10 meters.

Any user has also the possibility to register on the ArcGIS Online portal (www.arcgis.com), receiving further benefits, for example the possibility to export data in several formats, like shapefile, CSV, FGDB, GeoJSON, and Feature Collection.

4. Statistics and discussion

ArcGIS Online provides several tools for spatial analysis and for performing basic descriptive statistics of features and their attributes. The following histograms and pie diagrams (figs. 9 – 10 – 11 – 12 – 13 – 14) show the statistics of the most significant fields of the Site and Event tables. These fields contain the information that can better characterize a site or an event.

The histograms shown in this paragraph as well as the pie diagrams were created using Microsoft Excel. ArcGIS online provided only the numerical statistic values, except for the median that was obtained from Microsoft Excel.

Site

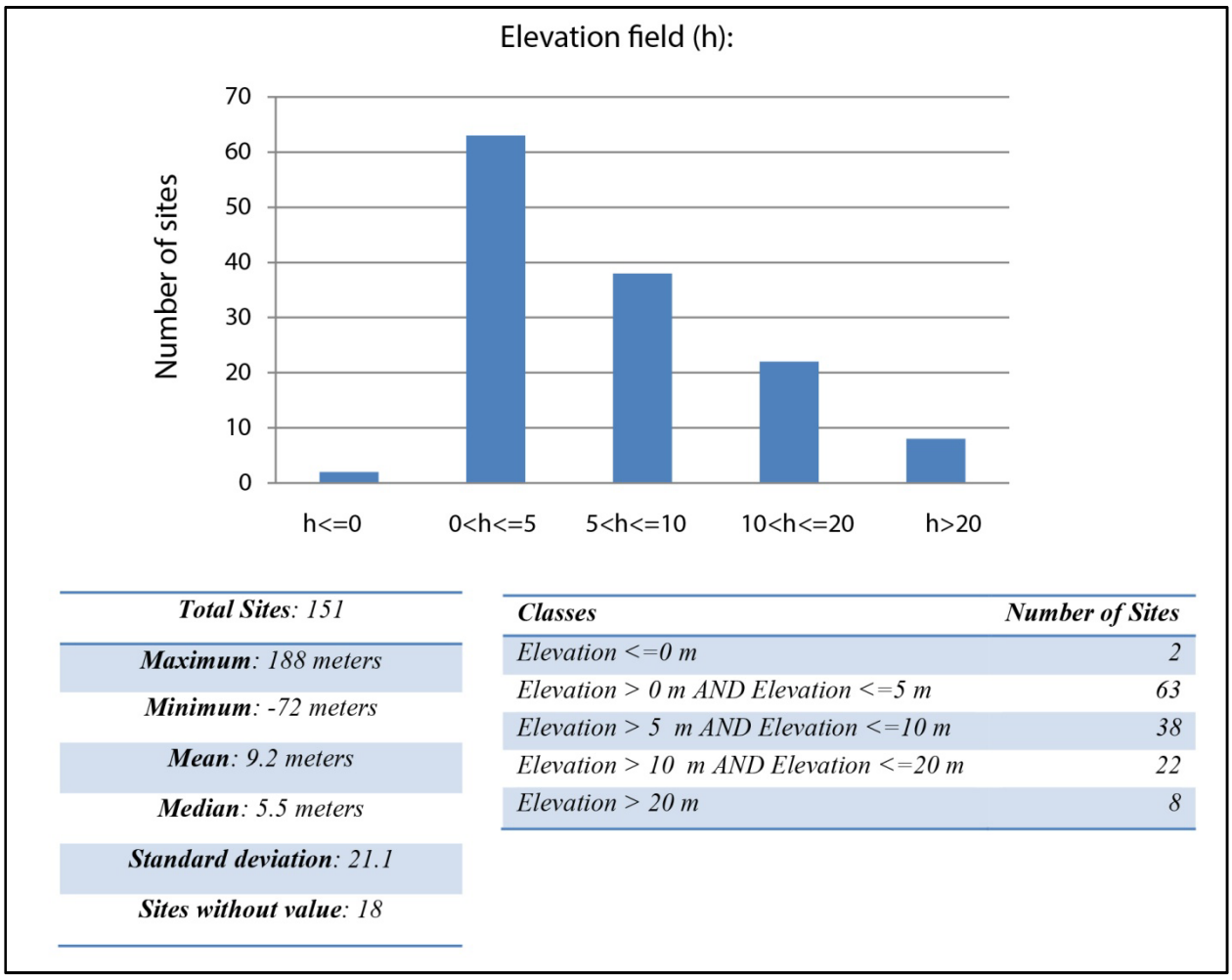

***Total Sites**: 151*
***Maximum**: 188 meters*
***Minimum**: -72 meters*
***Mean**: 9.2 meters*
***Median**: 5.5 meters*
***Standard deviation**: 21.1*
***Sites without value**: 18*

Classes	*Number of Sites*
Elevation <=0 m	*2*
Elevation > 0 m AND Elevation <=5 m	*63*
Elevation > 5 m AND Elevation <=10 m	*38*
Elevation > 10 m AND Elevation <=20 m	*22*
Elevation > 20 m	*8*

Fig. 9 - The histogram shows the distribution of the sites in relation to their elevation above the sea level. All elevations are referred to the present sea-level and all the data are provided by the authors, not calculated or derived. The related tables reports the five classes choose to better represent the elevation value and the statistical values derived from the Elevation field. From a general point of view, it is possible to note that 50% of the sites are below 5 m a.s.l. and that only 23% of the sites are elevated above 10 m a.s.l.. In fact, highly elevated sites are difficult to be reached and they need very high waves, but the deposition and preservation of the deposits depend on their geomorphologic setting.

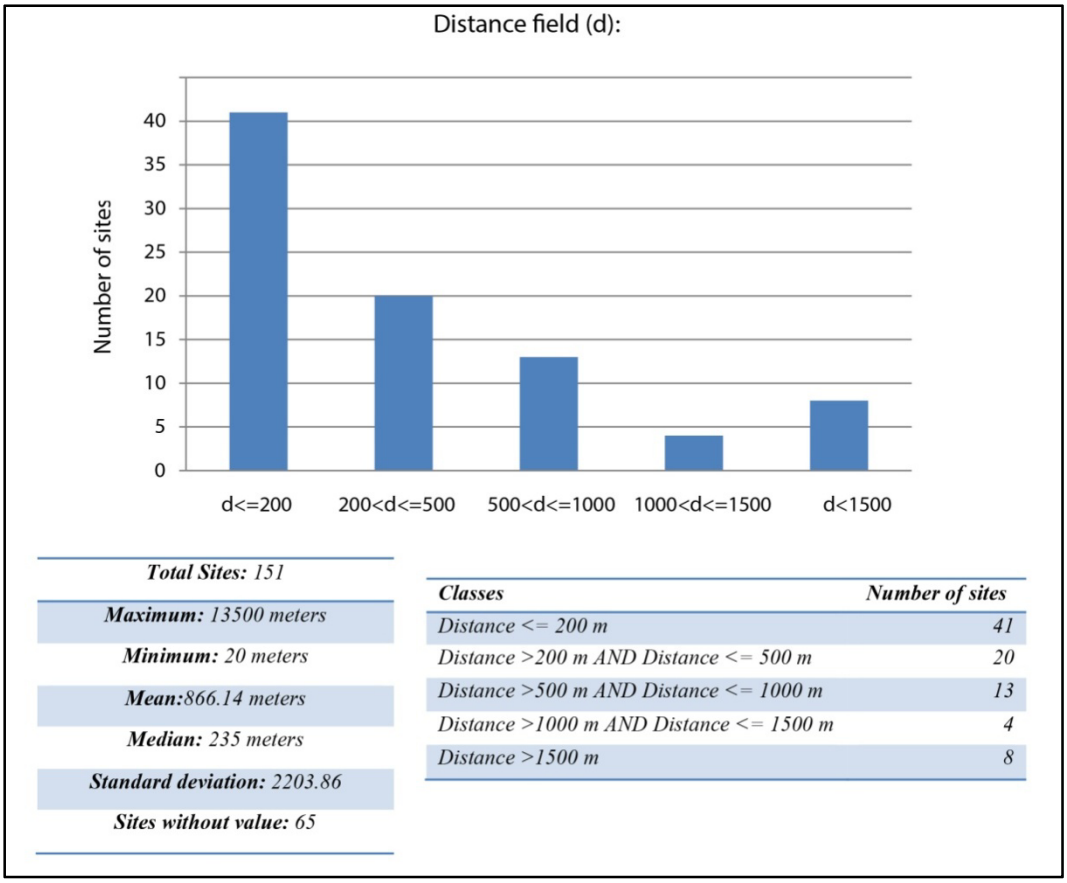

Total Sites: *151*
Maximum: *13500 meters*
Minimum: *20 meters*
Mean:*866.14 meters*
Median: *235 meters*
Standard deviation: *2203.86*
Sites without value: *65*

Classes	***Number of sites***
Distance <= 200 m	*41*
Distance >200 m AND Distance <= 500 m	*20*
Distance >500 m AND Distance <= 1000 m	*13*
Distance >1000 m AND Distance <= 1500 m	*4*
Distance >1500 m	*8*

Fig. 10 - The histogram shows the distribution of the sites in relation to their distance from the present shoreline. The related table reports the five classes choose to better represent the elevation value and the statistical values derived from the distance field. From a general point of view, it is possible to note that almost 50% of the sites are located within 200 m from the shoreline (notably the inundation limit of the storms; Morton et al., 2007) and that almost 30% of the sites are at distance greater than 0.5 km. Thus, even at long distances from the shoreline (more than 500 m) there are sites able to preserve “traces” of the tsunami inundation.

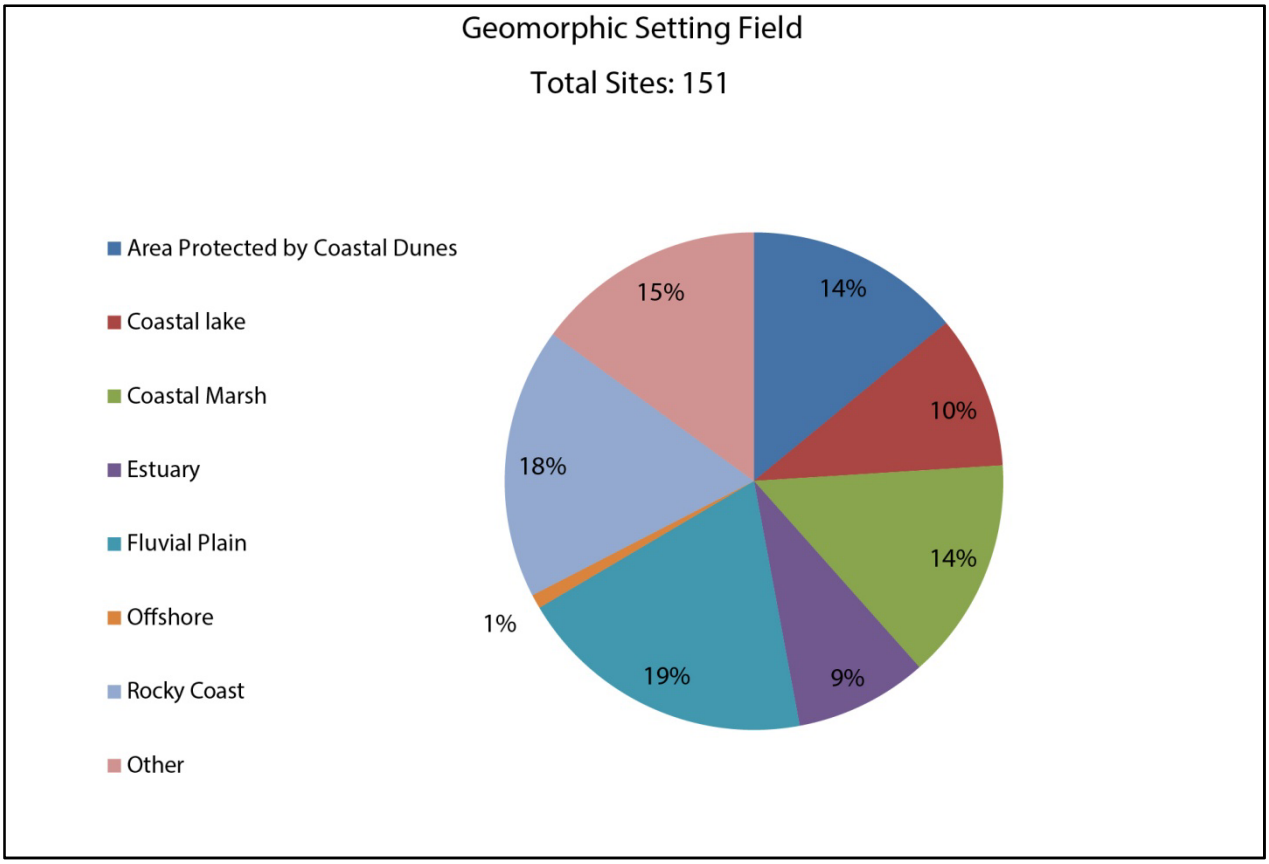

Fig. 11 - The pie diagram shows the geomorphological settings, divided according to their percentages, of all sites contained in the database. Note that each single site may have one or more geomorphic settings. It is possible to note that rocky coast and fluvial plains account almost 40 % of the total and that, from a general point of view, the proposed settings fit well with those investigated in the literature.

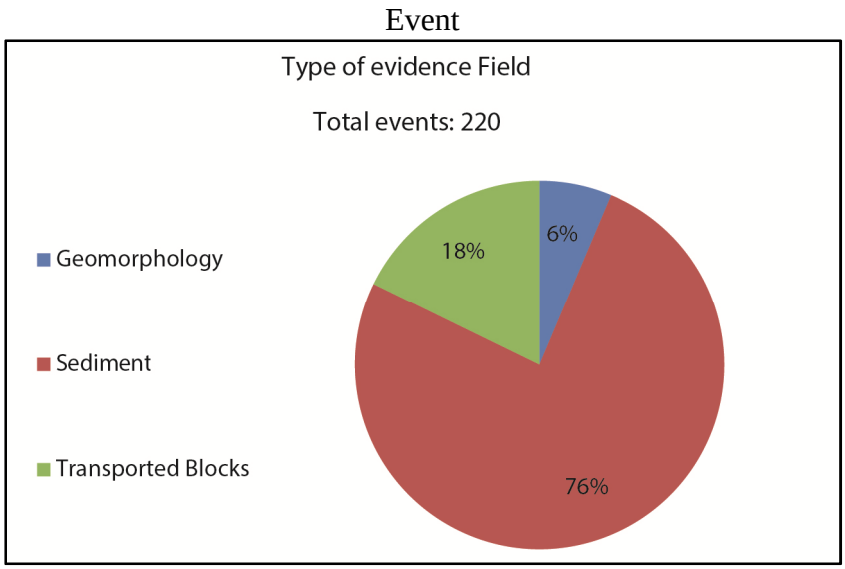

Fig. 12 - The pie diagram shows the different kinds of paleotsunami evidence present in all events recorded in the database. Tsunami sediments dominates with more than 75% while the geomorphic imprint of a paleotsunami is not an easy task to achieve.

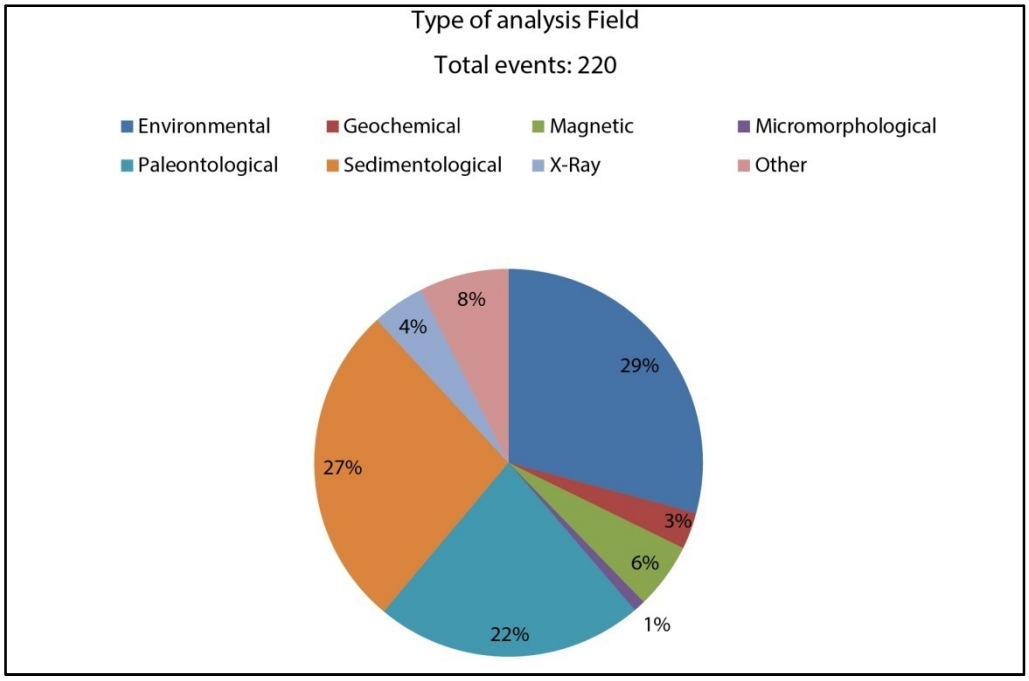

Fig. 13 - The pie diagram shows the distribution of the different approaches used to support the tsunami interpretation in all 220 events recorded in the database. It is possible to see that only the environmental, sedimentological and paleontological analyses are commonly used.

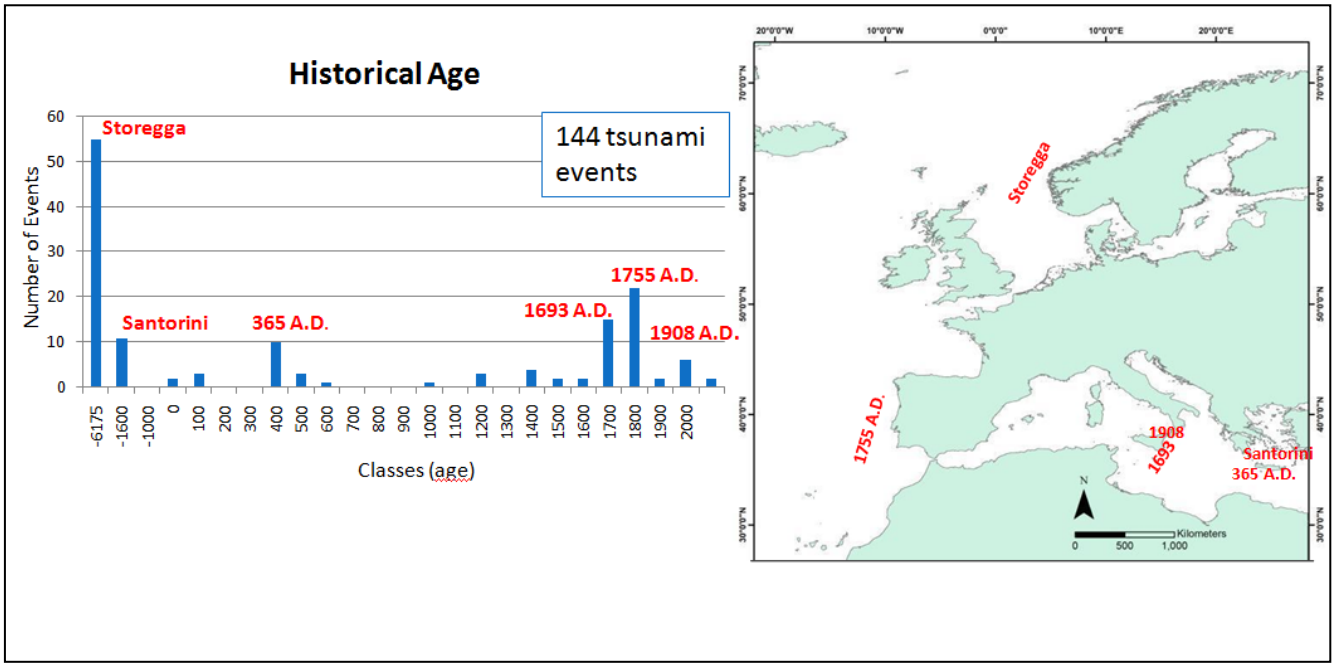

Fig. 14 - The histogram shows the distribution of the historical ages potentially related to 144 tsunami events recorded in the databases. Some of the main known tsunami events are directly related to the main peaks of the histogram. These events are reported in the histogram as well as in a map.

The database contains 151 individual sites with at least one paleotsunami deposit evidence. In specific, 220 tsunamis evidence (220 events) are recorded in the database. The statistics analysis applied to the elevation, distance and geomorphic setting site fields can be summarized as follow:

The coastal geomorphic setting of sites (fig. 11) may be divided in three categories: the first one includes all coastal settings characterized by a low energy sedimentation (e.g. coastal marsh, coastal lake). The second category covers those coastal settings characterized by estuary and by fluvial plain where the sedimentation environment could have been affected by continental high energy events due to the presence of paleo and actual fluvial systems. Most of fluvial plain settings, recorded in the database, is characterized by abandoned plains where fluvial processes didn't affect the sedimentation in recent time, favoring the preservation of tsunami sediment layers. The third and last category includes all site settled on rocky coasts.

The height of sites above the sea level (fig. 9) may be considered as a minimum run up value. This value is assumed to be "minimum" since the Holocene sea level was never higher than today (Fleming et al., 1998). Thus, a tsunami wave can reach sites located even farer inland (e.g. the 2011 Tohoku tsunami in the Sendai plain; Szczuciński et al., 2012), but without leaving a "signature" able to be preserved for long time (Szczuciński et al., 2012). On the base of the heights histogram (fig. 9), it is possible to approximate that 50% of the sites are below 5 m a.s.l. and that 23% of the sites are elevated above 10 m a.s.l. This classification perfectly reflects the site coastal settings; in fact, most sites are located in areas characterized by specific geomorphological setting (coastal marsh, lakes, fluvial plain, estuaries, back dune environment) which rarely tend to overcome 10 m a.s.l. Most of sites that exceed an elevation a.s.l. of 10 meters are located along the coast of the Norway, where the main historical tsunami event was attributed to the Storegga tsunami (dated about 8150 BP, Bondevik et al., 2012). These elevation values cannot be considered "real" since Bondevik et al., (1997) suggest that the relative sea level was higher than today because of the well known glacial unloading effect since the LGM (Last Glacial Maximum about 20 Ka, Clark et al., 2009) that uplifted most of the sites investigated in Norway.

The distance of the sites compared to the actual coastline (fig. 10) represents the maximum distance where the tsunami deposit was found. This value can be interpreted as the minimum inundation distance reached by the tsunami wave. It is possible to generalize that about half of the sites have a distance from the present shoreline <= 200 meters that represents the storms inundation limit (Morton et al., 2007) while 14% of the sites have distances > 1000 meters. Moreover, from a general point of view, we can assert that all sites, where the tsunami evidence is characterized by boulder accumulations, have a distance from the present shoreline of maximum 100 meters (with few exceptions), as the wave energy is not sufficient to carry away large blocks. Differently, all

sites where sediment tsunami layers were detected and recognized, present a variable distance from the present shoreline, exceeding the kilometer. For example, vary flat coastal morphologies (low elevations above the present sea level) can be inundated for several hundred meters. In fact, the coastal lowland of Pantano Morghella site, (Sicily, southern Italy) shows a maximum inundation distance of 1200 meters from the present coastline (Gerardi et al., 2012).
In the event table the most considerable field to analyze is the type of evidence (fig. 12). It provides the kind of geological evidence left by the tsunami wave onshore and offshore. 76 % of the deposit is represented by sediment, 18 % by transported blocks and only 6% by geomorphological signatures. This reflects the geomorphic setting noticed in the sites. In fact, a sediment deposit can be clearly recorded and preserved in a stratigraphic sequence of a coastal lake, coastal marsh, estuary or fluvial plain. Differently, transported blocks can only be observed along rocky coasts (that represent only 18% of geomorphic setting) like marine terraces gentle sloping toward the sea. Finally, it is possible to note that geomorphological evidence of paleotsunami are very rare (only 6%). This could be attributed to the difficult of preservation and recognition of morphological signatures left by a prehistorical/historical tsunami, especially because coastal geomorphological processes are able to erase old geomorphological tsunami signatures. For example, a coast under erosion will very hardly preserve geomorphological record of past tsunamis (Goff et al., 2007). Differently a prograding coast has a good chance to preserve the geomorphological tsunami signatures (Goff et al., 2007).

Querying the database, it was also possible to deduce the main approaches adopted in order to identify and characterize a tsunami deposit (fig. 13). From the analysis shown in pie diagram it emerged that environmental considerations together with paleontological and sedimentological analyses are the most used approaches. In fact, the most common tsunami layer differs from the underlying and overlying sediments because of its paleontological content mainly made of marine components and its granule dimension. The major part of tsunami deposit represented by sediments are characterized by a single sandy layer or by few sandy layers separated by mud laminations with an erosive contact at the base and a thickness generally less of 25 cm (Morton et al., 2007). The structure can be massive or normal graded fining upward (the inverse grading is rare) (Morton et al., 2007). Moreover, tsunami sediments may have also an important part of organic remains and fossils from offshore, such as foraminifera, diatoms, fragments of corals and bivalves (Morton et al., 2007).
144 tsunami events (among 220 in total) showing dating information are potentially correlated to a historical event (fig. 14). On the base of the dating constraints, the events can be summarized in

three distinct groups: the first one includes all tsunami occurred from 4000 BP to the present, the second group shows all sites affected by tsunami older than 4000 BP and a final group that includes all undated deposit or not correlated to any historical event. This distinction is well appreciable in the geographical distribution of tsunami deposits (fig. 14). In fact, paleotsunami deposits found in the Mediterranean Sea are all younger than 4000 BP (except 2 deposits related to an event potentially related to the 5000-years BP tsunami generated by the partial collapse of the modern Sciara del Fuoco; Tanner et al., 2004) while the oldest tsunami deposits are located in the Atlantic Ocean (e.g. an old event found at Canary Islands (Torrado et al., 2006) or the Storegga tsunami (Bondevik et al., 1997; Smith et al., 2004)). This is mainly due to the difficulty of preserving traces of the old events in coastal settings. In this context, it is very appreciable to note the distribution of the historical ages potentially related to 144 tsunami events recorded in the databases. Some of the main known tsunami events are directly related to the main peaks visible in the histogram (fig. 14). In detail, it is possible to note that the north-east Atlantic is characterized by two main events: the Storegga Slide tsunami occurred about 8150 years BP (Bondevik et al., 2012) and the 1755 Lisbon tsunami (NOAA/WDS tsunami database) that mainly hit the Portugal coasts. The Mediterranean Sea was especially affected by the 365 AD Crete tsunami and by the eruption/caldera collapse of Santorini volcano (NOAA/WDS tsunami database). The other two peaks, related to the 1693 and 1908 events, represents the two biggest known events occurred in Ionian Sea that struck the coasts of eastern Sicily (Italy) (De Martini et al., 2012; NOAA/WDS tsunami database).

4.1 A focus on Italy

At Italian level, all paleotsunami deposits are concentrated in the southern Italy. In detail, the regions of Apulia and Sicily host 25 sites with a total of 57 geological evidence of tsunami. As in the previous statistics analysis, even for Italy, the elevation and distance field histograms are reported together with the type of evidence and the geomorphic setting pie diagrams (figs. 15 – 16).
From the elevation field (fig. 15), it is possible to note that most of Italian sites place within 5 meters above the present sea level, while 5% present heights > 10 meters above the present sea level. The distance field (fig. 15) shows that 55% of the analyzed sites are located within 200 meters from the present shoreline and 27% has values greater than 500 m. As previously mentioned, inundation distances that exceed 500 meters are related to very flat coastal morphologies where the sea wave, thanks to the available landward space and low elevations above the sea level, takes more time to dissipate its energy. Fluvial plains, lowlands, coastal marshes or lagoons are the best candidates to favor a very long tsunami inundation. Heights more than 5 meters above the sea level are often attributed to rocky coastal sites, where marine terraces host transported blocks. From the

elevation histogram (fig. 15) it is possible to note that one site has an elevation > 10 meters above the present sea level. This particular case is related to a tsunami sediment located on a flank of the Stromboli volcano (Eolie islands, Sicily) (Tanner et al., 2004).

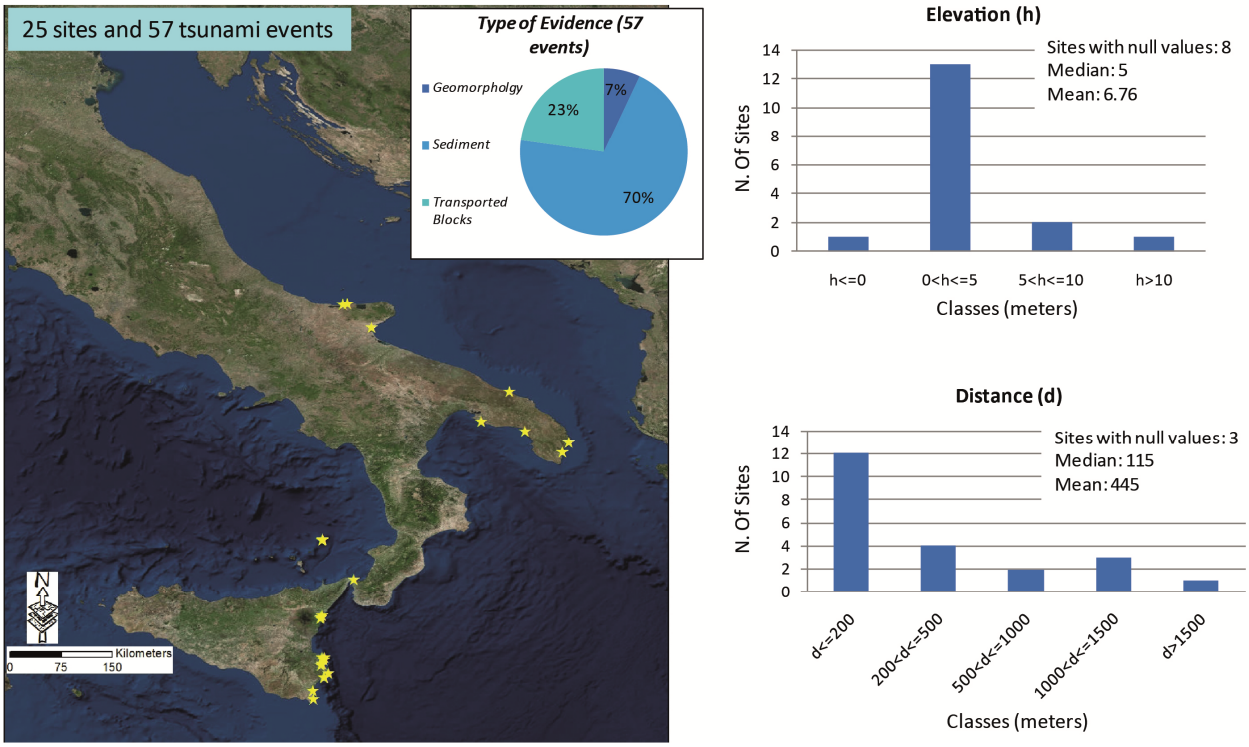

Fig. 15 – The map shows all Italian sites with at least one tsunami deposit evidence (25 sites and 57 tsunami events). The pie diagram (applied on all 57events) distinguishes the type of evidence, emphasizing a clear predominance of sediment layers. The histograms point out the relation between the sites and the corresponding distance from the present shoreline and height above sea level.

The database shows that most of paleotsunami deposits found along the coast of Italy are represented by sediment layers (70 %), followed by 23 % of transported blocks and 7% of geomorphological evidence. Even in this case, a solid relation between the type of evidence and the geomorphic setting exists. Taking into account that each site may have one or more geomorphic setting, from the figure 16 it is possible to note that coastal settings like marsh, lakes, fluvial plain, estuaries and back dune environment are suitable for the conservation and investigation of tsunami deposit represented by sediment and also by geomorphic features. Differently rocky coast are the most favorite settings for the detachment, transport and deposition of large boulders.

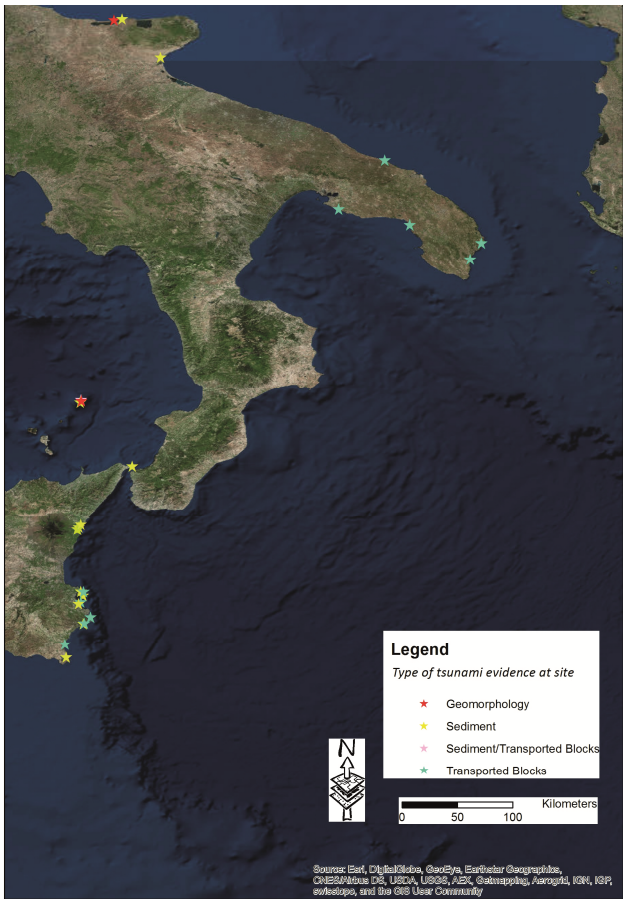

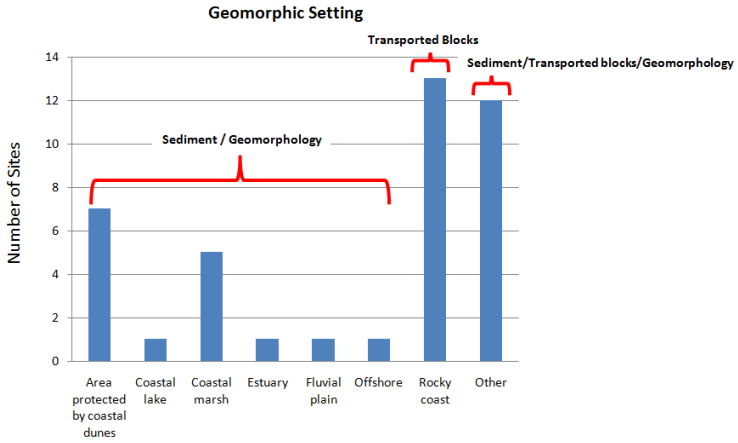

Fig. 16 - The map shows the type of paleotsunami geological evidence along the Italian coasts for each site. It is important to note that the symbols (colored stars) are referred to the sites and each site may have one or more associated paleotsunami deposit evidence (geomorphological evidence, sediment, transported blocks or a combination of them). The histogram shows the geomorphic setting of Italian sites in relation to the type of tsunami evidence (each site may have one or more geomorphic setting). Data for Italian coasts from: Barbano et al., 2009, 2010; De Martini et al., 2003, 2010, 2012; Gerardi et al., 2012; Gianfreda et al., 2001; Mastronuzzi et al., 2000, 2004, 2007, 2012; Pantosti et al., 2008; Scicchitano et al., 2007, 2010; Smedile et al., 2011; Tanner et al., 2004.

5. Conclusions

NEAM area

The collected and analyzed data for the NEAM can be summarized as follow:

- The Astarte Paleotsunami Deposits geodatabase – NEAM region contains 151 sites and 220 geological evidence of tsunami.
- The tsunami deposits are characterized by a predominance of sediment layers (76%), followed by transported blocks (18%) and geomorphological signatures (6%).
- Actually, in the geodatabase, 50% of the sites have an elevation above sea level within 5 meters while only 23 % of sites exceeds the value of 10 meters. In addition, about half of the analyzed sites have a distance from the present shoreline <= 200 meters (the storms inundation limit, Morton et al., 2007) and 14% of the sites overcomes 1000 meters. Very flat coastal morphologies, with low elevations above the sea level, are able to favor long inundation distances. Sites characterized by elevation > 10 a.s.l. are mainly located on rocky coasts, and volcano flanks. Moreover, there are several sites, with an elevation > 10 meters, located in Norway where the main tsunami event was attributed to the Storegga tsunami (dated about 8150 BP, Bondevik et al., 2012).
- From a scientific point of view, environmental, paleontological and sedimentological analysis seems to be the most resolute and used approaches in order to identify and characterize a tsunami deposit.

Italy

The collected and analyzed data for the Italy can be summarized as follow:

- At national level, all sites, where tsunami deposits were recognized so far, are located along the coasts of Sicily and Apulia regions (Southern Italy).
- The southern Italy presents 25 sites and 51 events, where 70 % of tsunami deposits is represented by sediment layers
- Most of run-up values (from the elevation of paleotsunami deposits) are within 5 meters above sea level. Note that 5% of the sites have an elevation > 10 meters.
- 55% of inundation distances are within 200 meters while 27% overcomes values of 500 meters. Very flat coastal morphologies (e.g. the Pantano Morghella site located in the southern east Sicily) are able to favor long inundation distances.

Data from elevation and distance fields (obtained from all NEAM sites) may be considered as minimum run-up heights and minimum inundation distances since we know that the Holocene sea level was never higher than today (Fleming et al., 1998). Therefore, a tsunami wave can reach sites located even farer inland but without leaving a ”signature” able to be preserved for long time (Szczuciński et al., 2104). These minimum values might define spatial limits of a future tsunami inundation. More in detail, a possible application of these values could be placed in tsunami simulations in order to have a minimum constraint to be inserted into the inundation models. In addition, this kind of data could be used as a benchmark even just to make a comparison between the geological data (heights and distances derived from deposits) and modeled inundations (from tsunami simulations). The use of the tsunami deposits spatial distribution was recently applied in several studies. For example, Sawai et al. (2012) modeled the 869 AD Jogan tsunami and compared the inundation results with the inundation areas obtained from mapping and distribution of the Jogan tsunami deposit in the Sendai plain. Butler et al., (2014) instead, set tsunami simulations on Makauwahi sinkhole (Island of Kaua‘I, Hawaii Islands) taking into account the spatial distribution of paleotsunami deposits. Results indicated that a giant earthquake in the eastern Aleutian Islands circa 1425–1665 AD created the paleotsunami deposit in Kaua‘i. Moreover, Jaffe et al., (2012) modeled sandy tsunami deposits near Sendai Airport using an inverse sediment transport model to investigate the spatial and temporal variation of tsunami flow speed in the 11March 2011 Tohoku-oki tsunami. The application of the inverse model procedure was complicated since results obtained were strongly dependent on the choice of Manning's n roughness coefficient.

Therefore, paleotsunami deposits, in the context of inundation modeling can be used either directly applying an inverse model and indirectly as benchmarks to be compared with modeling results.

This work will be submitted to Marine Geology:

The ASTARTE Paleotsunami Deposits data base –web-based references for tsunami research in the NEAM region (Paolo Marco De Martini, Simone Orefice, Alessandra Smedile, Antonio Patera, Raphael Paris, Pedro Terrinha, James Hunt, Gerassimos Papadopoulos, Daniela Pantosti, João Noiva, Ioanna Triantafyllou and Ahmet C. Yalciner).

References

Barbano M.S., De Martini P.M., Pantosti D., Smedile A., Del Carlo P., Gerardi F., Guarnieri P., Pirrotta C., (2009). In Search of Tsunami Deposits Along the Eastern Coast of Sicily (Italy): The State of the Art. Recent Progress on Earthquake Geology, chapter 5. ISBN: 978-1-60876-147-0 Nova Science Publishers, Inc.

Barbano M.S., Pirrotta C., Gerardi F., (2010). Large boulders along the south-eastern Ionian coast of Sicily: Storm or tsunami deposits?. Marine Geology, 275, 140 – 154.

Beccari B., (2009) Measurements and impacts of the Chilean tsunami of May 1960 in New South Wales, Australia. Report, NSW State Emergency Service, File no. 08/0576.

Bondevik S., Stormo S.K. & Skjerdal G.(2012). Green mosses date the Storegga tsunami to the chilliest decades of the 8.2 ka cold event. Quaternary Science Reviews, 45, 1–6.

Bondevik S., Svendsen J.I., Johnsen G., Mangerud J. & Kaland P.E. (1997). The Storegga tsunami along the Norwegian coast, its age and run-up. Boreas, 26, 29–53.

Butler R., Burney D., Walsh D., (2014). Paleotsunami evidence on Kaua‘i and numerical modeling of a great Aleutian tsunami. Geophysical Research Letters, 41, 19, 6795 – 6802. DOI: 10.1002/2014GL061232

Clark P.U., Dyke A.S., Shakun J.D., Carlson A.E., Clark J., Wohlfarth B., Mitrovica J.X., Hostetler S.W., McCabe A.M., (2009). The Last Glacial Maximum. Science, Vol. 325, Issue 5941, pp. 710-714. DOI: 10.1126/science.1172873

Costa P.J.M., Dawson S., Quintela M., Andrade C., Milne F., Dourado F. and Dawson A. (2016). Tsunami Deposits Database – Retrieved from http://tsunami.campus.ciencias.ulisboa.pt/.

De Martini P.M., Barbano M.S., Pantosti D., Smedile A., Pirrotta C., Del Carlo P., and Pinzi S. (2012). Geological evidence for past-tsunamis along eastern Sicily (Italy): an overview, Nat. Hazards Earth Syst. Sci., 12, 2569-2580, doi:10.5194/nhess-12-1-2012.

De Martini P.M., Barbano M.S., Smedile A., Gerardi F., Pantosti D., Del Carlo P., Pirrotta C., (2010). A unique 4000 year long geological record of multiple tsunami inundations in the Augusta Bay (eastern Sicily, Italy). Marine Geology, 276, 42-57, doi: 10.1016/j.margeo.2010.07.005

De Martini P.M., Burrato P., Pantosti D., Maramai A., Graziani L., Abramson H., (2003). Identification of tsunami deposits and liquefaction features in the Gargano area (Italy): paleoseismological implication. ANNALS OF GEOPHYSICS, VOL. 46, N. 5.

De Martini P.M., Patera A., Orefice S., Paris R., Volker D., Lastras G., Terrinha P., Noiva J., Smedile A., Pantosti D., Hunt J., Gutscher M.A., Migeon S., Papadopoulos G., Triantafyllou I., Yalciner A.C., (2017). The ASTARTE Paleotsunami and Mass Transport Deposits databases – web-based references for tsunami and submarine landslide research around Europe. Geophysical Research Abstracts, Vol. 19, EGU2017-15055, 2017, EGU General Assembly 2017.

De Martini P.M., Orefice S., Smedile A., Patera A., Paris R., Terrinha P., Hunt J., Papadopoulos G., Pantosti D., Noiva J., Triantafyllou I., Yalciner A.C. The Astarte Paleotsunami Deposits data – web – based references for tsunami research in the NEAM region. Astarte project, Deliverable D2.44.

Fischer P., Finkler C., Robke B. R., Baika K., Hadler H., Willershauser T., Rigakou D., Metallinou G., Vott A., (2016). Impact of Holocene tsunamis detected in lagoonal environments on Corfu (Ionian Islands, Greece): Geomorphological, Sedimentological and microfaunal evidence. Quaternary International, 401, 4 – 16.

Fleming K., Johnston P., Zwartz D., Yokoyama Y., Lambeck K., Chappel J., (1998). Refining the eustatic sea-level curve since the Last Glacial Maximum using far and intermediate-fields sites. Earth and Planetary Science Letters 163, 327-342.

Gerardi F., Smedile A., Pirrotta C., Barbano M. S., De Martini P. M. ,Pinzi S. , Gueli A. M., Ristuccia G. M., Stella G., and Troja S. O., (2012). Geological record of tsunami inundations in Pantano Morghella (south-eastern Sicily) both from near and far-field sources. Nat. Hazards Earth Syst. Sci., 12, 1185–1200. doi: 10.5194/nhess-12-1185-2012.

Gianfreda F., Mastronuzzi G., Sansò P., (2001). Impact of historical tsunamis on a sandy coastal barrier: an example from the northern Gargano coast, southern Italy. Natural Hazards and Earth System Sciences (2001) 1: 213–219, ©European Geophysical Society 2001.

Goff J., Cain G., (2016). Tsunami databases: The problems of acceptance and absence. Geoforum, 76, 114 – 117.

Goff J., Chaguè – Goff C., (2014). The Australian tsunami database: A review. Progress in Physical Geography 2014 38: 218. DOI: 10.1177/0309133314522282.

Goff J.R., Hicks D. M., Hurren H. Tsunami geomorphology in New Zealand. A new method for exploring the evidence of past tsunamis. NIWA Technical Report 2007.

Historical Tsunami Database for the World Ocean (HTDB/WLD) (Version 3.0 of December 31, 2006). Tsunami Laboratory Novosibirsk (NTL). Institute of Computational Mathematics and Mathematical Geophysics of Siberian Division of Russian Academy of Sciences.

Jaffe B.E., Goto K., Sugawara D., Richmond B.M., Fujino S., Nishimura Y., (2012). Flow speed estimated by inverse modeling of sandy tsunami deposits: results from the 11 March 2011 tsunami on the coastal plain near the Sendai Airport, Honshu, Japan Sedimentary Geology 282, 90–109

Japan Tsunami Trace database (Tsunami trace height information). Disaster Control Research Center (DCRC), Graduate School of Engineering, Tohoku University Japan Nuclear Energy Safety Organization (JNES). http://tsunami-db.irides.tohoku.ac.jp/

Mastronuzzi G., Pignatelli C., (2012). The boulders berm of Punta Sa Guerra (Taranto, Italy): a morphological imprint of the Rossano Calabro tsunami of April 24, 1836? Earth Planets Space, 64, 10 829-842.

Mastronuzzi G., Pignatelli C., Sansò P., Selleri G., (2007). Boulder accumulations produced by the 20th of February, 1743tsunami along the coast of south eastern Salento (Apulia region, Italy). Marine Geology 242,191–205.

Mastronuzzi G., Sansò P., (2000). Boulders transport by catastrophic waves along the Ionian coast of Apulia (southern Italy). Marine Geology 170, 93-103.

Mastronuzzi G., Sansò P., (2004). Large boulder accumulations by extreme waves along the Adriatic coast of southern Apulia (Italy). Quaternary International, 120, 173 – 184.

Minuora K., Imamura F., Sugawara D., Kono Y., Iwashita T., (2001). The 869 Jogan tsunami deposit and recurrence interval of large-scale tsunami on the Pacific coast of northeast Japan. Journal of Natural Disaster Science, Volume 23, Number 2, pp83-88.

Morris M. K., Mazengarb C., (2009). Historical accounts of tsunamis in Tasmania. Tasmanian Geological Survey Record 2009/04. Department of Infrastructure, Energy and Resources, Mineral Resources Tasmania.

Morton R.A., Gelfenbaum G., Jaffe B.E., (2007). Physical criteria for distinguishing sandy tsunami and storm deposits using modern examples. Sedimentary Geology, 200, 184 – 207.

New Zealand Palaeotsunami Database. 2017. https://ptdb.niwa.co.nz [10/07/2017]

Pantosti D., M.S. Barbano, A. Smedile, P.M. De Martini and G. Tigano, (2008). Geological evidence of paleotsunamis at Torre degli Inglesi (northeast Sicily). Geophysical Research Letter, 35, L05311, doi: 10.1029/2007GL032935.

Pérez-Torrado F.G., Paris R., Del Carmen Cabrera M., Schneider J.L., Wassmer P, Carracedo J.C., Rodriguez-Santana A, Santana F. (2006). Tsunami deposits related to flank collapse in oceanic volcanoes: The Agaete Valley evidence, Gran Canaria, Canary Islands. Marine Geology, 227, 1-2, 135-149.

NGDC/WDS Global Historical Tsunami Database, 2100 BC to present. doi:10.7289/V5PN93H7

Scicchitano G., Costa B., Di Stefano A., Longhitano S.G., Monaco C., (2010). Tsunami and storm deposits preserved within a ria-type rocky coastal setting (Siracusa, SE Sicily). Zeitschrift für Geomorphologie Vol. 54, Suppl. 3, 051-077.

Scicchitano G., Monaco, C., and Tortorici, L., (2007). Large boulder deposits by tsunami waves along the Ionian coast of south-eastern Sicily (Italy). Mar. Geol., 238, 75–91.

Smedile A., De Martini P. M., Pantosti D., Bellucci L., Del Carlo P., Gasperini L., Pirrotta C., Polonia A., and Boschi E., (2011). Possible tsunamis signatures from an integrated study in the Augusta Bay offshore (Eastern Sicily–Italy). Mar. Geol., 281,1–13.

Sawai Y., Namegaya Y., Okamura Y., Satake K., Shishikura M., (2012). Challenges of anticipating the 2011 Tohoku earthquake and tsunami using coastal geology. GEOPHYSICAL RESEARCH LETTERS, VOL. 39, L21309, doi:10.1029/2012GL053692.

Soloviev S. L., Solovieva O. N., Go C. N., Kim K. S., and Shchetnikov N. A., (2000). Tsunamis in the Mediterranean Sea 2000 B.C.–2000 A.D. Kluwer Academic Publishers, Dordrecht, 237 pp.

Sugawara D., Goto K., Imamura F., Matsumoto H., Minoura K. (2102). Assessing the magnitude of the 869 Jogan tsunami using sedimentary deposits: Prediction and consequence of the 2011 Tohoku-oki tsunami. Sedimentary Geology, 282, 14 -26.

Szczuciński W., Kokociński M., Rzeszewski M., Goff C.C., Cachão M., Goto K., Sugawara D., (2014). Sediment sources and sedimentation processes of 2011 Tohoku-oki tsunami deposits on the Sendai Plain, Japan — Insights from diatoms, nannoliths and grain size distribution. Sedimentary Geology 282, 40-56.

Tanner L.H., Calvari S., (2004). Unusual sedimentary deposits on the SE side of Stromboli volcano, Italy: products of a tsunami caused by the ca. 5000 years BP Sciara del Fuoco collapse?. Journal of Volcanology and Geothermal Research 137, 329– 340.

The Euro-Mediterranean Paleotsunami Database (http://paleotsunami.rm.ingv.it/). TRANSFER project (Tsunami Risk AN Strategies For the Europen Region.

The New Zealand Tsunami Database: Historical and Modern Records, Natural Hazards Databases, GNS Science, Lower Hutt [07/05/2017].

Chapter 2

Searching for Paleotsunami deposits

The second part of my research activity is focused on the research inland of potential paleotsunami deposits, along the coasts of eastern Sicily. This work is the result of a collaboration between four researcher of the Istituto Nazionale di Geofisica e Vulcanologia of Rome (INGV): Paolo Marco De Martini, Alessandra Smedile, Stefania Pinzi and myself. In this context, my work gave a solid contribution to all phases that characterized this kind of research, with a particular emphasis on the geomorphological analysis. In detail, I contributed both to field activity (Identification of potential sites able to preserve paleotsunami layers and coring campaigns) and to laboratory analyses (Stratigraphical description, sampling phase, micropaleontological analysis and sedimentological analysis). Moreover, all geomorphological interpretations are the product of my studies and considerations.

1. Introduction

It is well known from several historical studies that the Eastern Sicilian coast is one of the Italian most prone areas to tsunami hazard based on recorded tsunami inundations caused both by regional earthquakes (1169, 1693, 1908) as well as by far field earthquakes such as the AD 365 Crete event (Maramai et al., 2014). From a geological point of view, several paleotsunamis have been recognized along the coast of eastern Sicily (De Martini et al., 2012 and references therein). In detail, 29 distinct tsunami deposits–related inundations were recognized in the field from Augusta-Priolo to Pachino (De Martini et al., 2017).

Geological evidence of paleo- tsunami can provide us a record extendible back in time for the past 4–5 ka, whereas the present coastline and the sea level were relatively stable since then (Fleming et al., 1998). The knowledge of the distribution and characteristics of tsunami deposits can help us to define a minimum observed inundation distance and run up height for a specific tract of coast and to assume where a future tsunami could occur. A deterministic approach aimed to recognize coastal areas hit by tsunami in the past and potential recurrence of these extreme events, is an important way (from a geological point of view) to contribute in the assessment of the risk with the evaluation of the inundation hazard (Mastronuzzi et al., 2013).

Paleotsunami deposits are the symbol of high energy events and, as mentioned in the general introduction, can be represented by coarse clastic deposits (ranging from large pebbles to boulders; Terry and Goff, 2014) or by looses sediments. Geological evidence of tsunami are also represented by geomorphological features as dune modifications or washover fans (Gianfreda et al., 2001; Goff et al., 2007).

Below, I report a list of the main geological and physical characteristics that can better characterize a tsunami deposit (Tuttle et al., 2004; Morton et al., 2007, Shiki et al., 2008; Goff et al., 2012):

- ✓ Particle/grain sizes of tsunami deposits range from fine mud to boulders. A tsunami will usually transport whatever size ranges are available—it is sediment source-dependent.
- ✓ Sediment thickness range from few centimeters to 25 – 30 centimeters.
- ✓ Sediments generally fine inland. Deposits generally rise in altitude inland and can extend for several km inland and tens or hundreds of kilometers along shore.
- ✓ Sediments often show a normal grading (fining upwards) or a massive structure. Inverse grading is rare.
- ✓ Each tsunami wave can form a distinct sedimentary unit and/or sub-units often intercalated by mud laminations. Mud laminations are related to the sediment transport, in fact they can settle down between successive tsunami waves or can be introduced as soil eroded from surrounded slopes by the return flow.
- ✓ The deposit can contain intraclasts (rip-up clasts) of reworked material and an important part of organic remnants and fossils from offshore, such as foraminifera, diatoms, fragments of corals and bivalves, often with a poor preservation state.
- ✓ From a general point of view, tsunami deposits may differ from the storm deposits in terms of thickness (larger for storms), grain size characteristics (storm deposits are better sorted) and internal structure (storm deposits are often laminated and may show foreset and cross – bedding sedimentary structures).
- ✓ The deposit is sometimes associated with loading structures at base and may be associated with liquefaction features on the ground surface caused by local earthquake shaking.
- ✓ The deposit may contains micro-scale features as micro-rip-up clasts, millimetre-scale banding, organic entrainment, fining-up sequences and erosive contacts that may be visible only in thin section.
- ✓ Measurement of anisotropy magnetic susceptibility (AMS) combined with grain size analysis provides information on hydrodynamic conditions ‘typical’ during tsunami deposition. Essential when no sedimentary structures are visible. Magnetic properties of minerals (inc. magnetic susceptibility) provide information about depositional environment.
- ✓ Heavy mineral laminations often present but source-dependent. Normally near base of unit/sub-unit but not always. Composition and vertical distribution of heavy mineral assemblage may change from the bottom to top of the deposit.

With the aim to find new areas hosting paleotsunami sediments, it was decided to look for new evidence of such deposits in some selected sites that were evaluated positive for their deposition, preservation and dating. A coastal site able to preserve paleotsunami sediments has to be

characterized by a low – energy sedimentation coastal environment, where past high-energy marine inundations may have been recorded by deposits left on the ground and preserved in the stratigraphical record. Moreover, sites of investigation have to be chosen with a distance from the present shoreline of at least 200 meters in order to exclude or to limit the influence of the storms (Nanayama et al., 2000; Goff et al., 2004; Tuttle et al., 2004).

Two sites, housing natural reserves, were selected and investigated along the coasts of eastern Sicily. The southernmost site is called Torre Barbagianni and it is located in the central part of the Vendicari natural reserve area while northward the one called Vigne, is actually the "backyard" of the old Siracusa salt-pan (fig. 1).

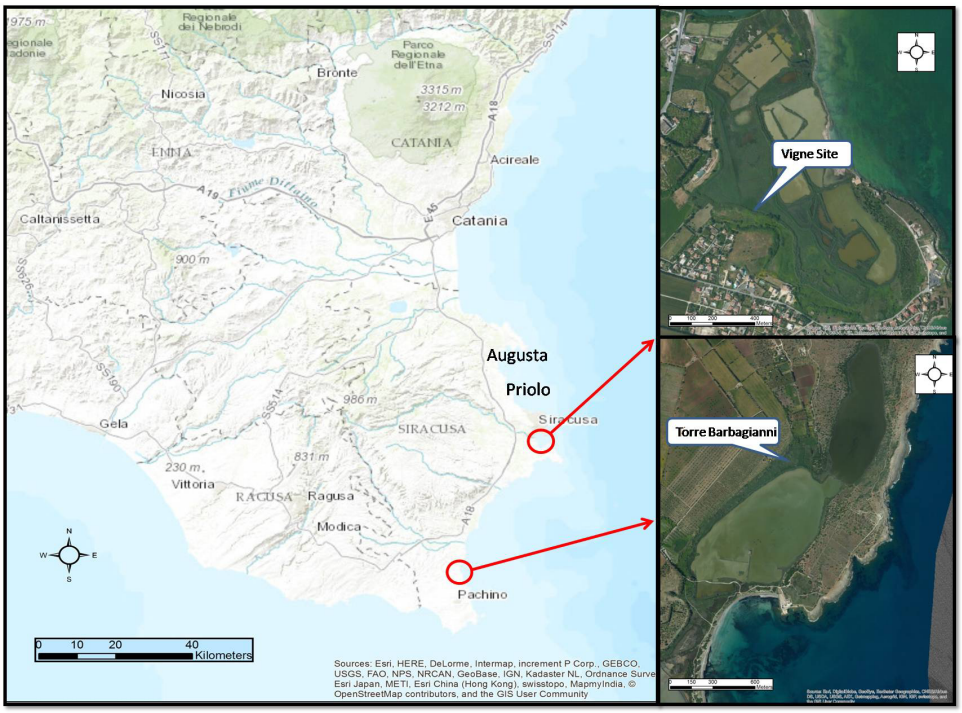

Fig. 1 - The figure shows the map of the eastern Sicily from Etna volcano (to the north) to Pachino town (to the south). The smaller maps represent the exact locations of the two selected and investigated sites: Vigne Site in the southernmost part of Siracusa town and Torre Barbagianni in the natural reserve of Vendicari (Maps from ESRI).

2. Methods

In the selected areas we carried out coring campaigns using a gasoline powered percussion hammer. Both open cores (windowed percussion gouge, which allows an immediate and direct observation of the sampled stratigraphy directly in the field) and closed PVC tubes were collected and localized by GPS measurement (fig. 2).

Detailed pictures of the sediments and quick stratigraphical description of each open core were performed directly in the field and once an interesting stratigraphic sequence was found, several long cores were collected in PVC tubes, each 1 m long. PVC cores were later opened in the

stratigraphic laboratory of INGV in Rome, in order to get several detailed photo shootings and to perform accurate stratigraphical, grain-size and textural descriptions.

A dedicated sampling procedure was set up for sedimentological and micropaleontological (foraminifera) analyses. Moreover, samples for AMS radiocarbon dating were collected on selected layers in order to constrain the age window of the whole stratigraphic record and of some specific layers. All these data were analysed and studied in order to better reconstruct the paleo-environmental evolution of the specific study sites and to identify, differentiate and characterize high-energy deposits of marine origin from the local low-energy sedimentation record.

Fig. 2 -The figure shows one of the several steps characterizing the extraction core-procedure. In detail, the operator drives the corer into the ground through the use of the percussion hammer.

2.1 Paleontological procedure

Micropaleontological analyses were carried out on 65 samples collected on all PVC studied cores. Collected samples were disaggregated using H_2O_2 and then washed on a 0.63 mm and 0.125 mm mesh sieves and dried. The dry residue was described under a stereomicroscope. An additional step was added on coarse deposits using a 0,5 mm mesh sieve in order to separate and better describe this latter fraction. Macro fossils specimens and grains were qualitatively analyzed in terms of taphonomic and morphoscopic characteristics. At least 100 benthic specimens were counted for each sample, where sufficient concentration was present, and they were identified at specific level. Conversely, the planktonic foraminifera that were simultaneously counted, were identified only at generic level due to their bad preservation grade. Classification, at genus level, was made according

to Loeblich and Tappan (1987), while species were determined according to major studies relative to the Mediterranean area (Cimerman and Langer, 1991; Sgarrella and Moncharmont-Zei, 1993). The whole paleontolongical assemblage was analysed by means of some key studies (Peres and Picard, 1964; Murray, 2006) in order to reconstruct the paleoenvironment of the collected sequences.

2.2 Sedimentological analysis

Sedimentological analyses were carried out on 12 samples collected on all studied PVC cores. All wet samples were weighted before being placed in a convection oven for 24 h at a temperature of 105^{o} C and re-weighted after drying, so to estimate the respective quantity of water.

Subsequently, they were disbanded in a solution of water and hydrogen peroxide and washed with distilled water in order to eliminate the content of organic matter.

The next step was to sift wet each sample with a sieve ASTM mesh 120 (125 μm) and dried again the obtained fractions.

Besides, the fractions >125 μm were dry sifted with sieve ASTM mesh 10, 18, 35, 60 (respectively 2000, 1000, 500, 250 μm) and each selected portion was weighted while the fractions <125 μm were analyzed with the optical grain-sizer LUMiReader, a multi-wavelength (870 nm, 630 nm, 470 nm) instrument, for the particle-sizing. LUMiReader employs the STEP-Technology, which allows obtaining space- and time-resolved extinction profiles over the entire sample length that can be recorded in user defined time. LUMiReader is able to measure grain size from 200 nm to 2 mm and analyzed samples with a grain size distribution from 500 nm to 300 μm.

Finally, the data yielded by the two different procedures were matched and elaborated in order to have a unique grain size distribution for each sample. The final results are plotted in histograms in which the ordinate axis represents the weight percentages and the abscissa axis represents the grain size in φ, see the Appendix at the end of this chapter for more details. In general, the results of the sedimentological analyses confirm the grain size evaluation done while making the log of the core and all the analyses done on samples are presented in the Appendix.

2.3 Radiocarbon dating

Radiocarbon dating by high-resolution mass spectrometry was performed at the Poznan Radiocarbon Laboratory (Poland) and at Beta Analytic Laboratory (London Bio Science Innovation Centre). Ten selected organic rich samples and charcoals were collected in order to constrain the age of the study sequences. C14 derived data include measured and calibrated ages according to Calib REV 7.10 by Stuiver and Reimer (1993) by using the intcal.13.14c calibration curve (Reimer et al., 2009).

3. Searching for paleotsunami deposits in the Vendicari Area

The study area is represented by a coastal lagoonal system located in the south-eastern portion of Sicily coast, exactly in the marine Reserve of Vendicari, about 30 km south of the Siracusa town. From a geological point of view, the Vendicari area is the emerged eastern part of the Hyblean foreland domain of the Apenninic Maghrebian Chain (Lentini et al., 1994; Lentini et al., 2006). The eastern Sicily, from Messina to the eastern flank of Mt. Etna, is characterized by the presence of NNE-SSW normal faults (mostly offshore) that join with the NNW-SSE Malta escarpment system to the south (fig. 3) (Pirrotta et al., 2013). The south-eastern edge of the Hyblean plateau is characterized by a coastal belt with carbonate rocks that form a gently sloping wave-cut platform occasionally characterized by the presence of cliffs and tight inlets (Barbano et al., 2010). Moreover, the platform, in some areas, shows fractures and an uplift related to a recent tectonic process (Barbano et al., 2010).

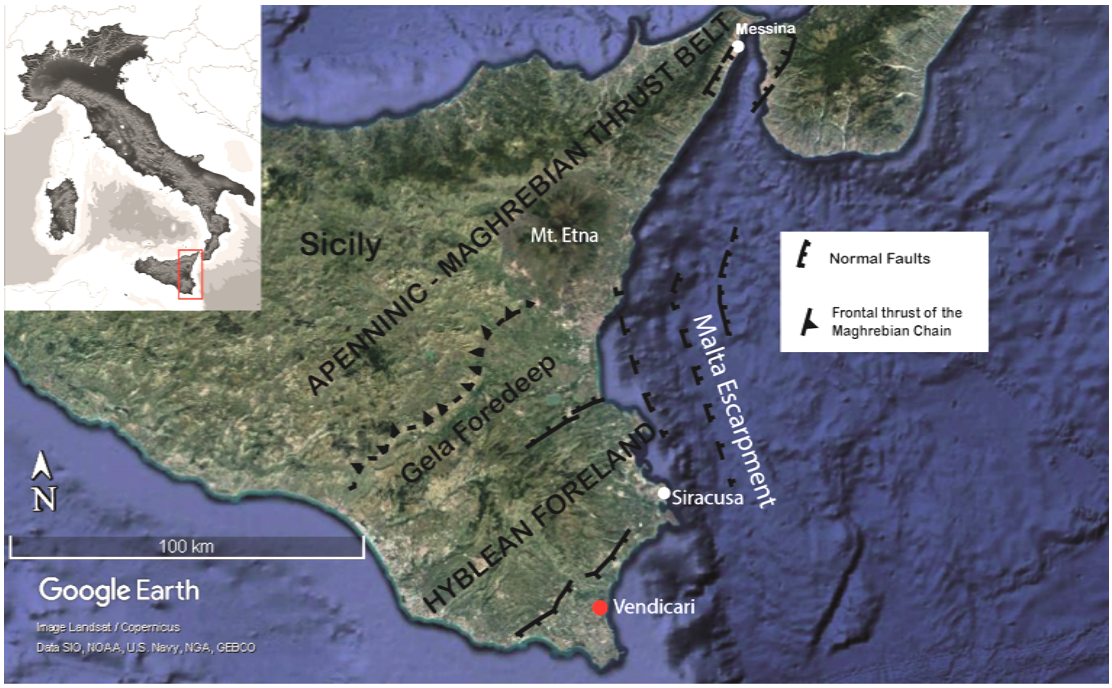

Fig. 3 - Map of Eastern Sicily showing the main structural domains and seismotectonic features: the Apenninic-Maghrebian Thrust Belt, the Hyblean Foreland affected by faults and bounded by the Malta Escarpment connecting the Hyblean Foreland to the Ionian Basin. The red dot displays the investigated area of Vendicari (Modified after Pirrotta et al., 2013).

Nowadays, the Vendicari lagoonal system stretched parallel to the coast for about 7 km (Amore et al., 1994) and is surrounded by a wave cut platform northward. The lagoonal system is characterized by the presence of three salt coastal lakes: Pantano Grande and Pantano Piccolo in the northern side and Pantano Roveto in the central and southern side. The two lagoons of Pantano

Grande and Pantano Piccolo are separated from the sea by a wave-cut platform that reaches an elevation of about 10 meters above the present sea level. To the south, the wave-cut platform leaves the place to a coastal sandy barrier that separates the Vendicari lagoonal system of Pantano Roveto from the sea (fig. 4). Therefore, the part of coastline section that stretches from the southern side of Pantano Grande to the end of Pantano Roveto can be considered a fully developed beach system, characterized by an emerged beach, a littoral sandy barrier and a wet back area. Moreover, the lagoonal system of Vendicari is connected to the sea by seasonal channels (partially man controlled) subjected to water level fluctuations between the winter overflows and the summer draining (Amore et al., 1994).

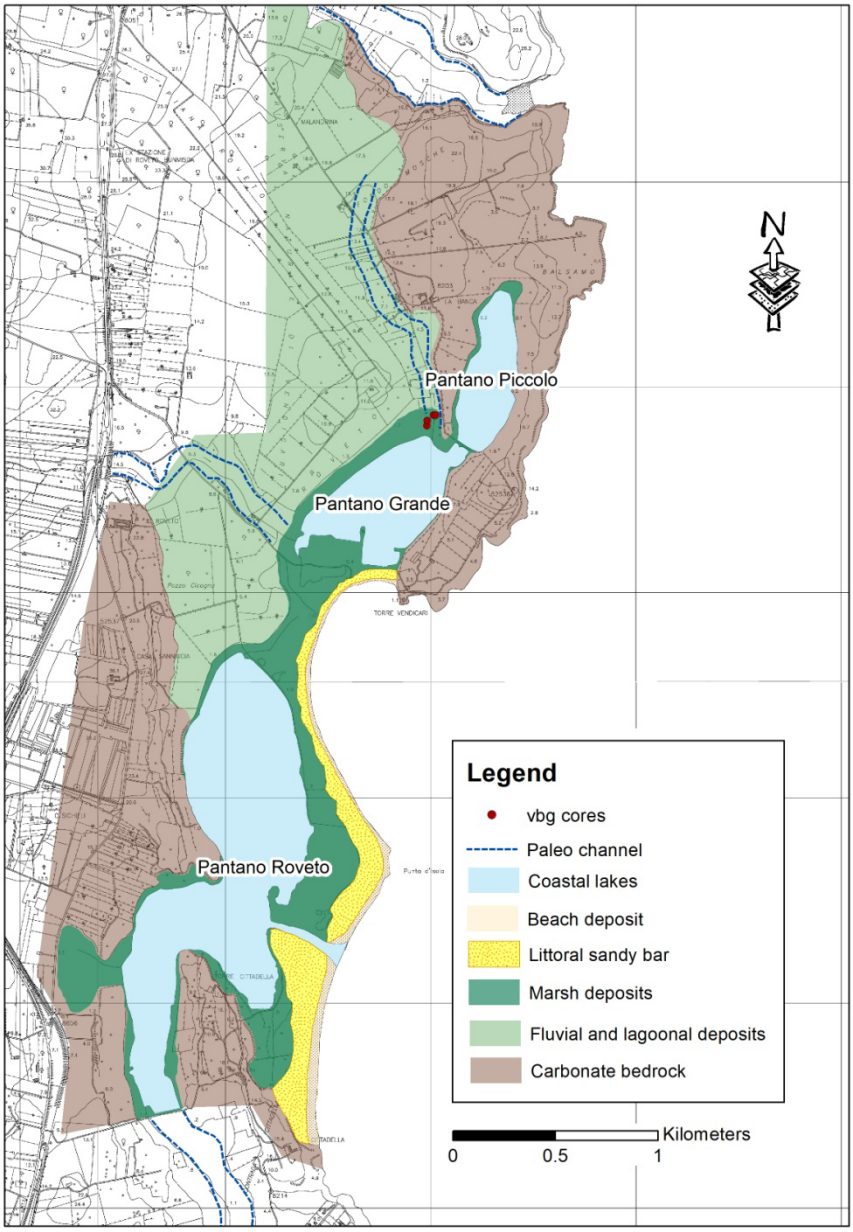

Fig. 4 – Sketch of the geomorphological map of the Vendicari area. The map shows the lagoonal system of Vendicari characterized by the two salt lagoons of Pantano Piccolo and Pantano Grande separated from the sea (on the east side) by a wave-cut platform that reaches an elevation of about 10 meters a.s.l. Conversely to the south, the Pantano Roveto

lagoon is separated from the sea by a coastal sandy barrier. The southern side of the Pantano Grande lagoon and the Pantano Roveto lake can be considered part of a developed beach system.

In the Vendicari lagoonal area, with the aim to find new areas hosting paleotsunami deposits, we selected and investigated a site, called Torre Barbagianni, potentially suitable for the deposition and preservation of paleotsunami deposits represented by sediment layers. The area was already studied by Barbano et al., (2010) highlighting the presence of large boulder deposits placing on the wave cut platform, potentially related to the 1693 tsunami event.

3.1 Torre Barbagianni site

The Torre Barbagianni site, within the natural reserve of Vendicari, is a salt marsh developed between the Pantano Grande and Pantano Piccolo coastal lakes (fig. 5). The distance of the site from the sea is about 800 meters and it was measured considering the distance from the beach (to the south) and not from the high rocky coast (on the eastern side, up to 10 m a.s.l.) because we believe that only the sandy beach with its narrow 1 m-high bar represented and still is a preferential path for tsunami waves.

In this site, five cores were dug down to maximum 3,1 m in depth forming a transect in the NE-SW direction paralleling the coastline (fig. 6). Among them, three are open cores (VBG-S1, VBG-S2, VBG S3, stratigraphic logs in Appendix) while two are closed PVC tubes (VBG-S4and VBG-S5).

The north-easternmost VBG-S1 and VBG-S2 cores reached a maximum depth of 1 m and recovered a stratigraphic sequence made by brown to gray silt (in the uppermost 90 cm) lying on a yellowish-white altered calcarenite, down to the cores bottom. The VBG-S3, VBG-S4 and VBG-S5 cores were collected close to the permanent lake “Pantano Grande” and recovered a 3 m-long stratigraphic sequence characterized by clayey silt alternating to silty clay layers, apart from a single coarser sandy deposit, found at about 1 m in depth.

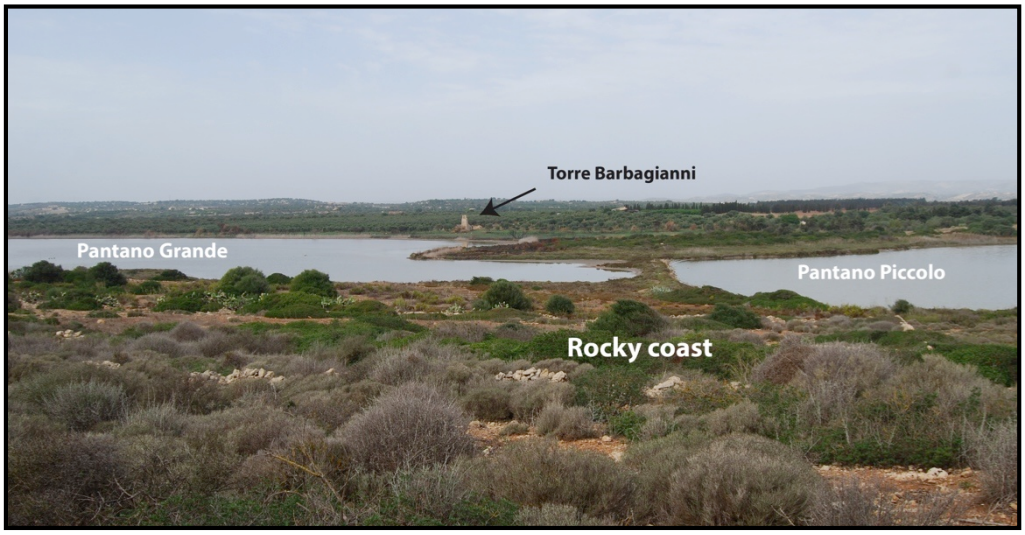

Fig. 5 - Picture of the study site, looking westward, taken from the about 200 m wide rocky coast that separates the Pantano Grande and Pantano Piccolo coastal lakes from the Ionian Sea.

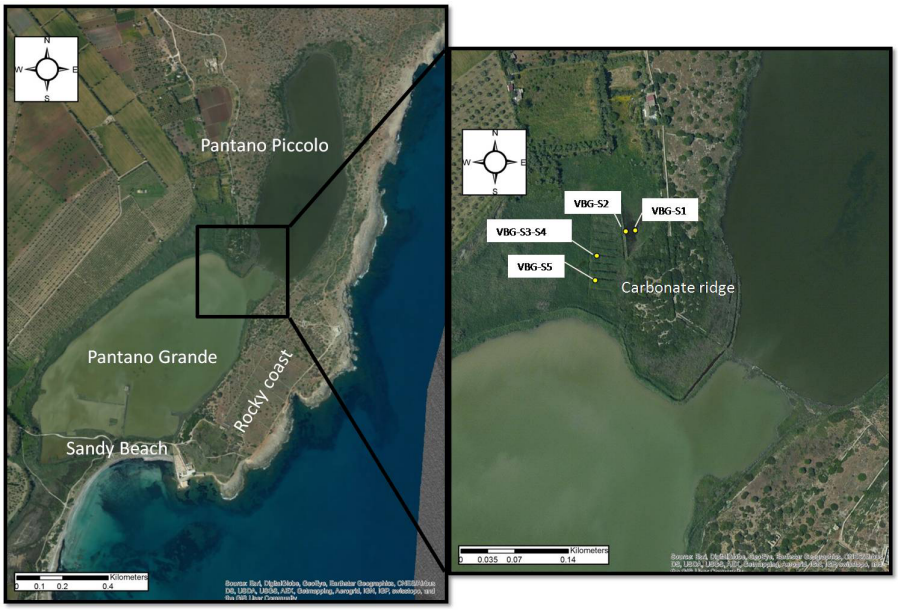

Fig. 6 – The map on the left shows the Torre Barbagianni site while the zoom presents the exact location of the VBG cores, immediately behind a small carbonate ridge to the east of our site (Maps from ESRI)

3.2 Stratigraphic sequence

The VBG-S4 core (fig. 7) that can be used as reference for this study site, even if some layers are better preserved in VBG-S5 (fig. 8).

The VBG-S4 core presents a brown to gray clayey silt deposit from the surface, where a very thin dark brown silty soil developed, down to about 80 cm, with vegetal remnants and oxidized patches concentrated between 34-38 and 70-80 cm in depth. This fine sequence is interrupted from 80 to 115 cm by a coarser deposit. This peculiar interval, displaying a sharp basal contact, is characterized by hazel to gray sandy and silty sediments with shell fragments. Moreover, we should

mention that in VBG-S5 core (fig. 8), this sandy interval looks slightly different in terms of grain size and texture but presenting again a sharp basal contact. In fact, the VBG-S5 core sandy interval is characterized by 25 cm thick fine sand, structureless and massive with many shell fragments and roots. Moreover, in the VBG-S5 core, the fine sand displays few cm thick clayey sand and clayey silt intervals rich in shell fragments, both at its bottom and top. Moving downward in VBG-S4 core, from 115 to 135 cm, a gray clayey silt interval with many shell fragments and mm in size clasts is present (fig. 7). Notice that the same interval in VBG-S5 core displays two extra bioclastic layers within it. From 210 cm to the core bottom (310 cm), the VBG-S4 core presents a gray to dark gray clayey silt, containing vegetal remnants, whole shells and shell fragments, followed downwards by whitish silty clay to clayey silt sediments rich in vegetal remnants and in rounded to sub-rounded carbonate clasts up to 2-3 cm in size, particularly abundant toward the base.

3.3 Paleoenvironmental reconstruction

The micropaleontological study was performed on two cores (VBG-S4 and VBG-S5) and, as for the stratigraphic description, we decided to synthetize the main results referring solely to the VBG-S4 core (fig.7). However, the list, description and interpretation of all samples collected for the micropaleontological analysis are reported in table 1 for the VBG-S4 core and in table 2 for the VBG-S5 core.

In the VBG-S4 core starting from the bottom to ca. 190 cm in depth, the analyzed samples were characterized by a poor foraminiferal assemblage typical of marginal marine environment (mainly *Ammonia* spp. and *Haynesina germanica*) with an important amount of reworked specimens, both planktonic and benthic, from old marine sediments. Notice that among planktonics, few specimens of *Globorotalia puncticulata*, a biostratigraphical marker from the Pliocene, were identified. This assemblage suggests the presence of a brackish ponding environment with significant fluvial/alluvial input, as testified by the recovery of a bad preserved reworked microfauna (fig. 7).

Moving upwards, the previously described reworked assemblage seems to drop down (at ca. 160 and 130 cm, samples Micro 4 and Micro 5 respectively), as a dominant oligothipic assemblage, made of *H. germanica*, is displayed. Moreover, in these samples many vegetal remnants with brackish gastropods (*Hydrobia* spp.) and the dominant brackish ostracod *Cyprideis torosa* are also present. Consequently, the occurrence of an oligothipic assemblage together with vegetal remnants and brackish macro- and ostracoda- fauna can point to a fully lagoonal paleoenvironment, even if a fluvial/alluvial input cannot be excluded due to a seldom recovery of reworked taxa (both planktonic and benthic). At the depth of 115 cm, in correspondence with the coarse sandy interval (samples Micro 6, 7 and 8 in fig. 7) the bioclastic component increases (many whole and shell

fragments with Sponge spicules and sea-urchin remnants) and two different foraminifera assemblages are detected. In fact, a smaller in size ($0.125<\Phi<0.250$ mm) and reworked assemblage (rich in both planktonic and benthic foraminifera from old marine terrains) is present together with benthic foraminiferal taxa from vegetated and coarse sea bottom typical of the inner shelf (e.g. *Ammonia* spp., *Cibicides lobatulus*, *Elphidium crispum*, *Miliolids*, *Miniacina miniacea*, *Nubecularia lucifuga*, *Peneroplis* spp., *Rosalina* spp.). Thus, the coarsening of the VBG-S4 sequence (from 115 to 80 cm in depth) may suggest the development of a foreshore beach paleoenvironment, probably due to the establishment of a direct connection to the sea water with respect to the previously restricted lagoon.

Moving upwards, from 80 cm in depth up to 10-20 cm , important amount of Ammonia spp. and *H. germanica* together with the abundance of some shallow depth marine species and brackish macro- and micro-fauna (among others *Hydrobia* spp. and *C. torosa*) point out to a recovery of protected shallow marine condition as it is today (figs. 7 and 8). It is worth to note that also in the uppermost part (Micro 9, Micro 10, Micro 11) a notable amount of reworked species from the Pliocene is displayed, suggesting a long-lasting sedimentary fluvial/alluvial contribution. Finally, the topmost sample (Micro 11) in VBG-S4 shows an assemblage suggesting a low Salt Marsh environment due to the contemporary recovery of *Ammonia spp*., *H. germanica* together with some agglutinated taxa as *Cribrostomo ides jeffreysi*, *Jadammina macrescens* and *Trochammina inflata*. The low Salt Marsh is the environment that is possible to observe nowadays when we sampled the cores.

3.4 Age constraints

Radiocarbon dating was performed on 4 samples from core VBG S4 and VBG S5 (Table 3, each sample is labeled with site code, core number, and depth in cm). The ages obtained are in stratigraphic order and suggest that the studied sequence is about 4500 years old. Radiocarbon samples were collected above and below the environmental change in the VBG S4 core and only below the environmental change in the VBG S5 core. In order to constrain the bottom of the sand (environmental change) an average stable sedimentation rate of 0.5-0.6 mm/yr was derived. The sedimentation rate was estimated for both cores taking into account the stratigraphic interval between two ages and also considering the stratigraphic position of every age with respect to the whole cores. If we apply this sedimentation rate to the lagoonal/alluvial deposits overlaid by the beach sands, it is possible to derive a maximum age of the sand bottom of BC 280 – 230 AD.

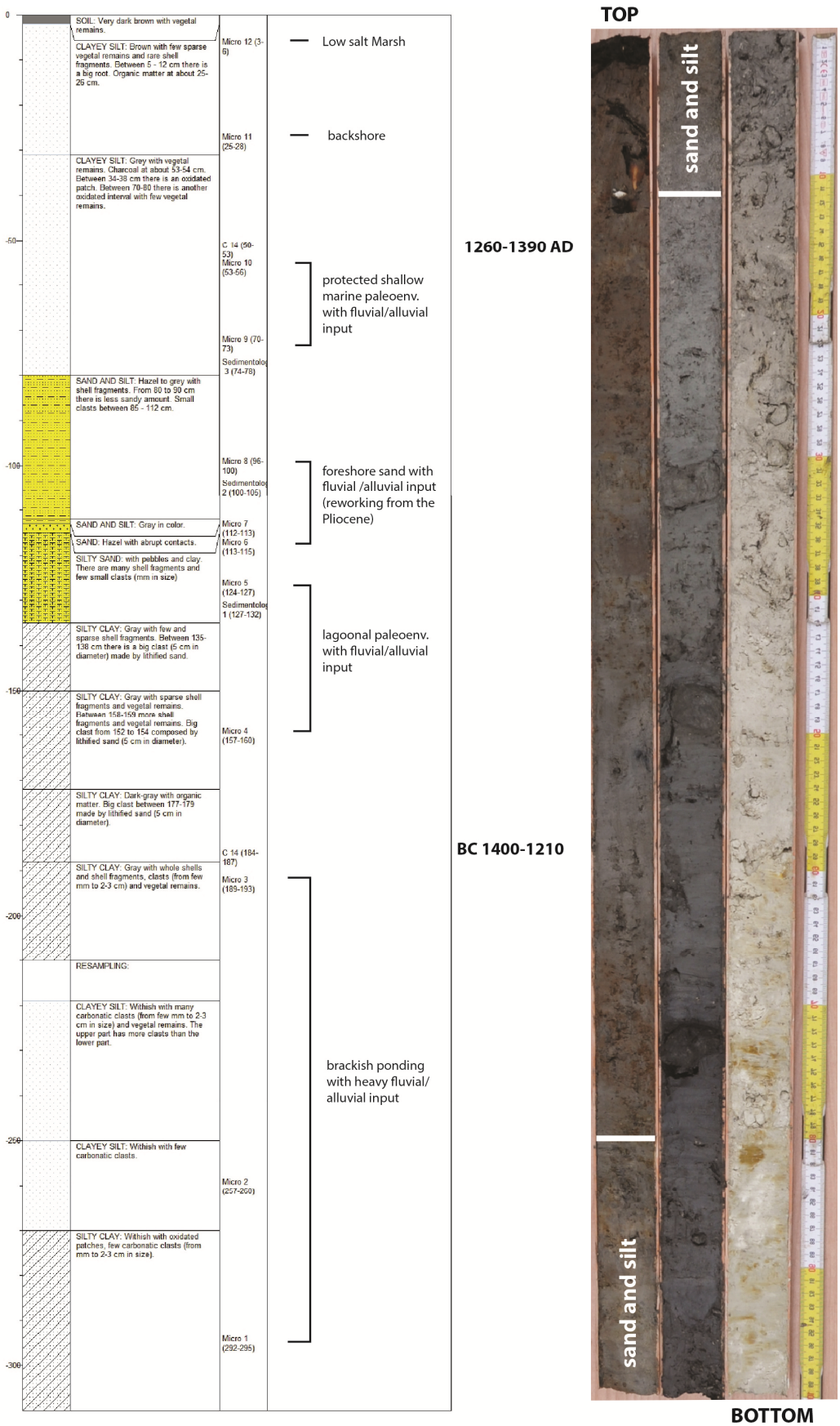

Fig. 7- VBG-S4 log within a brief paleoenvironmental reconstruction based on micropaleontological analysis and the age result of a radiocarbon dating. On the right, the picture of the whole sequence collected with PVC tubes, 1 m long. In the core picture the presence of the coarse unit mainly characterized by sand is highlighted.

ID Sample	Depth (cm)	Paleontological content	Paleoenvironment
VBG S4-I-12	3-6	Benthic forams: *A. tepida, Cribrostomoides jeffreysi, H. germanica, Jadammina macrescens, T. inflata* Other remarks: vegetal remnants, mollusk fragments, ostracods	Low salt marsh
VBG S4-I-11	25-28	Benthic forams: almost absent and in bad condition except some *C. lobatulus*. Other remarks: sea-urchin remnants, vegetal remains,	Backshore
VBG S4-I-10	53-56	Benthic forams: *A. tepida, Asterigerinata mamilla, Bolivina* spp.*, *C. lobatulus, Cibicidoides* spp., *Elphidium* spp.*, *H. germanica, N. lucifuga, Quiqueloculina* spp*., *R. bradyi* Macrofossils: *Hydrobia* spp., mollusk fragments Other remarks: sponge spicules, sea-urchin remnants, vegetal remnants, ostracods	Marginal marine paleoenvironment with fluvial/alluvial input
VBG S4-I-9	70-73	Benthic forams: *A. tepida, C. lobatulus, Cibicidoides* spp., *Elphidium* spp.*, *H. germanica, N. lucifuga, Quiqueloculina* spp*. *R. bradyi* Macrofossils: *Hydrobia* spp., mollusk fragments, sponge spicules, sea-urchin remnants Other remarks: vegetal remnants, ostracods	Marginal marine paleoenvironment with fluvial/alluvial input
VBG S4-I-8	96-100	Benthic forams: *A. tepida, Bolivina* spp.*, *C. lobatulus, Cibicidoides* spp.*, *Elphidium* spp.*, *H. germanica, N. lucifuga, R. bradyi, Quinqueloculina* spp., *Rosalina* spp.*, *S. costata* Macrofossils: *Hydrobia* spp., sponge spicules, sea-urchin remnants, mollusk fragments Other remarks: vegetal remnants, ostracods	Foreshore
VBG S4-II-7	112-113	Benthic forams: *Ammonia tepida, Elphidium* spp.*, *C. lobatulus, Cibicidoides* spp.*, *H. germanica, N. lucifuga, Quinqueloculina* spp., *Rosalina obtusa, Sigmoilinita costata* Macrofossils: *Hydrobia* spp., sponge spicules, sea-urchin remnants Other remarks: ostracods	Foreshore
VBG S4-II-6	113-115	Benthic forams: *Asterigerinata mamilla*, Cibicides lobatulus, Cibicidoides pachyderma*, H. germanica, Nubecularia lucifuga, Quinqueloculina* spp., *Rosalina bradyi** Macrofossils: *Hydrobia* spp., *Cerithium vulgatum*, sponge spicules and sea-urchin remnants	Foreshore
VBG S4-II-5	124-127	Benthic forams*: H. germanica* Macrofossils: *Hydrobia* spp., mollusk fragments, whole and broken *Cardium* sp. Other remarks: vegetal remnants, ostracods	Lagoon with fluvial/ alluvial input
VBG S4-II-4	157-160	Benthic forams: *Cibicides* sp., *H. germanica* Macrofossils: *Hydrobia* spp. Other remarks: vegetal remnants, ostracods	Lagoon with fluvial/alluvial input

VBG S4-II-3	189-193	Benthic forams*: A. Parkinsoniana, H. germanica, Elphidium* spp*	Brackish ponding/lagoonal with fluvial/ alluvial input
VBG S4-III-2	257-260	Benthic forams*: Ammonia parkinsoniana, Elphidium* spp.*	Brackish ponding with heavy fluvial/alluvial input
VBG S4-III-1	292-295	Benthic forams*: Ammonia* spp., *Haynesina germanica, Elphidium* sp.	Brackish ponding/lagoonal with fluvial/ alluvial input

Table 1: List of all samples collected and analyzed for micropaleontological analyses from PVC core VBG S4 dug in Torre Barbagianni site. The table shows the ID sample, the depth with respect to the ground surface and a very brief description of the paleontological content and the related interpreted paleoenvironment. Note that * is used when forams are in very bad condition.

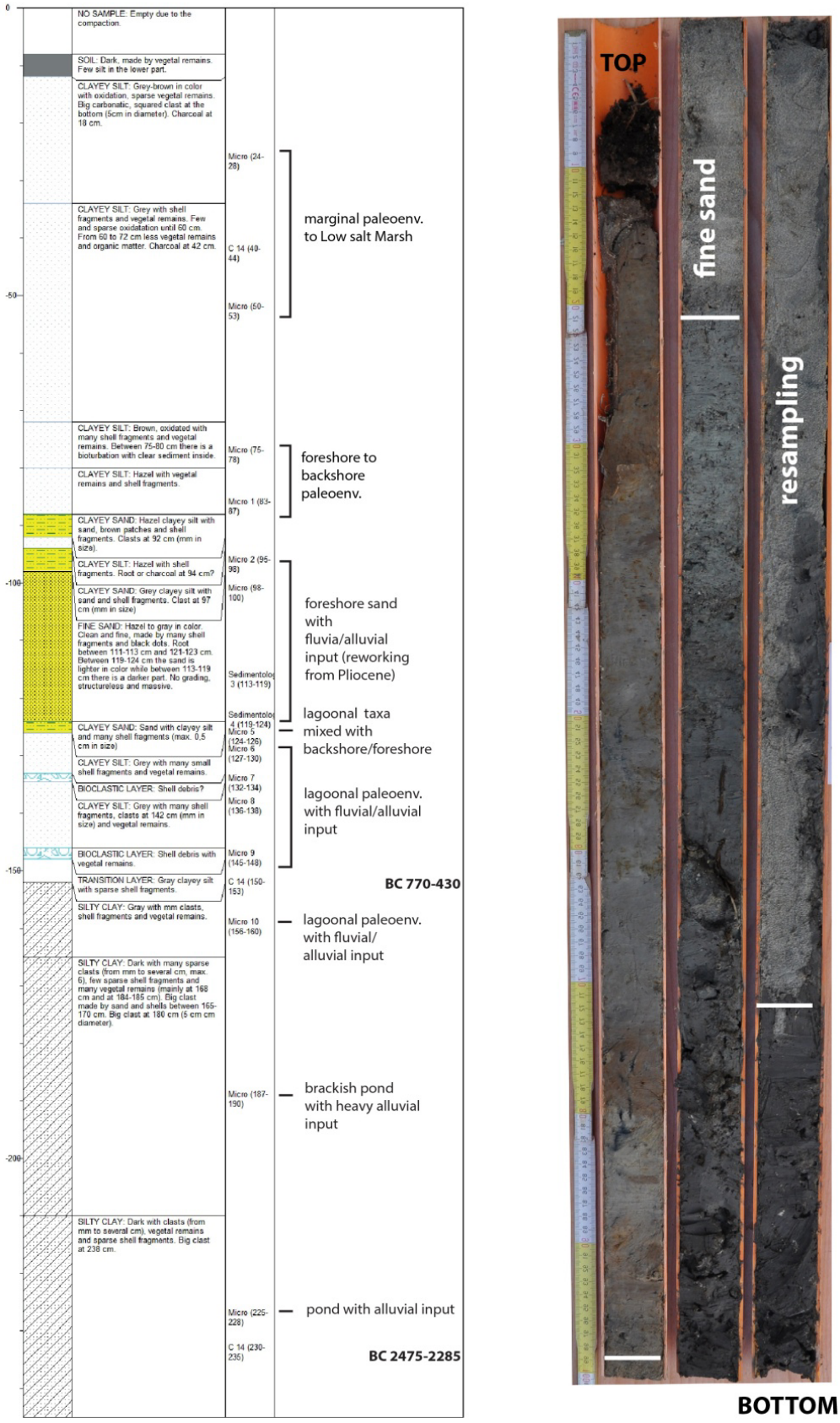

Fig. 8 - VBG-S5 log within a brief paleoenvironmental reconstruction based on micropaleontological analysis and the age result of a radiocarbon dating that constrain the whole sedimentary core sequence. On the right, the picture of the whole collected sequence with PVC tubes, 1 m long. In the core picture the presence of the sandy unit and of a thick resampling interval are highlighted.

ID Sample	Depth (cm)	Paleontological content	Paleoenvironment
VBG S5-I	24-28	Benthic forams: *Cibicides lobatulus, Cibicidoides* sp., *Haynesina germanica Rosalina* sp. Macrofossils: *pirenella conica*, mollusk fragments, ostracods Other remarks: sea-urchin remnants	Marginal marine to low marsh
VBG S5-I	50-53	Benthic forams: *Haynesina germanica, Trochammina inflata* Other remarks: vegetal remnants, oogonium, mollusk fragments, ostracods	Marginal marine to low marsh
VBG S5-I	75-78	Benthic forams: *Ammonia* spp., *Bolivina* spp.*, *Cibicides lobatulus, Cibicidoides* spp.*, Miliolids, *Rosalina* spp. Macrofossils: *Hydrobia* spp., mollusk fragments Other remarks: vegetal remnants,	Foreshore to backshore
VBG S5-I-1	83-87	Benthic forams: *Asterigerinata mamilla, Asterigerinata planorbis, C. lobatulus Cibicidoides* spp., *Elphidium crispum, H. germanica, Planorbulina mediterranensis, Quinqueloculina* spp. *Rosalina bradyi, Rosalina obtusa* Macrofossils: *Hydrobia* spp., mollusk fragments, sea-urchin remnants Other remarks: vegetal remnants, ostracods, oogonium	Foreshore to backshore
VBG S5-I-2	95-98	Benthic forams: *C. lobatulus, Cibicidoides* spp.*, *Elphidium* spp.*, *H. germanica, P. mediterranensis, Quinqueloculina* spp. Macrofossils: *Hydrobia* spp., sea-urchin remnants Other remarks: vegetal remnants, shell fragments, ostracods	Foreshore with fluvial/alluvial input
VBG S5-I	98-100	Benthic forams: *Asterigerinata* spp., *Bolivina* sp.*, *C. lobatulus, Elphidium* spp.*, *miliolids*, P.mediterranensis, Quinqueloculina* spp. Macrofossils: *Planorbis sp.** and mollusk fragments Other remarks: ostracoda	Foreshore with fluvial/alluvial input
VBG S5-II-3S	113-119	Benthic forams: *C. lobatulus, Cibicidoides* spp.*, *Nubecularia lucifuga, Quinqueloculina spp., Rosalina* spp. Macrofossils: *Cerithium vulgatum*, sponge spicules Other remarks: ostracods	Foreshore with fluvial/alluvial input
VBG S5-II-4S	119-124	Benthic forams: *C. lobatulus, N. lucifuga, P. mediterranensis, Quinqueloculina* spp., *Rosalina* spp.	Foreshore with fluvial/alluvial input
VBG S5-II-5	124-126	Benthic forams: *Asterigerinata* spp., *C. lobatulus, E.crispum*, H. germanica, Quinqueloculina* spp., *R. bradyi, R. obtusa* Macrofossils: *Hydrobia* spp., sea-urchin remnants Other remarks:, vegetal remnants, shell fragments, ostracods	Lagoon mixed with foreshore or backshore? Transitional environment
VBG S5-II-6	127-130	Benthic forams: *Ammonia tepida, Cibicidoides spp.*, H. germanica, Quinqueloculina* spp.	Lagoonal with fluvial/alluvial input

		Macrofossils: *Hydrobia* spp. Other remarks: shell fragments, ostracods, vegetal remnants	
VBG S5-II-7	132-134	Benthic forams: *A. tepida, C. Lobatulus, H. germanica* Macrofossils: *Cerastoderma glaucum, Hydrobia* spp. Other remarks: shell fragments, ostracods, vegetal remnants	Lagoonal with fluvial/alluvial input
VBG S5-II-8	136-138	Benthic forams:, *Ammonia perlucida, A. tepida, H. germanica, Cibicidoides* spp.*, *C. lobatulus, Quinqueloculina* spp. Macrofossils: *Hydrobia* spp., *Cerastoderma glaucum* Other remarks: shell fragments, ostracods	Lagoonal with fluvial/alluvial input
VBG S5-II-9	145-148	Benthic forams: *Cibicidoides* spp.*, *E. crispum**, *H. germanica, Quinqueloculina* Macrofossils: *Hydrobia* spp. Other remarks: shell fragments, vegetal remnants	Lagoon with fluvial/alluvial input
VBG S5-II-10	156-160	Benthic forams: *Cibicides* sp., *Cibicidoides spp.**, *H. germanica* Macrofossils: *Hydrobia* spp., *Planorbis* sp., *Ovatella myosotis* Other remarks: vegetal remnants, ostracods, mollusk fragments	Lagoon with fluvial/alluvial input
VBG S5-II	187-190	Benthic forams: *Ammonia* spp.*, *H. germanica* Macrofossils: *Hydrobia* spp., Other remarks: ostracods, vegetal remnants, mollusk fragments	Brackish ponding with heavy alluvial input
VBG S5-III	225-228	Barren Other remarks: vegetal remnants	Ponding with alluvial input

Table 2: List of all samples collected and analyzed for micropaleontological analyses from PVC core VBG S5 dug in Torre Barbagianni site. The table shows the ID sample, the depth with respect to the ground surface and a very brief description of the paleontological content and the related interpreted paleoenvironment. Note that * is used when forams are in very bad condition.

Sample/depth (cm)	Lab code	δ 13 C	Conventional age years B.P.	Calibrated age 2σ	Probability distribution
VBG-S4-I (50-53)	Beta - 467101	-26.8	700 +/- 30	AD 1260 – 1310 AD 1360 - 1387	0.775 0.179
VBG-S4-II (187)	POZ 80752	-27.2	3035 +/- 30	BC 1400- 1210	1.000
VBG-S5-II (150-153)	Beta - 467102	-23.3	2480 +/- 30	BC 774 – 482 BC 441 - 434	0.949 0.05
VBG-S5-III (235)	POZ 80754	-22	3900 +/- 35	BC 2480- 2290 BC 2250- 2240	0.998 0.002

Table 3 - Measured and calibrated ages of the collected samples at Torre Barbagianni site.

4. Searching for paleotsunami deposits in the Siracusa Area

4.1 Vigne Site

The Vigne site is located in the southernmost part of Siracusa town where old salt-pans were active from about 1600 to 1980/90. The site, from a geomorphological point of view, is on an abandoned fluvial plain related to the Anapo and Ciane rivers, filled by alluvial and colluvial silt and clay sediments, potentially related to a low-energy over-flooding environment (figs. 9, 10, 11). The fluvial plain is surrounded by yellowish, coarse and organogenic calcarenite and sands (the "Panchina" unit), with cross bedding. At the base, polygenic gravel and conglomerate are present (from A.A.V.V., 1986. Carta Geologica del Settore Nord-Orientale Ibleo. S.El.Ca. Firenze). This unit is carved by the local fluvial system, which developed a proto-delta mouth. Three cores (SSV-S1, SSV-S2 and SSV-S3, with the first being an open core, its log is available in the Appendix) were dug down to ca. 5 m in depth (fig. 9). The cores were collected in an agricultural field located ca. 2 meters above the sea level, with a maximum distance of 470 meters from the present shoreline, close to an escarpment due to the fluvial erosion.

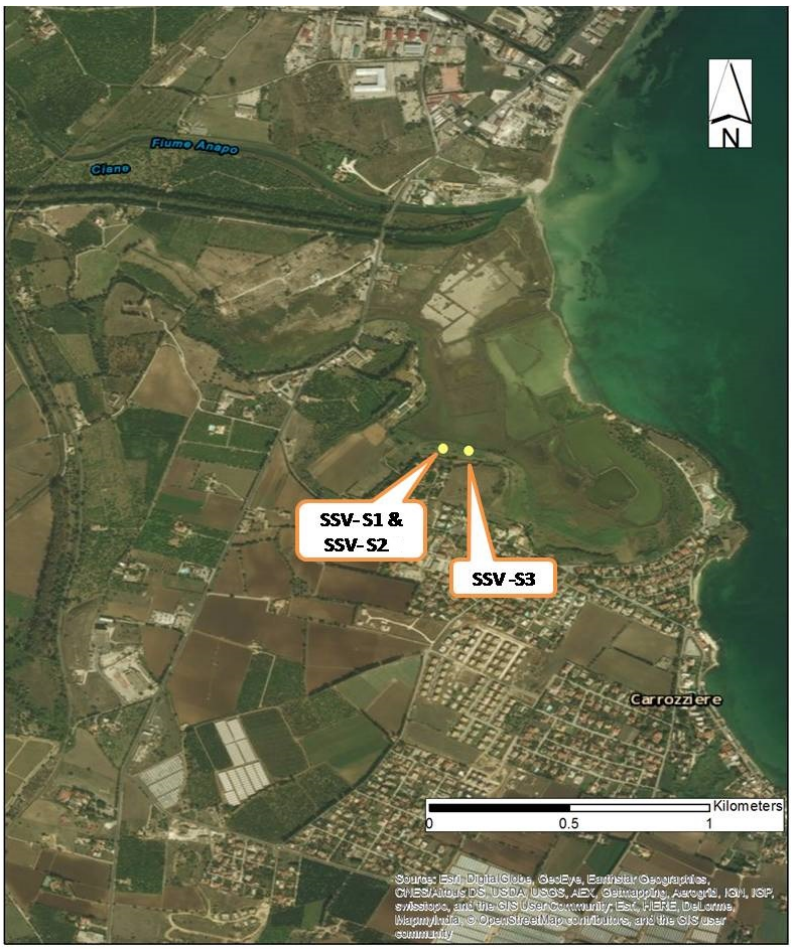

Fig. 9 - Map of Vigne Site. The location of SSV-S1, SSV-S2 and SSV-S3 cores is shown (Map from ESRI).

Fig. 10 - Picture of the Vigne study site seen from a southern stretch of rocky coast.

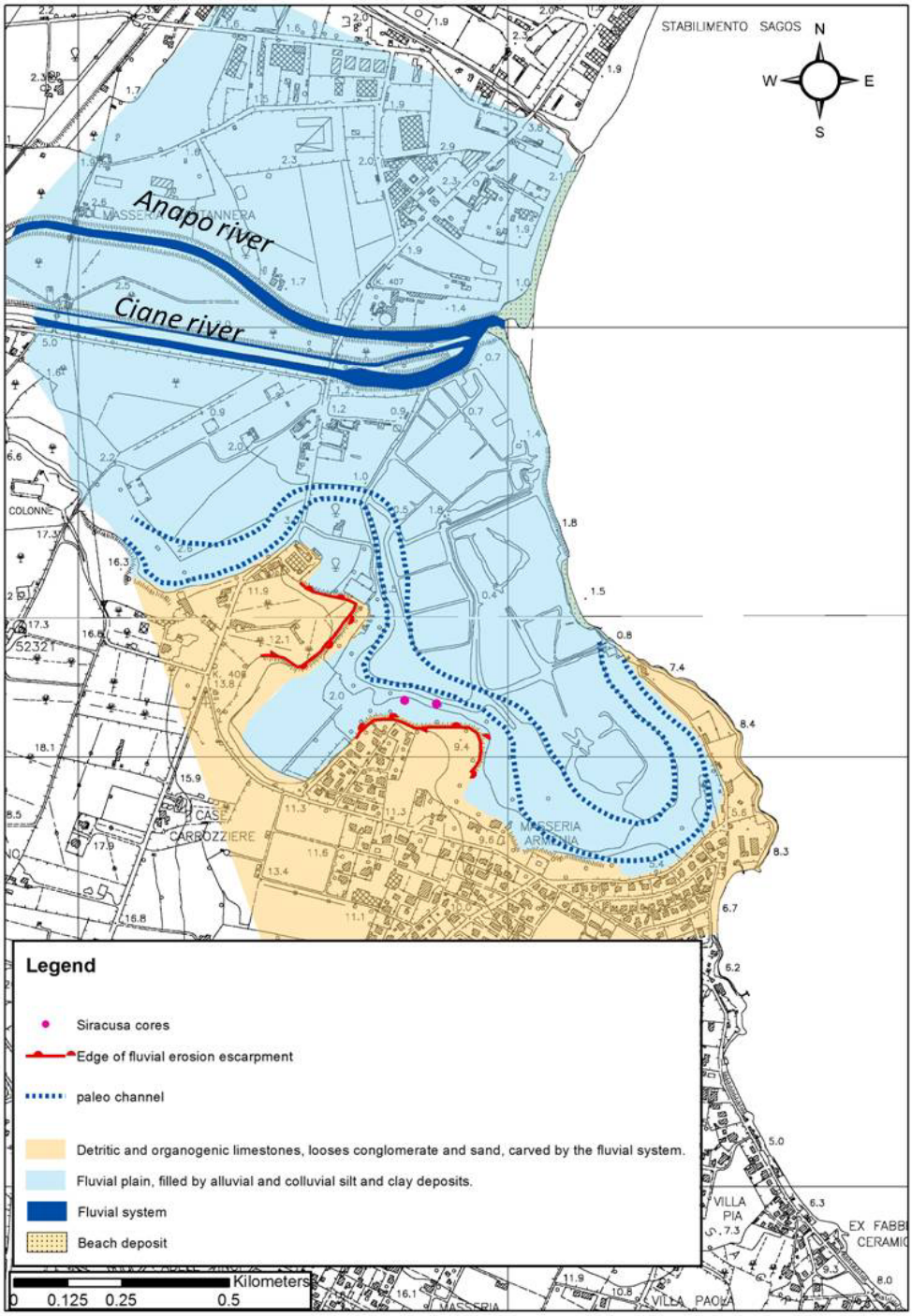

Fig. 11 – Sketch of the geomorphological map of the Vigne site area. In detail it' possible to note that the coring site is located in an abandoned fluvial plain related to the Anapo and Ciane rivers, filled by alluvial and colluvial silt and clay sediments, potentially related to a low-energy over-flooding environment.

4.2 Stratigraphic sequence

The three collected cores are quite similar in terms of stratigraphy and thus we decided to describe the 5.2 m long SSV-S2 core sequence (fig. 12) as reference to synthetize the stratigraphy of the study site, being the more complete and rich among the three. Starting from the bottom (520 cm in depth) its stratigraphy consists of 20 cm of light gray to blue, massive clayey unit. From the study

of SSV-S3 core (fig.13) we know that the light gray to blue clayey interval may have a maximum thickness up to 150 cm with sparse oxidized patches and small carbonate rounded pebbles. From 500 to 448 cm, it is possible to observe a coarser interval made of rounded pebbles and sub-angular clasts (likely of fluvial origin) in a silty sand matrix. This latter coarse interval presents an erosive basal contact on the underlying unit. From 448 cm up to 225 cm, the stratigraphy is characterized by dark gray to gray clayey-silt alternating with several coarse layers (four bioclastic layers mainly made by shell debris and one bioclastic calcarenite) and with a thin peat deposit (395-402 cm) lying on a gray to brown organic silt with important bioclastic content. In general, this latter clayey silt unit contains shell fragments together with whole shells (small gastropods and bivalves) between 303-305 and 346-355 cm in depth. Moving upwards, from 225 to 75 cm in depth, a brown sandy clayey silt is found, quite rich in carbonate clasts (Φ max 5 cm) at the depths of 143-147, 130-136 and 120-125 cm, gray in color from 225 to 175 cm in depth. Finally, the top of the core is characterized by 75 cm of thick brown silt layer, rich in roots and calcarenite pebbles.

4.3 Paleoenvironmental recostruction

The micropaleontological study was performed on two cores (SSV-S2 and SSV-S3). The list of samples with their description and interpretation is reported in table 4 for SSV-S2 core and in table 5 for SSV-S3 core. The analysis suggested the development of different paleoenvironments for both cores, especially in the lower and upper portion of the stratigraphic sequence.

In the SVV-S2 core (fig. 12), starting from the bottom to ca. 502 cm in depth, the analyzed samples show a benthic foraminifera assemblage (e.g. *Bolivina alata*, *Bolivina spathulata*, *Bulimina aculeata*, *Bulimina etnea*, *Cassidulina carinata*, *Hyalinea balthica*, *Uvigerina mediterranea*, *Uvigerina peregrina*) pointing out to an upper bathyal paleoenvironment even if poorly preserved taxa (*Ammonia* spp., *Asterigerinata mamilla*, *Cibicides lobatulus*) from the inner platform are also present. This latter shallow water assemblage together with Sea Urchins, Gastropods and Bivalves of the SVMC biocenosis (sensu Perés and Picard; 1964) are also displayed. The deep assemblage pertains to a geological formation “the gray-blue clay”, Lower Pleistocene in age, outcropping in the study area and sampled at the bottom core, probably intercalated to shallow water and more recent terrains eroded and transported from the river action. In fact, from 502 to 448 cm of depth, the presence of a rounded pebbles level, showing an erosional basal contact, confirms the presence of a fluvial system. Moving upwards, the sample collected from a bioclastic layer (Micro 16) reveals a marginal marine paleoenvironment (dominated by *Ammonia* spp. and *H. germanica*) with fluvial input as testified by the presence of bad preserved planktonic and benthic foraminifera taxa from the Pleistocene and ruined and broken macrofossils. From 433 to 395 cm in depth, the

protected marine paleoenvironment developed to ponding condition as suggested by the unique presence of few reworked foraminifera as well as by the sedimentation of organic silt followed by the development of a peaty layer. From a geomorphological point of view, the above described paleonvironmmetal changes, starting from ca. 450 to 395 cm could be interpreted as an opening and a subsequently closure of the depositional system and environment in relation to the sea action.
From 393 to 239 cm in depth, the analyzed samples showed an oligopthipic assemblage dominated by *Ammonia* spp. and *H. germanica* related to a shallow marine protected paleoenvironment (most probably a shallow lagoon connected to the sea). Nevertheless, the continuous recovery of bad preserved reworked foraminifera in all the samples (bathyal species from Pleistocene terrains), suggest a long-lasting sedimentary fluvial/alluvial contribution. This latter contribution disappears within the interval 270-299 cm of depth, suggesting an ending for the river action. Likely, the recovery of a bioclastic layer at 282-294 cm, that suggests a thanatocoenosis, can be related to a sudden change of salinity and /or temperature thanks to no more river supply. Following, the above described marginal marine paleoenvironment, is interrupted by a 12 cm thick bioclastic calcarenite layer (226-239 cm of depth), showing an erosive basal contact and an inverse grading. It is important to note that the calcarenite clasts belong to the "Panchina" formation (the geological unit outcropping in the studied area). Immediately above the bioclastic calcarenite layer, the sample Micro 3 is almost barren, highlighting the closure of the connection of the environment to the sea. Moving upwards, from ca 200 cm in depth up to the top core, the analyzed samples show a marginal marine paleoenvironment (based on the analysis of one sample at 192-197 cm) evolving towards a continental/alluvial condition due to the solely recovery of barren samples up to ca. 100 cm in depth. No more samples were collected in the uppermost 1 m but we can hypothesize that a long-lasting continental paleoenvironment followed up to nowadays.

The SSV-S3 stratigraphic sequence (fig. 13), with respect to the SSV-S2 core, shows a 2 m thick gray-blue clay layer within a typical assemblage from the upper bathyal paleoenvironment eroded by a ca. 20 cm of overlying fluvial pebbles (from the bottom of the core to 364 cm of depth). It is worth to note that in the SSV-S3 core no ponding condition developed and overlying directly on the fluvial pebbles a long lasting shallow marginal marine paleoenvironment took place (from 364 to 246 cm of depth), as suggested the by recovery of an oligothipic assemblage made by *Ammonia* spp. and *H. germanica*. Nevertheless, as also seen in the SSV-S2 samples, an important fluvial input from 364 to 300 cm of depth is also present due to the continuous recovery of bad preserved marine foraminifera (bathyal species from Pleistocene terrains). In the following, the marginal marine paleonenvironment closes its connection to sea, as suggested by a barren sample collected at

250-253 cm of depth. The overlying bioclastic calacarenite layer at 229-246 cm of depth, shows, as for the SSV-S2 core; an erosional basal contact and an inverse grading. This coarse layer, belonging to the "Panchina" formation, could represent a high energy event that changed the local morphological and environmental settings. In fact, the sample collected just above the bioclastic calcarenite at 222-225 cm in depth shows two poor assemblages: i) a bad preserved marine and reworked foraminifera assemblage (*Ammonia* spp., *Asterigerinata* sp. *Cibicidoides* spp, *Heterolepa* sp., *Oridorsalis umbonatus*); ii) a lagoonal paleoenvironment with well preserved and few specimens of *H. germanica*, suggesting a backshore paleoenvironemnt. Moving upwards, a 78 cm thick layer made of calcarenite clasts (up to 5 cm in size) within a grey to brown clayey silt is shown. This interval was interpreted as a local event potentially related to a rocky landslide from the fluvial terrace flank. In fact, a fluvial terrace is just located behind the coring site. Moreover, the clasts found in this interval have the same lithology of the fluvial terrace (the geological unit called "Panchina"). From ca.140 to 80 cm of depth, the collected samples displayed only *H.germanica* as dominant taxa with few *Ammonia* spp. and reworked marine taxa (both planktonic and benthic foraminifera from the Pleistocene) suggesting a marginal marine paleoenvironment evolving towards ponding condition in its upper part. No samples were collected from the uppermost 90 cm of SSV-S3 core but we can hypothesize that similarly to SSV-S2 the paleoenvironment evolved towards a continental/alluvial plain as it is nowadays.

4.4 Age constraints

Radiocarbon dating was performed on 6 samples collected from core SSV S2 and SSV S3 (Table 6, each sample is labeled with site code, core number, and depth in cm). The ages obtained are in stratigraphic order and suggest that the studied sequence is very old. In fact, the oldest ages of SSV S2 and SSV S3 are respectively about 5300 and 4300 year BP, while the bottom of both cores is represented by the "gray-blue clay unit" of the lower Pleistocene. Taking into account radiocarbon ages it was possible to derive sedimentation rates for both cores. The sedimentation rate was computed from the stratigraphic position of every sample with respect to the whole core. SSV-S2 core shows sedimentation rates of about 0.82, 0.90, 2.2 mm/yr, while SSV-S3 core has sedimentation rates of about 0.77, 0.87, 0.85 mm/yr. Comparing these values, it is clear that both cores exhibit similar sedimentation rates except for the value of 2.2 mm /yr, recorded above the calcarenite clasts interval of the SSV-S3 core. This value should be discarded in the average sedimentation rate calculation because the calcarenite clasts interval most probably eroded part of the stratigraphic sequence, changing the sedimentation rate in the upper part of the SSV-S3 core. Thus, we considered an average sedimentation rate of about 0.82 mm/yr for both cores.

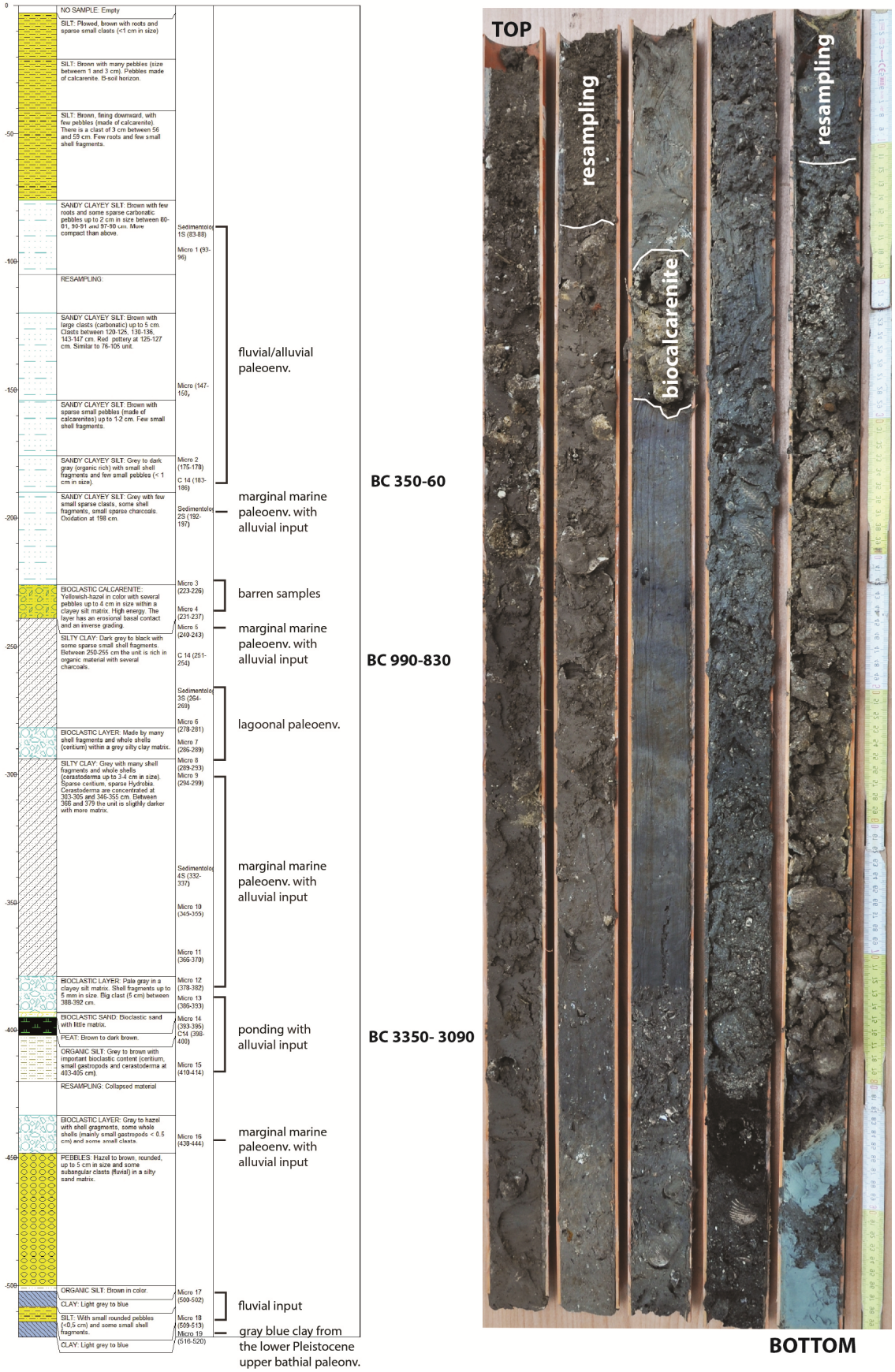

Fig. 12 – SSV-S2 core log with a brief paleoenvironmental reconstruction based on micropaleontological analysis and 14C calibrated ages. On the right, a picture of the whole collected sequence with PVC tubes, 1 m long.

ID Sample	Depth (cm)	Paleontological content	Paleoenvironment
SSV S2-II-1	93-96	Barren Other remarks: only inorganic fraction	Alluvial/fluvial paleoenvironment
SSV S2-II	147-150	Recorded only one *Ammonia*sp.*	Alluvial/fluvial paleoenvironment
SSV S2-II-2	175-178	Barren	Alluvial/fluvial paleoenvironment
SSV S2 2S	192-197	Benthic forams: *Ammonia* spp. Macrofossils: *Cerithium vulgatum*, *Hydrobia* spp., sea-urchin remnants, mollusk fragments, Other remarks: carbonatic clasts	Marginal marine with alluvial input
SSV S2-III-3	223-226	Only inorganic fraction, Very few badly preserved benthic forams.	Marginal marine
SSV-S2-III-4	231-237	Benthic forams badly preserved Other remarks: carbonatic clasts	High energy event
SSV-S2-5	240-243	Benthic forams: *Ammonia* spp. Other remarks: vegetal remnants, mollusk fragments	Marginal marine with alluvial input
SSV S2 3S	264-269	Benthic forams: *Ammonia* spp., *H. germanica* Other remarks: shell fragments	Lagoon
SSV S2-III-6	278-281	Benthic forams: *Ammonia* spp., *Haynesina germanica* Other remarks: shell fragments, ostracods, vegetal remnants	Lagoon
SSV S2-III-7	286-289	Benthic forams: *Ammonia* spp., *H. germanica* Macrofossils: *Hydrobia* spp., *Cerithium vulgatum*, *Cerastoderma glaucum* Other remarks: vegetal remnants, shell fragments, ostracods	Lagoon
SSV S2-III-8	289-293	Benthic forams: *Ammonia* spp., *H. germanica* Macrofossils: *Cerastoderma glaucum*, *Cerithium vulgatum*, *Hydrobia* spp., *Pirenella conica* Other remarks: vegetal remnants, shell fragments, ostracods, carbonatic clasts	Lagoon
SSV S2-III-9	294-299	Benthic forams: *Ammonia*, *H. germanica* Macrofossils: *Cerastoderma glaucum*, *Cerithium vulgatum*, *Pirenella conica* Other remarks: shell fragments, carbonatic clasts	Marginal marine with alluvial input
SSV S2 4S	332-337	Benthic forams: *Ammonia*, *H. germanica* Macrofossils: *Cerastoderma glaucum*, *Cerithium vulgatum*, *Hydrobia* spp., sponge spicules Other remarks: ostracods, oogonium, shell fragments	Marginal marine with alluvial input
SSV S2-IV-10	345-355	Benthic forams: *Ammonia*, *H. germanica* Macrofossils: *Cerastoderma glaucum*, *Cerithium vulgatum*, *Loripes lacteus* Other remarks: shell fragments, vegetal remnants, sea-urchins remnants	Marginal marine with alluvial input
SSV S2-IV-11	366-370	Benthic forams: *Ammonia*, *H. germanica* Macrofossils: *Cerithium vulgatum*, *Hydrobia* spp., *Pirenella conica* Other remarks: shell fragments, vegetal remnants, Ostracods	Marginal marine with alluvial input

SSV S2-IV-12	378-382	Benthic forams: *Ammonia, H. germanica* Macrofossils: *Cerastoderma glaucum, Cerithium vulgatum, Hydrobia* spp., *Loripes lacteus, Pirenella conica* Other remarks: small clasts, whole shells and shells fragments	Marginal marine with alluvial input
SSV S2-IV-13	386-393	Almost barren. Only few benthic forams badly preserved Macrofossils: *Cerithium vulgatum, Loripes lacteus, Pirenella conica* Other remarks: clasts, mollusk fragments	Ponding with alluvial input
SSV S2-IV-14	393-395	Only few benthic forams badly preserved Other remarks: mollusk fragments	Ponding with alluvial input
SSV S2-V-15	410-414	Benthic forams: *Ammonia* spp., *Asterigerinata* sp., *Cibicidoides* spp., *Hyalinea balthica* Other remarks: sample characterized only by reworked material, shell fragments, sea-urchins remnants	Ponding with alluvial input
SSV S2-V-16	438-444	Benthic forams: *Ammonia tepida, Bolivina spathulata, Cassidulina carinata, Cibicidoides* spp.*, *Elphidium* spp.*, *H. germanica, Uvigerina* spp.* Macrofossils: *Cerastoderma glaucum, Cerithium vulgatum, Hydrobia* spp., *Loripes lacteus, Pirenella conica, Planorbis* sp., *Truncatella subcylindrica* Other remarks: sea-urchins remnants, mollusks fragments	Marginal marine with alluvial input
SSV S2-VI-17	500-502	Barren	Fluvial input
SSV S2-VI-18	509-513	Benthic forams: *Ammonia* spp.*, *Cibicidoides* spp.*, *Elphidium crispum** Macrofossils: *Cerithium vulgatum, Pirenella conica* Other remarks: mollusks fragments, clasts (maybe carbonatic of fluvial origin)	Fluvial input
SSV S2-VI-19	516-520	Benthic forams: *B. spathulata, C. carinata, H. balthica, Uvigerina mediterranea, Uvigerina peregrina* Macrofossils: *Bittium reticulatum, Truncatella hammersmithi* Other remarks: ostracods, mollusk fragments, clasts, sea-urchin fragments	Upper bathyal Grey-blue clay from the lower Pleistocene

Table 4: List of all samples collected and analyzed for micropaleontological analyses from PVC core SSV-S2 dug in Vigne site. The table shows the ID sample, the depth with respect to the ground surface and a very brief description of the paleontological content and the related interpreted paleoenvironment. Note that * is used when forams are in very bad condition.

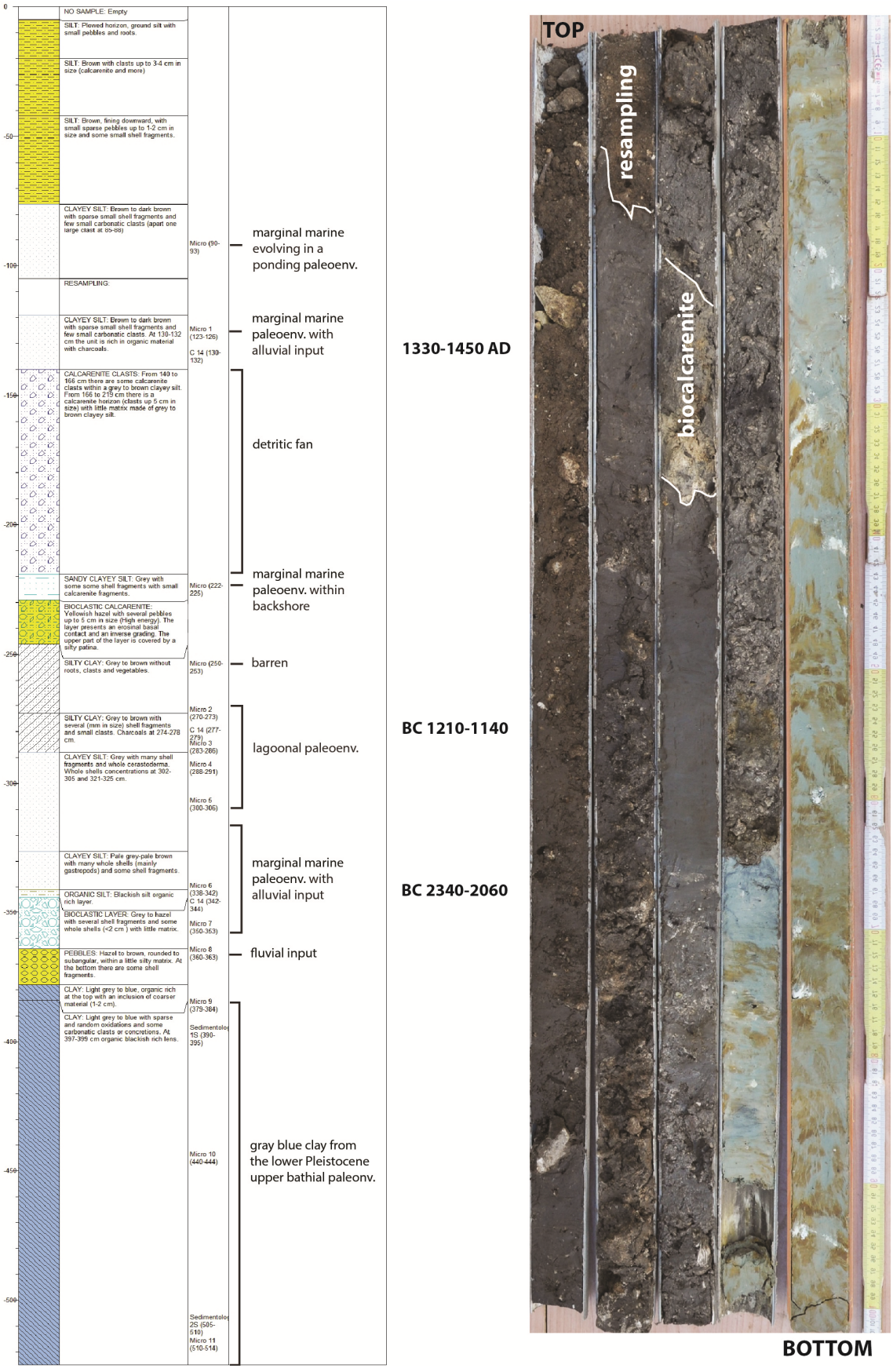

Fig. 13 - SSV-S3 core log with a brief paleoenvironmental reconstruction based on micropaleontological analysis and 14C calibrated ages. On the right, a picture of the whole collected sequence with PVC tubes, 1 m long.

ID Sample	Depth (cm)	Paleontological content	Paleoenvironment
SSV S3-I	90-93	Benthic forams: *Ammonia* spp., *Haynesina germanica*, Other remarks: ostracods	Marginal marine evolving in a ponding
SSV S3-II-1	123-126	Benthic forams: *H. germanica* Macrofossils: *Hydrobia* spp., *Pirenella conica*, *Planorbis* sp. Other remarks: ostracods, whole shells and shell fragments	Marginal marine with alluvial input
SSV S3-III	222-225	Benthic forams: *Ammonia* spp.*, *H. germanica*, *Elphidium* spp.* Other remarks: sea-urchin fragments, shell fragments, clasts	Marginal marine within backshore
SSV S3-III	250-253	Barren with rare ostracods	Lagoon
SSV S3-III-2	270-273	Benthic forams: *Ammonia* spp., *H. germanica*	Lagoon
SSV S3-III-3	283-286	Benthic forams: *Ammonia* spp., *H. germanica* Macrofossils: *Hydrobia* spp. Other remarks: ostracoda, mollusk fragments Honed material	Lagoon
SSV S3-III-4	288-291	Benthic forams: *Ammonia* spp., *H. germanica* Macrofossils: *Cerastoderma glaucum*, *Hydrobia* spp., *Loripes lacteus* Other remarks: whole shells and shell fragments, ostracods	Lagoon
SSV S3-IV-5	300-306	Benthic forams: *Ammonia* spp., *H. germanica* Macrofossils: *Cerithium vulgatum*, *Cerastoderma glaucum*, *Pirenella conica* Other remarks: whole shells and shell fragments	Lagoon
SSV S3-IV-6	338-342	Benthic forams: *Ammonia*, *H. germanica* Macrofossils: *Cerastoderma glaucum*, *Cerithium vulgatum*, *Hydrobia* spp., *Loripes lacteus*, *Pirenella conica* Other remarks: whole shells and shell fragments, ostracods	Marginal marine with alluvial input
SSV S3-IV-7	350-353	Benthic forams: *Ammonia* spp., *H. germanica* Macrofossils: *Cerithium vulgatum*, *Hydrobia* spp., *Pirenella conica* Other remarks: shell and shell fragments, carbonatic clasts	Marginal marine with alluvial input
SSV S3-IV-8	360-363	Benthic forams*: Ammonia* spp*, *Bolivina spathulata*, *Cibicidoides* spp.*, *Elphidium crispum** Macrofossils: *Cerastoderma glaucum*, *Cerithium vulgatum*, *Hydrobia* spp., *Pirenella conica* Other remarks: whole shells and shell fragments	Fluvial input
SSV S3-IV-9	379-384	Benthic forams*: Ammonia* spp*, *B. spathulata*, *Bulimina aculeata*, *Cassidulina carinata*, *Cibicides lobatulus**, *Elphidium spp.**, *Globocassidulina subglobosa* Macrofossils*: Hydrobia* spp., *Pirenella conica*	Grey-blue clay from the lower Pleistocene. Upper bathial paleoenvironment

		Other remarks: whole shells and shell fragments. The assemblage is badly preserved	
SSV S3-V-10	440-444	Benthic forams: *Bulimina aculeata, Bulimina marginata, B. spathulata, C. carinata, C lobatulus, G.subglobosa, H. balthica, Melonis barleeanum, Uvigerina peregrina* Other remarks: clasts	Upper bathyal Grey-blue clay from the lower Pleistocene
SSV S3-VI-11	510-514	Benthic forams: *B. aculeata, B. marginata, B. spathulata, C.carinata, H.balthica, U. peregrina, Textularia* spp. Other remarks: sea-urchins fragments, ostracods	Upper bathyal Grey-blue clay from the lower Pleistocene

Table 5: List of all samples collected and analyzed for micropaleontological analyses from PVC core SSV-S3 dug in Vigne site. The table shows the ID sample, the depth with respect to the ground surface and a very brief description of the paleontological content and the related interpreted paleoenvironment. Note that * is used when forams are in very bad condition.

Sample/depth (cm)	Lab code	δ 13 C	Conventional age years B.P.	Calibrated age 2σ	Probability distribution
SSV-S2 (398-400)	Poz-91255	-25.2	4500 +/-35	BC 3354- 3090	1.000
SSV-S2 (251-254)	Poz-91253	-21.1	2765 +/-30	BC 994- 985 BC 980- 834	0.023 0.977
SSV-S2 (183-186)	Poz-91259	-26.5	2140 +/-30	BC 353- 295 BC 229- 219 BC 213- 87 BC 78- 56	0.203 0.015 0.748 0.034
SSV-S3 -IV (342-344)	Poz-91258	-18.7	3790 +/-35	BC 2342-2132 BC 2083-2059	0.978 0.022
SSV-S3-III (277-279)	Poz-91257	-26.6	2905 +/-30	BC 1207- 1140 BC 1134-1008	0.211 0.789
SSV-S3-II (130-132)	Poz-91256	-23.6	505 +/- 30	AD 1331-1338 AD 1397-1447	0.022 0.978

Table 6 - Measured and calibrated ages of the collected samples at Vigne site.

5. Discussion and conclusions

The two sites investigated by coring exhibit interesting data that could suggest some consideration in terms of extreme events.

In fact, considering the data collected and elaborated at Torre Barbagianni site (Vendicari Natural Reserve area), it is possible to underline that an abrupt change in depositional environment from lagoonal/alluvial to marine (testified by a clear basal erosional contact of the sandy marine deposits overlaying the lagoonal/alluvial finer sediments), occurred at about 1 m in depth (fig. 14; fig.15A and 15B). Amore et al. (1994), studying the sediments of this protected area (by means of 1 m long cores on very recent deposits), already evidenced this phenomenon but nothing is available in terms of timing. The related marine interval (about 30-40 cm thick) is most probably due to the development of a foreshore beach paleoenvironment at the study site, intrinsically related to the

establishment of a direct connection to the sea (fig. 15B), presently at about 800 m far from the coring site.

The latter sediments are not a typical tsunami related deposit but we are tempted to interpret them as potentially related to a local earthquake or tsunami wave(s) that produced a significant modification of the coastline, disrupting the morphologic sandy coastal barrier able to protect the site area, thus favoring a direct connection to the sea and providing a large amount of sediment (due to the tsunami wave erosional action).

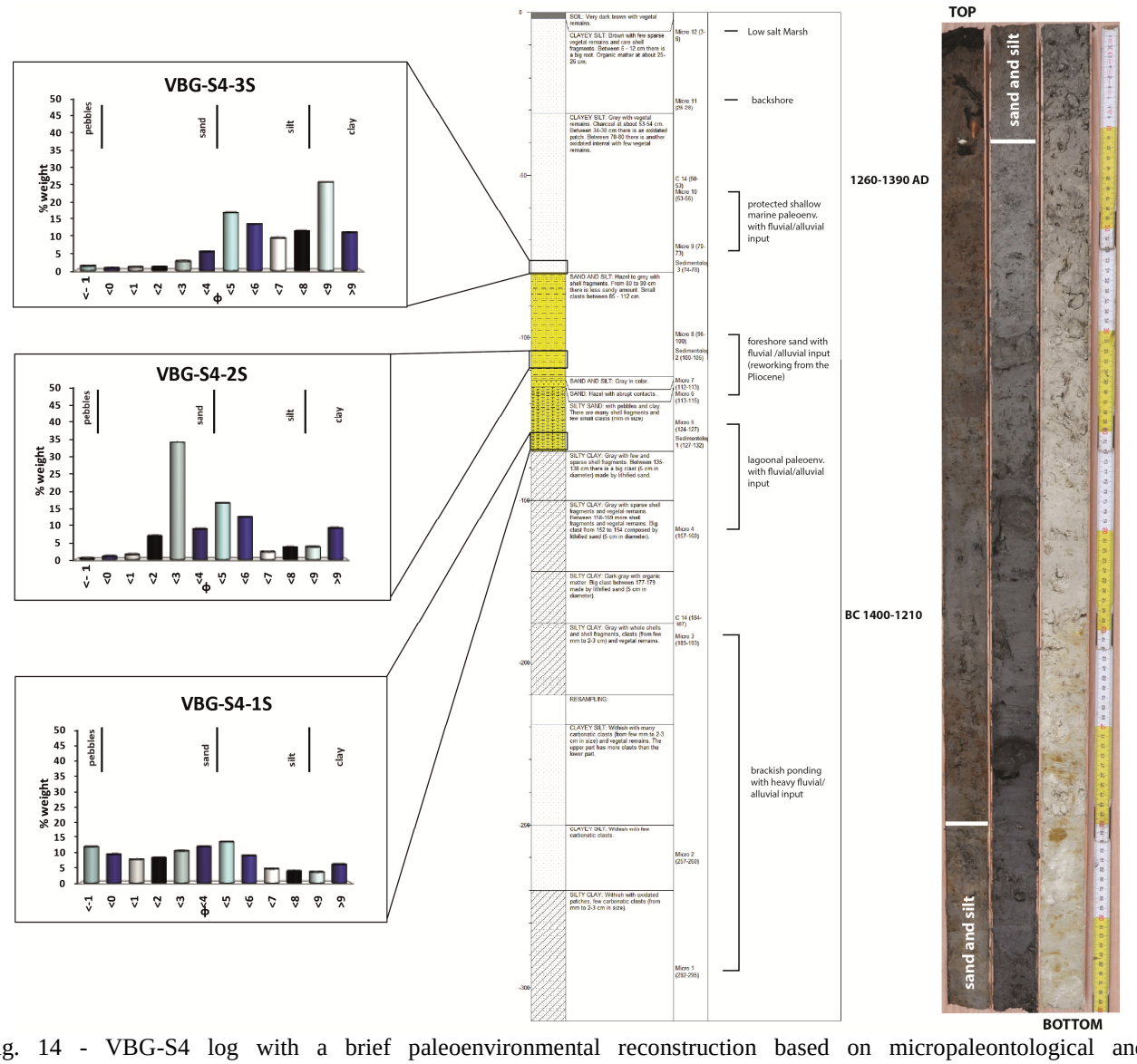

Fig. 14 - VBG-S4 log with a brief paleoenvironmental reconstruction based on micropaleontological and sedimentological analysis and the age result from radiocarbon datings. The picture of the whole sequence with PVC tubes, 1 m long is displayed on the right side. In the core picture the presence of on coarse unit mainly characterized by sand and silt is highlighted. On the left side some plots showing grain size analysis. The plot from the sample VBG-S4-1S highlight a badly sorted sample testifying the continuous alluvial/fluvial input in the lagoon while the sample collected in correspondence of the coarser layer (VBG-S4-2S) presents a bimodal grain-size distribution showing an important contribution of a fine sand in a quiet environment. Finally, in the uppermost plot (VBG-S4-3S) a recovery of the protected shallow environment with finer sediments is testified.

Today, it is known that large tsunami waves are able to drastically modify coastal morphologies. In fact, after the 2004 Indian Ocean tsunami, many scientific papers described the coastal erosion due to tsunami wave action (Umitsu et., 2007; Paris et al., 2009). Most of the erosional features such as erosion escarpments in soils, beaches, banks, riverbeds, and slopes were well described in literature by Maramai and Tinti, (1997) during the 1994 tsunami in Southeast Java, by Shi et al., (1995) for the 1992 tsunami in Flores and by Gelfenbaum et al., (2003) for the 1998 tsunami in Papua New Guinea. The Erosion of sand barriers was also reported by Andrade, (1992) for the 1755 Lisbon tsunami. Moreover, processes able to rebuild coastal landforms (e.g. beaches or coastal spits) eroded and modified by an extreme event were observed and reported (Koiwa et al., 2017). In fact, Koiwa et al. (2017) observed the recovery of the barrier spit of Pakarang Cape (southern Thailand) after the erosion caused by the 2004 Indonesia tsunami. They found that the new volume of sediment for the barrier recovery was two times larger than that of the estimated erosion by the tsunami, thus giving life to a new geomorphic feature. However, the recovery speed in restoration processes is dependent on sediment availability (Tanaka et. al., 2012) where the littoral processes (e.g. coastal current and storm waves) play a fundamental role in the sediment distribution.

De Martini et al. (2010) found a similar environmental change, from alluvial to marine, in a site called Augusta Hospital, (located few kilometers north of Siracusa town) that shows a geomorphological setting similar to Vendicari site. Even in this case, the deposit investigated was not a characteristic tsunami deposit. Authors, on the base of the analysis undertaken, related the sudden environmental change to an extreme event that caused a significant geomorphological coastal modification.

In terms of timing of this hypothesized strong event, recorded in the Vendicari area, it is possible to add that from both cores we got a radiocarbon constrained average sedimentation rate, very similar and stable, of about 0.5 mm/yr. If we apply this sedimentation rate to the lagoonal/alluvial deposits overlaid by the beach sands, we may derive a maximum age of the sand bottom (called here 03) windowed between BC 280 – 230 AD. This age is defined as maximum value because, if we take into account the presence of its clear erosive contact, we could have missed some cm of sediments, but we do not have a reasonable approach to calculate and not even to estimate it.

Finally, it is noteworthy to mention that this age compare well with the age of some tsunami deposits found in the nearby areas (De Martini et al., 2012), in particular with respect to the Ex event (from offshore data in the Augusta Bay, Smedile et al., 2011), PR-02 event (from Priolo Reserve site, De Martini et al., 2010), and MOR-T2 event (from Pantano Morghella site, Gerardi et al., 2012) that were potentially related to the 365 AD Crete tsunami (fig. 17).

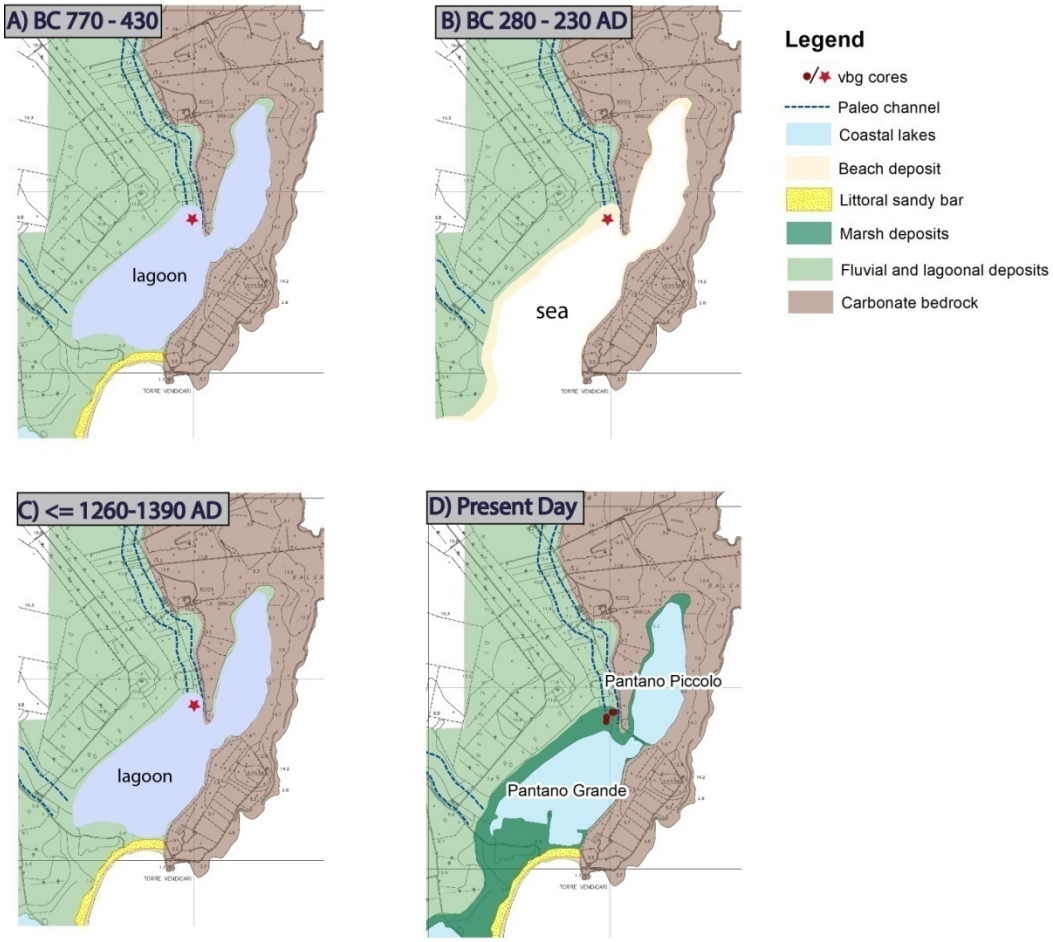

Fig. 15 - Summary of the paleoenvironment development for the Vendicari coring site. A) Lagoonal paleoenvironment at the coring site around BC 770-430. B) Beach at the coring site around BC 280-230 AD due to a marine sedimentation in the whole lagoon (Amore et al., 1994) likely due to the rupture of the morphological sandy barrier. C) Development of a lagoonal paleoenvironment with the recovery of the coastal sandy barrier (<= 1260-1390 AD). D) Present day phase with the two salt coastal lakes of Pantano Grande and Pantano Piccolo with their related marsh deposits.

In the Siracusa salt pans area (at Vigne site) we tentatively suggest a paleoenvironmental reconstruction based on the data collected from cores SSV-S2 and SSV-S3 and related analyses. Starting from the cores bottom, the micropaleontological study performed revealed the development of a fluvial environment, eroding and depositing on the grey-blue Lower Pleistocene marine clay, evolving towards a marginal marine environment (BC 2340-2060). In core SSV-S2, the latter environmental change occurred together with a clear ponding phase as testified by the presence of a peat layer (BC 3350-3090). Moreover, the site experienced a progressive closure of the system with the development of a lagoonal environment (BC 1210-1140) up to the deposition of a well distinct clean bioclastic calcarenite layer, with inverse grading and very little matrix.

Interestingly, both cores testify the successive development of a marginal marine environment (fig. 16a), that as for SSV-S3 is abruptly interrupted by the deposition of a detritic fan (fig. 16b), potentially related to a local cliff collapse (the terrace outer edge located just behind the coring site).

This fan is interpreted as responsible for the different environmental evolution recorded in the two cores. In fact, SSV-S2 is somehow protected with respect to the sea and thus evolved towards a continental deposition (fig. 16b, c, d) by fluvial/alluvial phases, while SSV-S3 evolves from a fluvial (fig. 16c) to a marginal marine environment (fig. 16d, 1330-1450 AD). Finally, both cores register the salt pan construction (fig. 16e, around 1600 AD) and the environment turned towards a pure continental deposition up to the present day phase (fig. 16f).

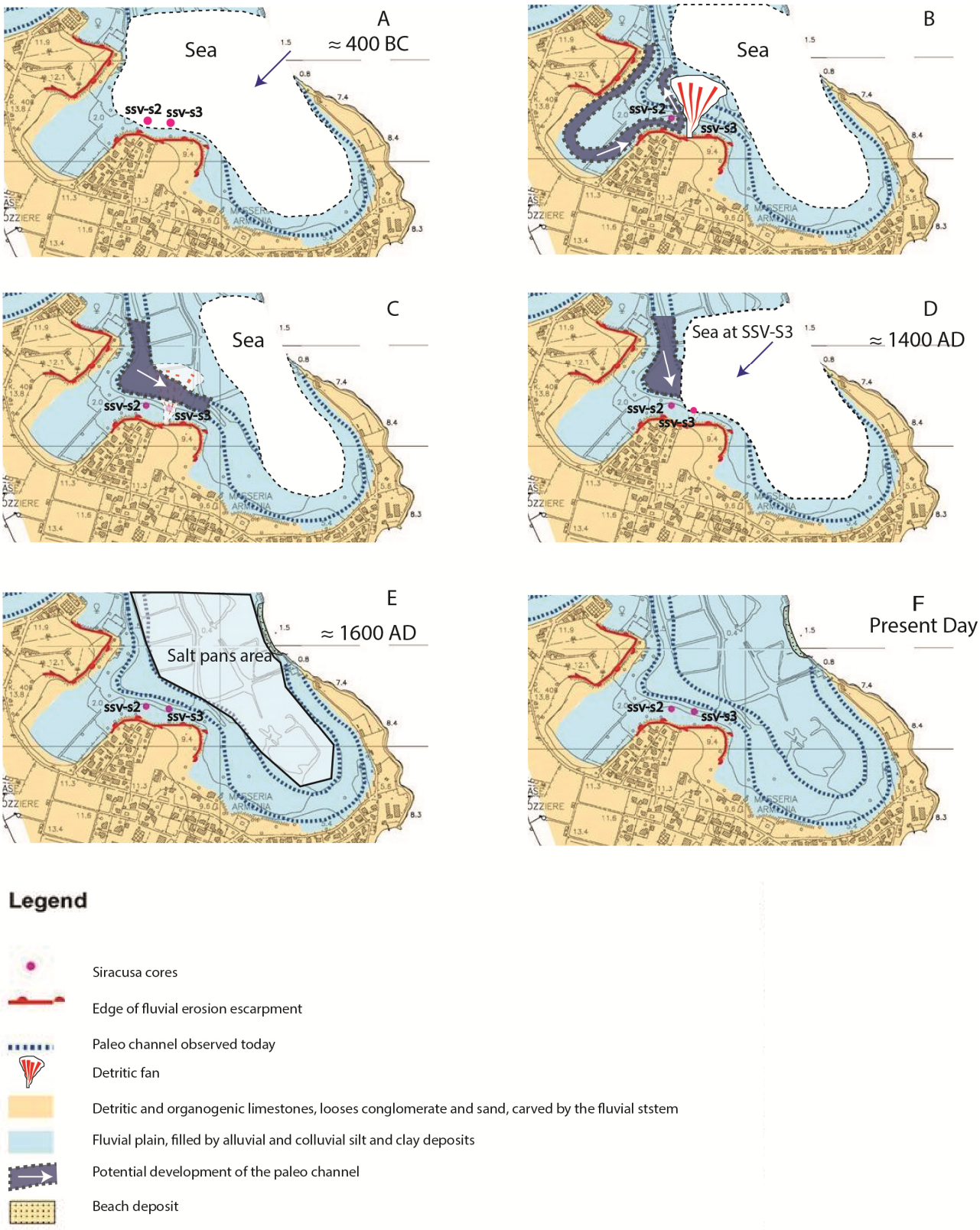

Fig. 16 – Summary of the paleoenvironment development for both cores after the deposition of the bioclastic calcarenite: A) Marginal marine environment for both cores. B) The deposition of a detritic fan, potentially related to a local cliff collapse, interrupted the marginal marine environment for SSV-S3. C), D) SSV-S2 is protected with respect to the sea and evolved towards a continental deposition by fluvial/alluvial phases, while SSV-S3 evolves from a fluvial

to a marginal marine environment. E), F) Both cores register the salt pan construction (around 1600 AD) and the environment turned towards a pure continental deposition up to the present day phase.

In the Siracusa area at the Vigne Site, we recorded only one single high energy unit, a distinct bioclastic calcarenite layer (deposited after BC 990-830 and before BC 350-60) with unclear provenance. This layer has some tsunami deposit features such as a sharp basal contact and a slightly inverse grading (that could suggest a fast deposition) but lacks of any marine content. Despite this, however, applying an average sedimentation rate of 0.82 mm/yr, the age of the high energy event (called here Sr1, fig 17) is ca. 750 BC. This age is comparable with some tsunami deposits found in the nearby areas, dated between 975 – 500 BC (De Martini et al., 2010; Smedile et al., 2011): AU-01, AU-02, PR-03,E8, E9, E10 (fig 17).

Even if a tsunami origin is not fully supported for this layer, it is worth to mention that a similar deposit, gravel layer made by subangular carbonatic clasts, found in the Augusta bay (AU-01 in De Martini et al., 2010) and interpreted as of tsunami origin based on micropaelontological analysis, display a very similar age (BC 600-400) temping us for correlating the two deposits.

Finally, if the bioclastic calcarenite layer is correctly interpreted as a tsunami deposit, it would be possible to derive a minimum inundation distance of about 470 meters from the shoreline and a minimum run up height of about 2 meters above the present sea level.

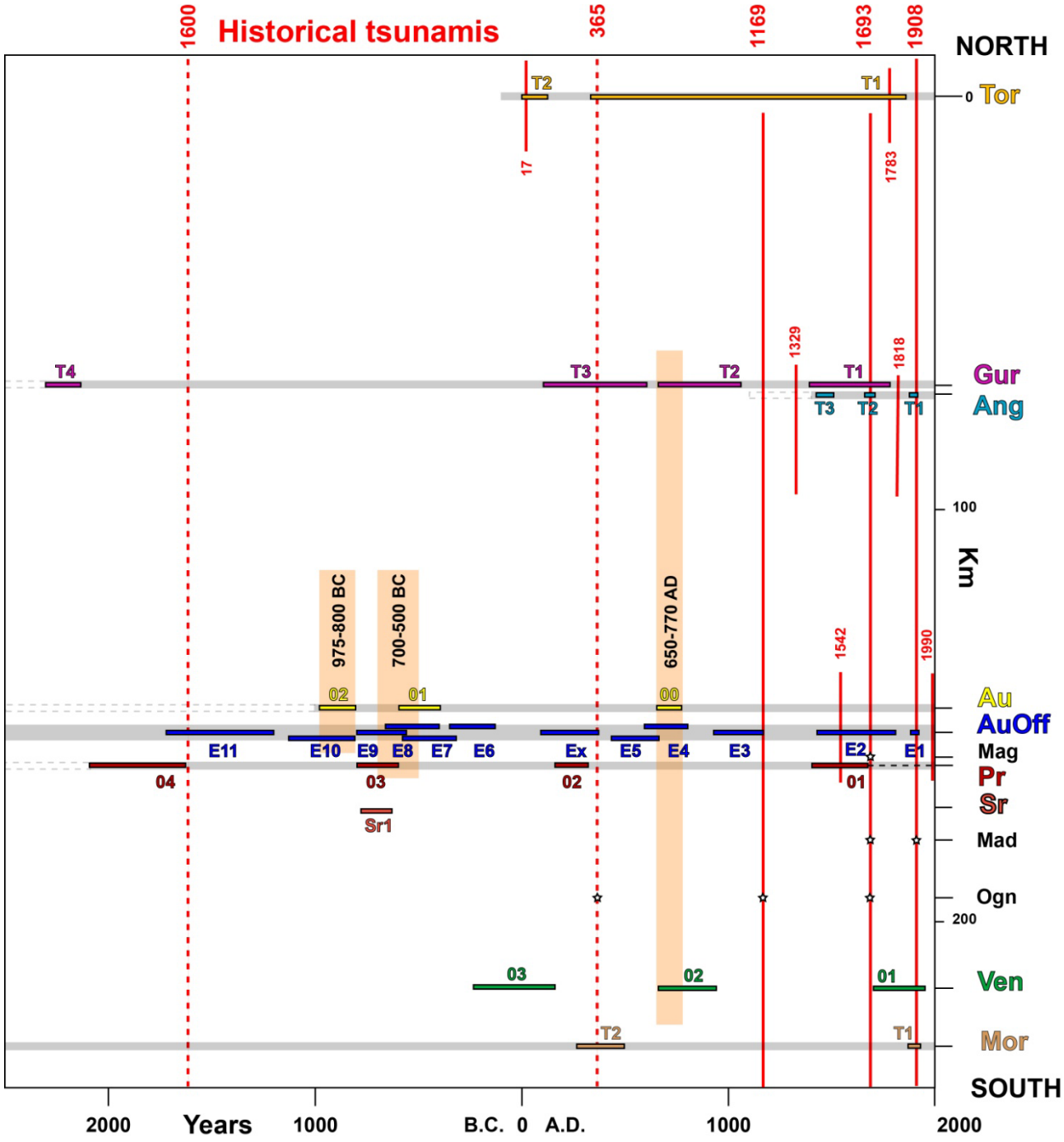

Fig. 17 – Space-time plot of the tsunamis identified along the coast of eastern Sicily (modified after De Martini et al., 2012). The distance (km) from the northern tip to the southern one of the rectified coastline is on the y-axis, while time (years) is on the x-axis. The sites investigated along the coast of eastern Sicily (De Martini et al., 2012; Scicchitano et al., 2007, 2010 and data from this thesis) are reported on the y axis: Tor=Torre degli Inglesi; Gur=Gurna; Ang=Anguillara; Au=Augusta; AuOff=Augusta Offshore; Pr=Priolo; Sr=Siracusa; Ven=Vendicari; Mor=Morghella; Mag=Magnisi P.; Mad=Maddalena P.; Ogn=Ognina). The horizontal coloured bars are the age intervals of the tsunamis (Scicchitano et al., 2007, 2010 events are marked with a star); horizontal light gray bars represent the time interval investigated at each site, it is dashed when extrapolated. The new potential events of Vendicari (Ven 03) and Siracusa (Sr1) are reported. Historical tsunamis dates are plotted with vertical red lines proportional to the known inundation

extent along the coast (dashed when inundation sites are unknown, e.g., 365 AD tsunami), while vertical hazel bars show the hypothesized best fitting age ranges for unknown tsunamis.

This work will be presented in a paper to be submitted to Annals of Geophysics:

High energy events in the Holocene stratigraphy: the Astarte EU Project Siracusa test site case study, SE Sicily, Italy (Simone Orefice, Alessandra Smedile, Stefania Pinzi and Paolo Marco De Martini).

References

Amore C., Costa B., Di Geronimo I., Giuffrida E., Randazzo G., Zanini A. (1994). Temporal evolution, sediments and fauna of the Vendicari lagoons (Siracusa), Studies on Ecology and Paleoecology of Benthic Communities, R. Matteucci et al. (eds). Boll. Soc. Paleont.Ital., Spec. Vol. 2, Mucchi, Modena, pp. 1-15.

Andrade C., (1992). Tsunami generated forms in the Algarve barrier island (South Portugal). In: Dawson, A.G. (Ed.), European Geophysical Union 1992 Tsunami Meeting. Science of Tsunami Hazard, vol. 10, pp. 21–34.

A.A.V.V., 1986. Carta Geologica del Settore Nord-Orientale Ibleo. S.El.Ca.Firenze.

Barbano M.S., Pirrotta C., Gerardi F., (2010). Large boulders along the south-eastern Ionian coast of Sicily: Storm or tsunami deposits?. Marine Geology, 275, 140 – 154.

Cimerman F., Langer M., (1991). Mediterranean foraminifera slovenska akademija znanosti in umetnosti, academiascientiarumartiumslovenica, classis IV, 1991. Historia Naturalia 30, Ljubliana.

De Martini P.M., Barbano M.S., Pantosti D., Smedile A. ,Pirrotta C. , Del Carlo P., and Pinzi S. (2012). Geological evidence for past-tsunamis along eastern Sicily (Italy): an overview, Nat. Hazards Earth Syst. Sci., 12, 2569-2580, doi:10.5194/nhess-12-1-2012.

De Martini, P.M., Barbano, M.S., Smedile, A., Gerardi, F., Pantosti, D., Del Carlo, P., Pirrotta, C, (2010). A unique 4000 year long geological record of multiple tsunami inundations in the Augusta Bay (eastern Sicily, Italy). Marine Geology, 276, 42-57, doi: 10.1016/j.margeo.2010.07.005

Fleming K., Johnston P., Zwartz D., Yokoyama Y., Lambeck K., Chappel J., (1998). Refining the eustatic sea-level curve since the Last Glacial Maximum using far and intermediate-fields sites. Earth and Planetary Science Letters 163, 327-342.

Gelfenbaum, G., Jaffe, B., (2003). Erosion and sedimentation from the 17 July, 1998 Papua New Guinea tsunami. Pure and Applied Geophysics 160, 1969–1999.

Gerardi F., Smedile A., Pirrotta C., Barbano M. S., De Martini P. M. ,Pinzi S. , Gueli A. M., Ristuccia G. M., Stella G., and Troja S. O., (2012). Geological record of tsunami inundations in Pantano Morghella (south-eastern Sicily) both from near and far-field sources. Nat. Hazards Earth Syst. Sci., 12, 1185–1200. doi: 10.5194/nhess-12-1185-2012.

Gianfreda F., Mastronuzzi G., Sansò P., (2001). Impact of historical tsunamis on a sandy coastal barrier: an example from the northern Gargano coast, southern Italy. Natural Hazards and Earth System Sciences (2001) 1: 213–219, ©European Geophysical Society 2001.

Goff J., Goff C.C., Nichol S., Jaffe B., Dominey-Howes D., (2012). Progress in palaeotsunami research Sedimentary Geology 243–244, 70–88

Goff J.R., Hicks D. M., Hurren H. Tsunami geomorphology in New Zealand. A new method for exploring the evidence of past tsunamis. NIWA Technical Report 2007.

Goff J., McFadgen B.G., Chagué-Goff C., (2004). Sedimentary differences between the 2002 Easter storm and the 15th century Okoropunga tsunami, southeastern North Island, New Zealand. Marine Geology 204, 235–250. doi:10.1016/S0025-3227(03)00352-9.

Koiwa N., Takahashi M., Sugisawa S., Ito A., Matsumoto H., Tanavud C., Goto K., (2017). Barrier spit recovery following the 2004 Indian Ocean tsunami at Pakarang Cape, southwest Thailand. Geomorphology (Accepted Manuscript), doi: 10.1016/j.geomorph.2017.05.003.

Lentini F., Carbone S., and Catalano S., (1994). Main structural domains of the central Mediterranean region and their Neogene tectonic evolution, Boll. Geofis. Teor. Appl., 36, 103–125.

Lentini F., Carbone S., and Guarnieri P., (2006). Collisional and postcollisional tectonics of the Apenninic-Maghrebian Orogen (Southern Italy), in: Post collisional tectonics and magmatism in the Mediterranean region and Asia, edited by: Dilek, Y. and Pavlides, S., Geological Society of America Special Papers, 409, 57–81.

Loeblich R., Tappan H., (1987). Foraminiferal Genera and Their Classification. Van Nostrand Reinhold, New York

Mastronuzzi G., Bruckner H., De Martini P.M., Regnauld H., (2013). Tsunami: from the open sea to the coastal zone and beyond: Mambretti S. (Ed), Tsunami: From Fundamentals to Damage Mitigation. WIT Press, Southampton, 1-36 pp.

Maramai A., Brizuela B., Graziani L. (2014). The Euro-Mediterranean Tsunami Catalogue. Annals of Geophysics, 57, 4, S0435. Doi: 10.4401/ag-6437

Maramai, A., Tinti, S., (1997). The 3 June 1994 Java tsunami: a post-event survey of the coastal effects. Natural Hazards 15 (1), 31–49.

Morton R.A., Gelfenbaum G., Jaffe B.E., (2007). Physical criteria for distinguishing sandy tsunami and storm deposits using modern examples. Sedimentary Geology, 200, 184 – 207.

Murray J.W., (2006). Ecology and Applications of Benthic Foraminifera. Cambridge University Press, Cambridge.

Nanayama F., Shigeno K., Satake K., Shimokawa K., Koitabashi S., Miyasaka S., Ishii M., (2000). Sedimentary differences between the 1993 Hokkaido–Nansei–Oki tsunami and the 1959 Miyakojima typhoon at Taisei, southwestern Hokkaido, northern Japan. Sedimentary Geology 135, 255–264

NGDC/WDS Global Historical Tsunami Database, 2100 BC to present. doi:10.7289/V5PN93H7

Paris R., Wassmer P., Sartohadi J., Lavigne F., Barthomeuf B., Desgages E., Grancher D., Baumert, P., Vautier F., Brunstein D., Gomez C., (2009). Tsunamis as geomorphic crises: Lessons from the December 26, 2004 tsunami in Lhok Nga, West Banda Aceh (Sumatra, Indonesia). Geomorphology 104(1–2), 59-72.

Peres J. M. and Picard J. (1964). Nouveau manuel de Bionomie bentique de la mer Mediterran´ee. Rec. Trav. Station Marine d'Endoume, 31, 1–137.

Pirrotta C., Barbano M. S., Pantosti D., De Martini P. M., (2013). Evidence of active tectonics in the Augusta Basin (eastern Sicily, Italy) by Chirp sub-bottom sonar investigation. Annals of Geophysics, 56, 5 S0562. doi:10.4401/ag-6371.

Reimer P. J., Baillie M. G. L., Bard E., Bayliss A., Beck J. W., Blackwell P. G., Bronk Ramsey C., Buck C. E., Burr G. S., Edwards R. L., Friedrich M., Grootes P. M., Guilderson T. P., Hajdas I., Heaton T. J., Hogg A. G., Hughen K. A., Kaiser K. F., Kromer B., McCormac F. G., Manning S. W., Reimer R. W., Richards D. A., Southon J. R., Talamo S., Turney C., S. M., Van Der Plicht J., and Weyhenmeyer C. E.(2009): IntCal09 andMarine09 radiocarbon age calibration curves, 0–50,000 years calBP, Radiocarbon, 51, 1111–1150.

Scicchitano G., Costa B., Di Stefano A., Longhitano S.G., Monaco C., (2010). Tsunami and storm deposits preserved within a ria-type rocky coastal setting (Siracusa, SE Sicily). Zeitschrift für Geomorphologie Vol. 54, Suppl. 3, 051-077.

Scicchitano G., Monaco, C., and Tortorici, L., (2007). Large boulder deposits by tsunami waves along the Ionian coast of south-eastern Sicily (Italy). Mar. Geol., 238, 75–91.

Sgarrella F., Moncharmont-Zei M., (1993). Benthic Foraminifera of the Gulf of Naples (Italy): systematics and autoecology. Bollettino della Società Paleontologica Italiana 32, 145–264.

Shiki T., Tachibana T., Fujiwara O., Goto K., Nanayama F., Yamazaki T., (2008). Characteristic features of tsunamiites. In: Shiki, T., Tsuji, Y., Yamazaki, T., Minoura, K. (Eds.), Tsunamiites — Features and Implications. Elsevier, Amsterdam, pp. 319–340.

Smedile A., De Martini P. M., Pantosti D., Bellucci L., Del Carlo P., Gasperini L., Pirrotta C., Polonia A., and Boschi E., (2011). Possible tsunamis signatures from an integrated study in the Augusta Bay offshore (Eastern Sicily–Italy). Mar. Geol., 281,1–13.

Shi, S., Dawson, A.G., Smith, D.E., (1995). Coastal sedimentation associated with the December 12th, 1992 tsunami in Flores, Indonesia. Pure and Applied Geophysics 144, 525–536.

Stuiver, M. and Reimer, P.J. (1993). Extended 14C database and revised CALIB radiocarbon calibration program. Radiocarbon, 35, 215-230, (last access: October 2016).

Tanaka, H., Tinh, N.X., Umeda, M., Hirao, R., Pradojoko, E., Mano, A., Udo, K., (2012). Coastal and estuarine morophology changes induced by the 2011 Great East Japan Earthquake Tsunami. Coastal Engineering Journal 54(1), 1250010-1-1250010-25.

Tanner L.H., Calvari S., (2004). Unusual sedimentary deposits on the SE side of Stromboli volcano, Italy: products of a tsunami caused by the ca. 5000 years BP Sciara del Fuoco collapse?. Journal of Volcanology and Geothermal Research 137, 329– 340.

Terry J.P.; Goff J., (2014). Megaclasts: Proposed Revised Nomenclature At the Coarse End of the Udden-Wentworth Grain-Size Scale for Sedimentary Particles. Journal of Sedimentary Research, 84(3-4):192-197.

Umitsu, M., Tanavud, C., Patanakanog, B., (2007). Effects of landforms on tsunami flow in the plains of Banda Aceh, Indonesia, and Nam Khem, Thailand. Marine Geology 242, 141-153.

Tuttle M.P., Ruffman A., Anderson T., Jeter H., (2004). Distinguishing tsunami from storm deposits in eastern North America: the 1929 Grand Banks tsunami versus the 1991 Halloween storm. Seismological Research Letters 75, 117–131.

Appendix

Stratigraphic logs

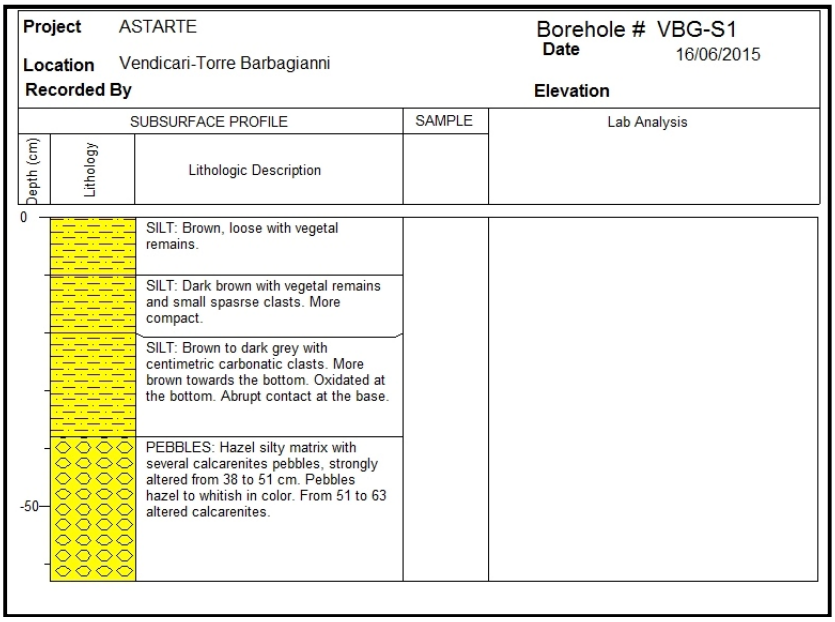

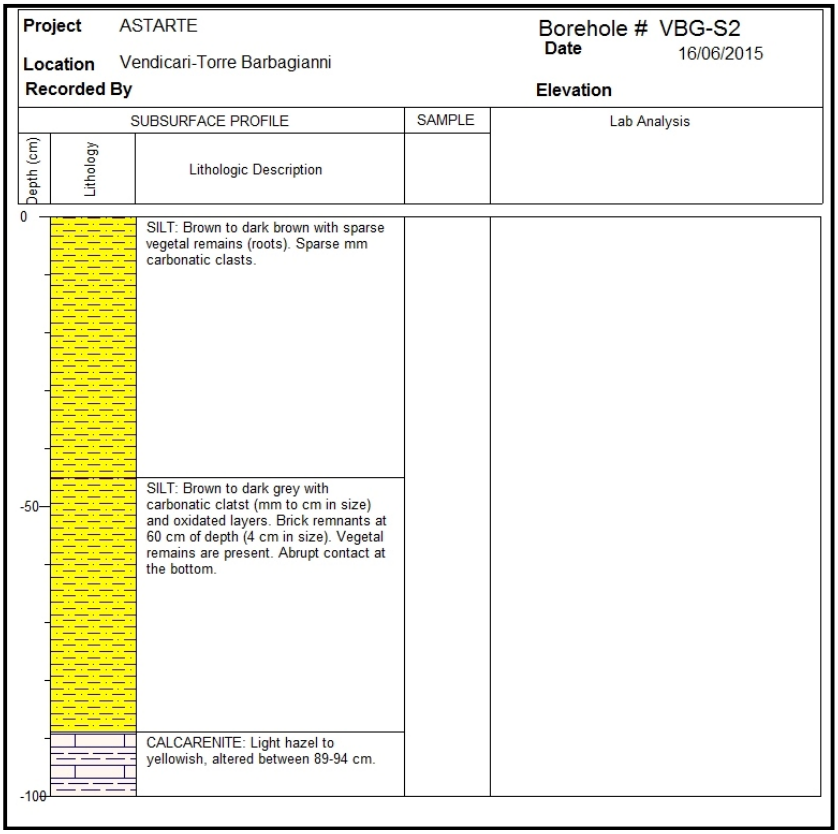

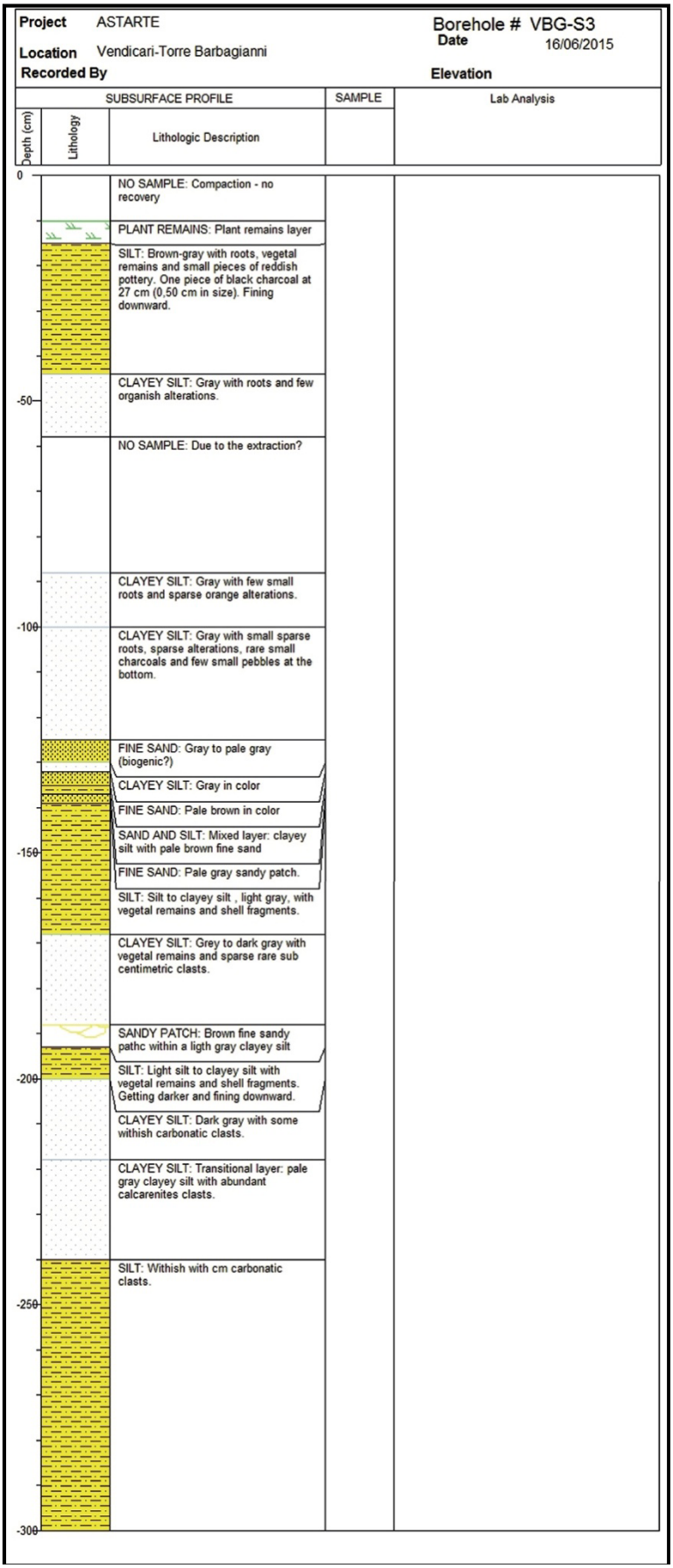
Project ASTARTE
Borehole # VBG-S3
Location Vendicari-Torre Barbagianni
Date 16/06/2015
Recorded By
Elevation
SUBSURFACE PROFILE
SAMPLE
Lab Analysis
Depth (cm)
Lithology
Lithologic Description
0
-50
-100
-150
-200
-250
-300
NO SAMPLE: Compaction - no recovery
PLANT REMAINS: Plant remains layer
SILT: Brown-gray with roots, vegetal remains and small pieces of reddish pottery. One piece of black charcoal at 27 cm (0,50 cm in size). Fining downward.
CLAYEY SILT: Gray with roots and few organish alterations.
NO SAMPLE: Due to the extraction?
CLAYEY SILT: Gray with few small roots and sparse orange alterations.
CLAYEY SILT: Gray with small sparse roots, sparse alterations, rare small charcoals and few small pebbles at the bottom.
FINE SAND: Gray to pale gray (biogenic?)
CLAYEY SILT: Gray in color
FINE SAND: Pale brown in color
SAND AND SILT: Mixed layer: clayey silt with pale brown fine sand
FINE SAND: Pale gray sandy patch.
SILT: Silt to clayey silt , light gray, with vegetal remains and shell fragments.
CLAYEY SILT: Grey to dark gray with vegetal remains and sparse rare sub centimetric clasts.
SANDY PATCH: Brown fine sandy pathc within a ligth gray clayey silt
SILT: Light silt to clayey silt with vegetal remains and shell fragments. Getting darker and fining downward.
CLAYEY SILT: Dark gray with some withish carbonatic clasts.
CLAYEY SILT: Transitional layer: pale gray clayey silt with abundant calcarenites clasts.
SILT: Withish with cm carbonatic clasts.

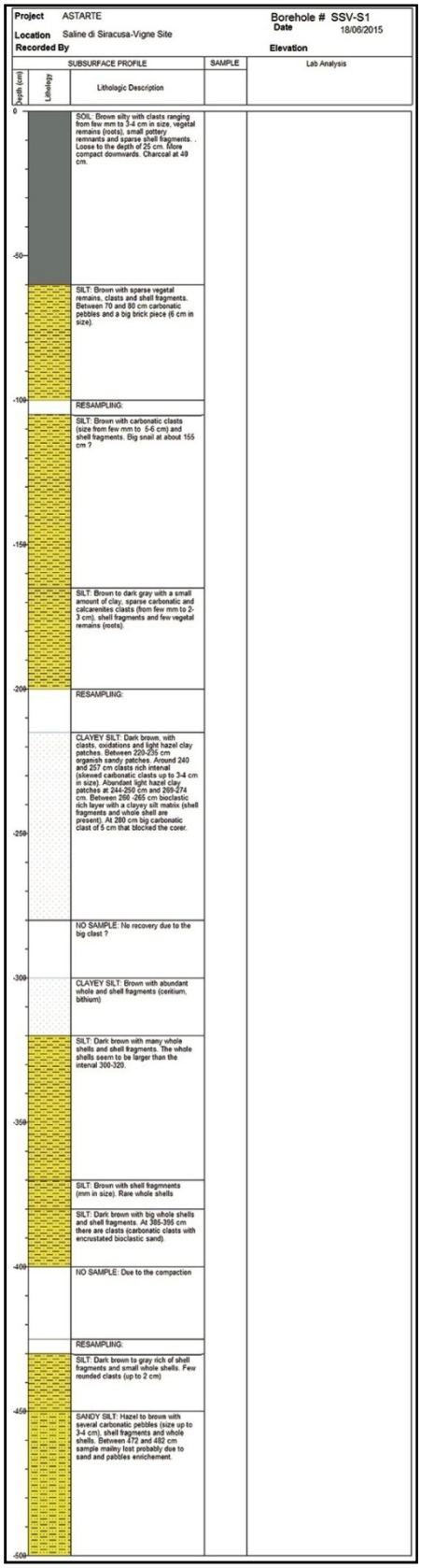
Project ASTARTE
Borehole # SSV-S1
Location Saline di Siracusa-Vigne Site
Date 18/06/2015
Recorded By
Elevation
SUBSURFACE PROFILE
SAMPLE
Lab Analysis
Depth (cm)
Lithology
Lithologic Description
0
-50
-100
-150
-200
-250
-300
-350
-400
-450
-500
SOIL. Brown silty with clasts ranging from few mm to 3-4 cm in size, vegetal remains (roots), small pottery remnants and sparse shell fragments. . Loose to the depth of 25 cm. More compact downwards. Charcoal at 49 cm.
SILT: Brown with sparse vegetal remains, clasts and shell fragments. Between 70 and 80 cm carbonatic pebbles and a big brick piece (6 cm in size).
RESAMPLING:
SILT: Brown with carbonatic clasts (size from few mm to 5-6 cm) and shell fragments. Big snail at about 155 cm ?
SILT: Brown to dark gray with a small amount of clay, sparse carbonatic and calcarenites clasts (from few mm to 2-3 cm), shell fragments and few vegetal remains (roots).
RESAMPLING:
CLAYEY SILT: Dark brown, with clasts, oxidations and light hazel clay patches. Between 209-235 cm organish sandy patches. Around 240 and 257 cm clasts rich interval (sheved carbonatic clasts up to 3-4 cm in size). Abundant light hazel clay patches at 244-250 cm and 269-274 cm. Between 260 -265 cm bioclastic rich layer with a clayey silt matrix (shell fragments and whole shell are present). At 280 cm big carbonatic clast of 5 cm that blocked the corer.
NO SAMPLE: No recovery due to the big clast ?
CLAYEY SILT: Brown with abundant whole and shell fragments (centium, bithium)
SILT: Dark brown with many whole shells and shell fragments. The whole shells seem to be larger than the interval 300-320.
SILT: Brown with shell fragmnents (mm in size). Rare whole shells
SILT: Dark brown with big whole shells and shell fragments. At 385-395 cm there are clasts (carbonatic clasts with encrustated bioclastic sand).
NO SAMPLE: Due to the compaction
RESAMPLING:
SILT: Dark brown to gray rich of shell fragments and small whole shells. Few rounded clasts (up to 2 cm)
SANDY SILT: Hazel to brown with several carbonatic pebbles (size up to 3-4 cm), shell fragments and whole shells. Between 472 and 482 cm sample mainly lost probably due to sand and pebbles enrichement.

Sedimentological data

VBG-S4-0S (291-292 cm)

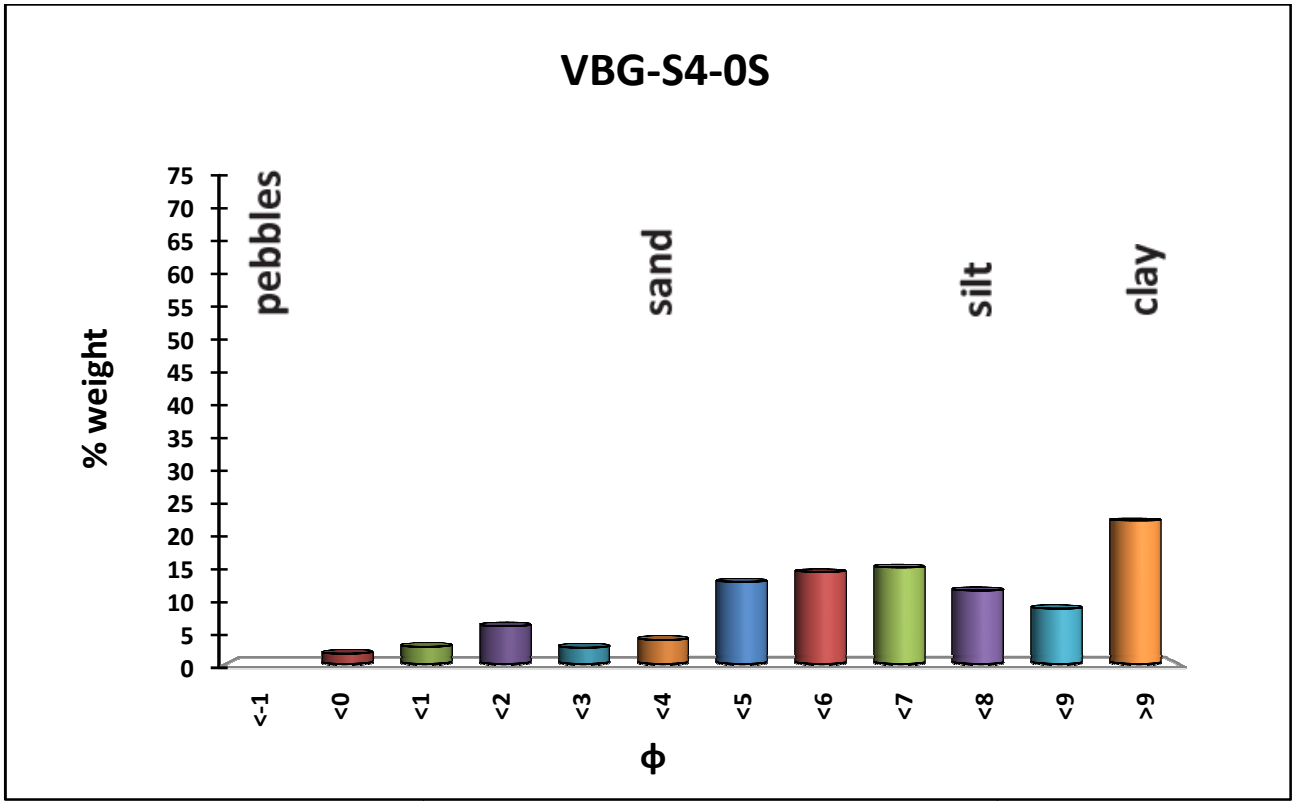

Total clay 30, 70%
Total silt 53, 09%
Total sand 16,21%
The sample can be defined a clayey silt with sand

VBG-S4-1S (127-132 cm)

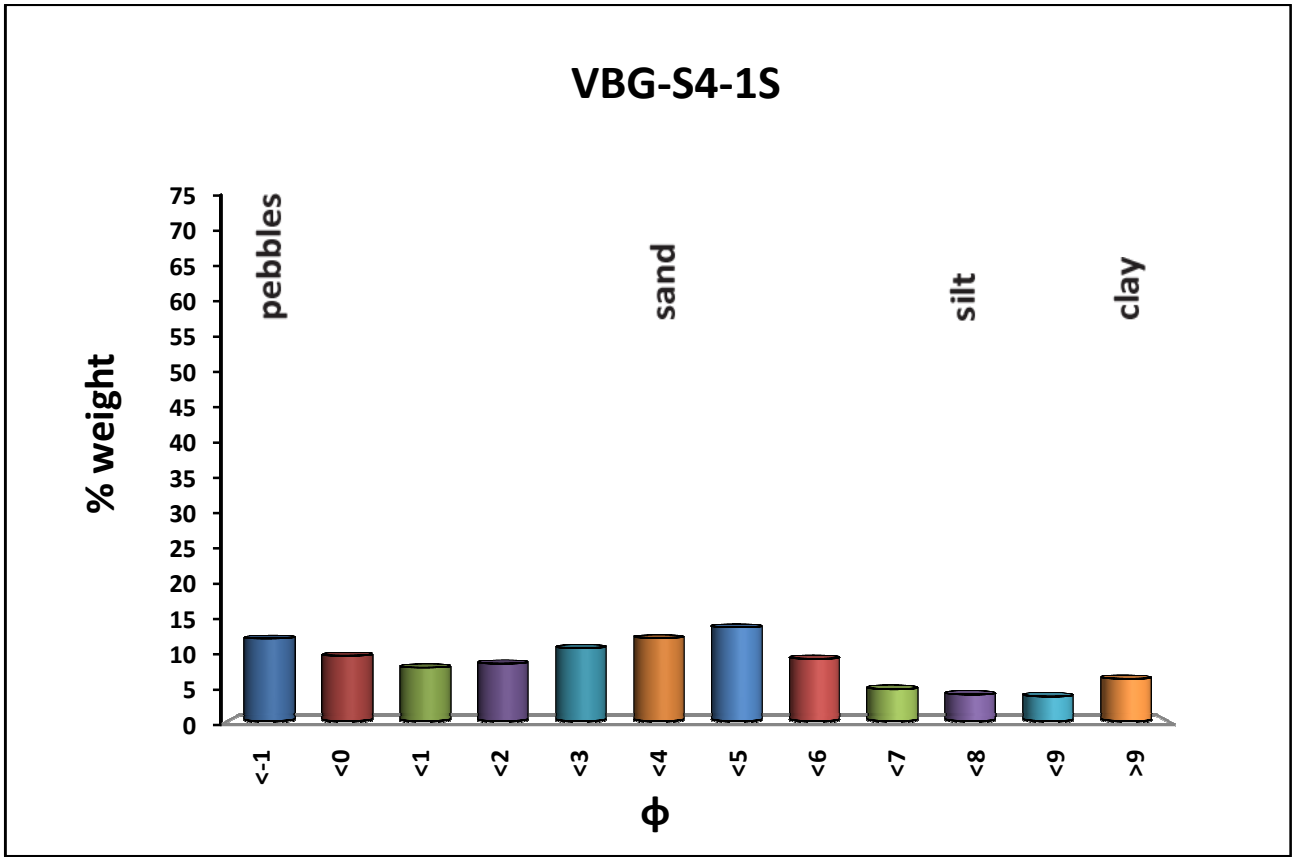

Total clay 9,60%
Total silt 30,83%
Total sand 47,71 %
Total pebbles 11,86%
The sample can be defined a silty sand with pebbles and clay

VBG-S4-2S (100-105 cm)

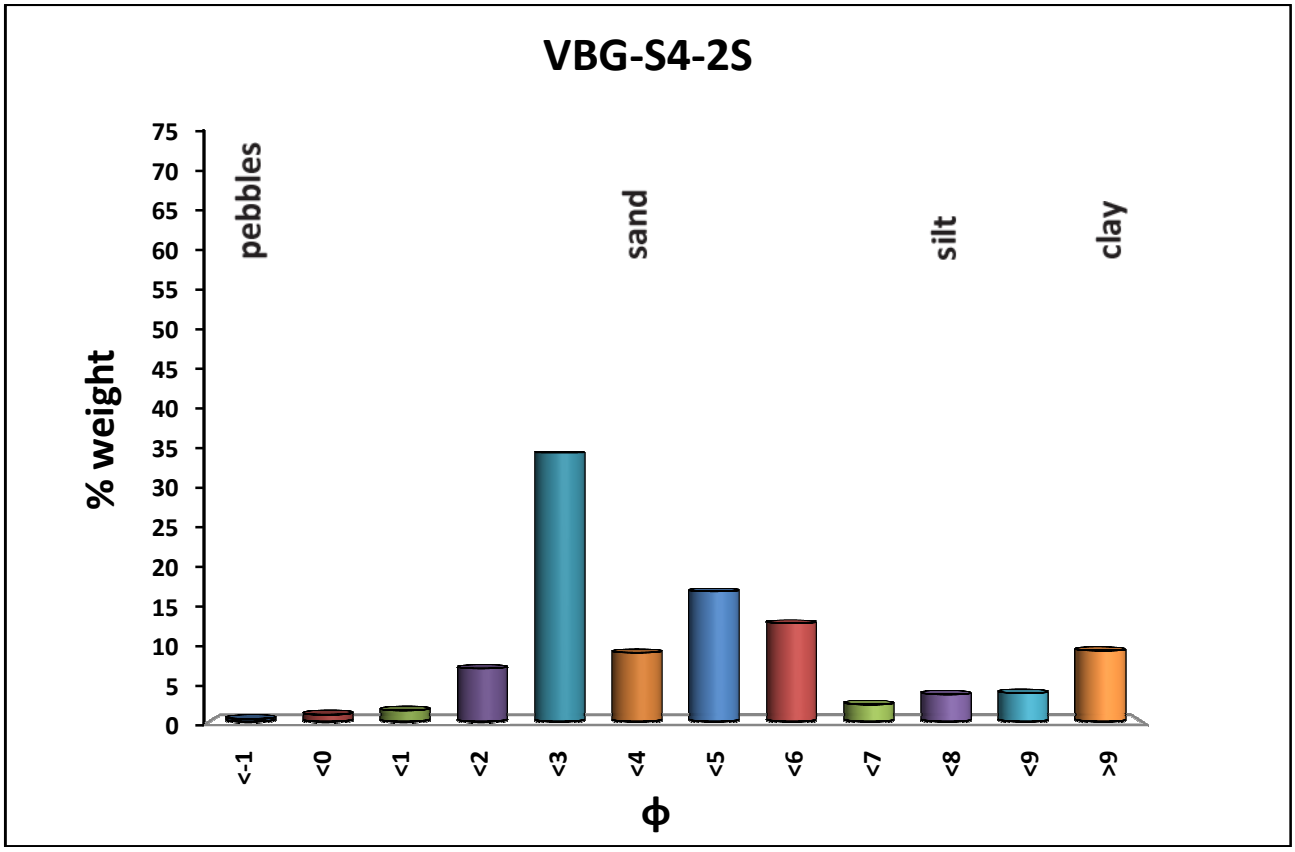

Total clay 12,68%
Total silt 34,81%
Total sand 52,19%
Total pebbles 0,32%
The sample can be defined a silty sand with clay

VBG-S4-3S (74-78 cm)

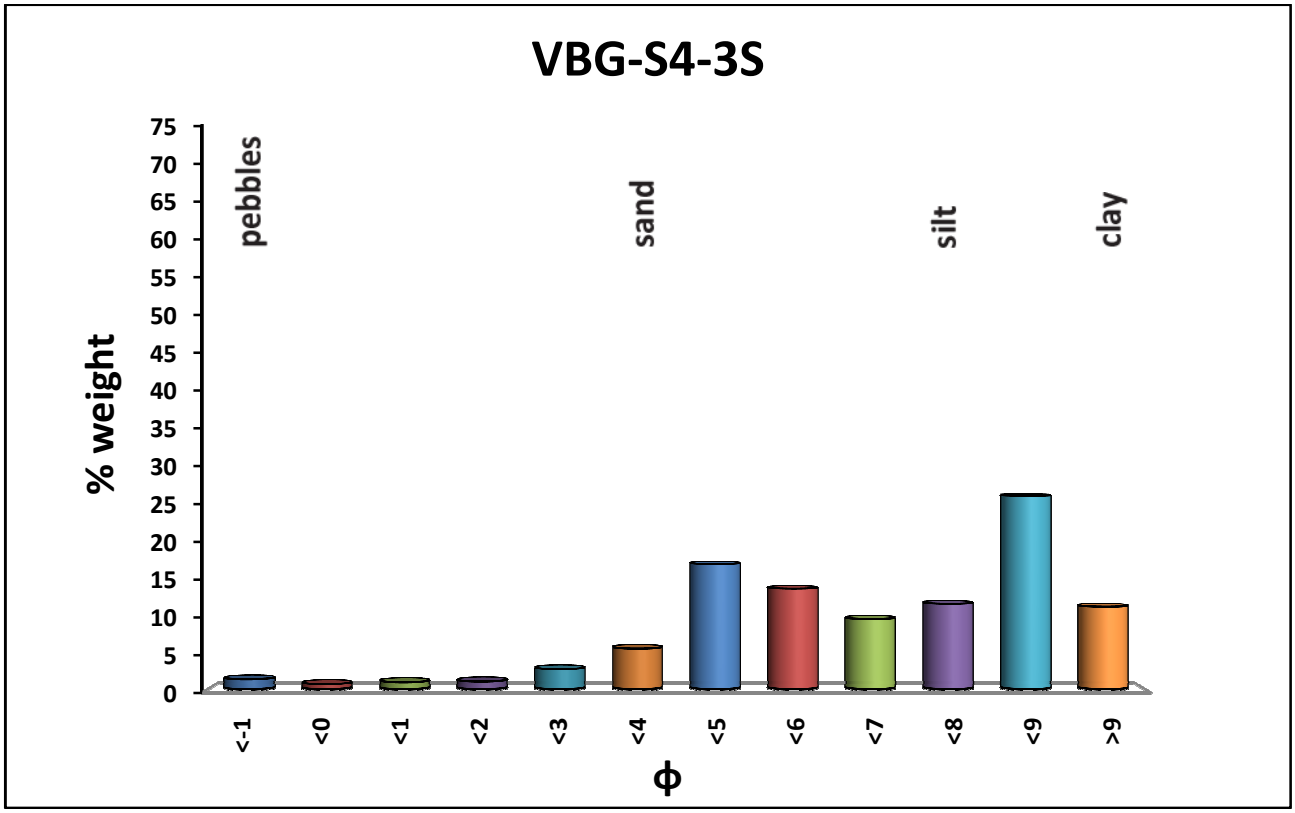

Total clay 36,92%
Total silt 51,02%
Total sand 10,74%
Total pebbles 1,32%
The sample can be defined a clayey silt with sand

VBG-S5-3S (113-119 cm)

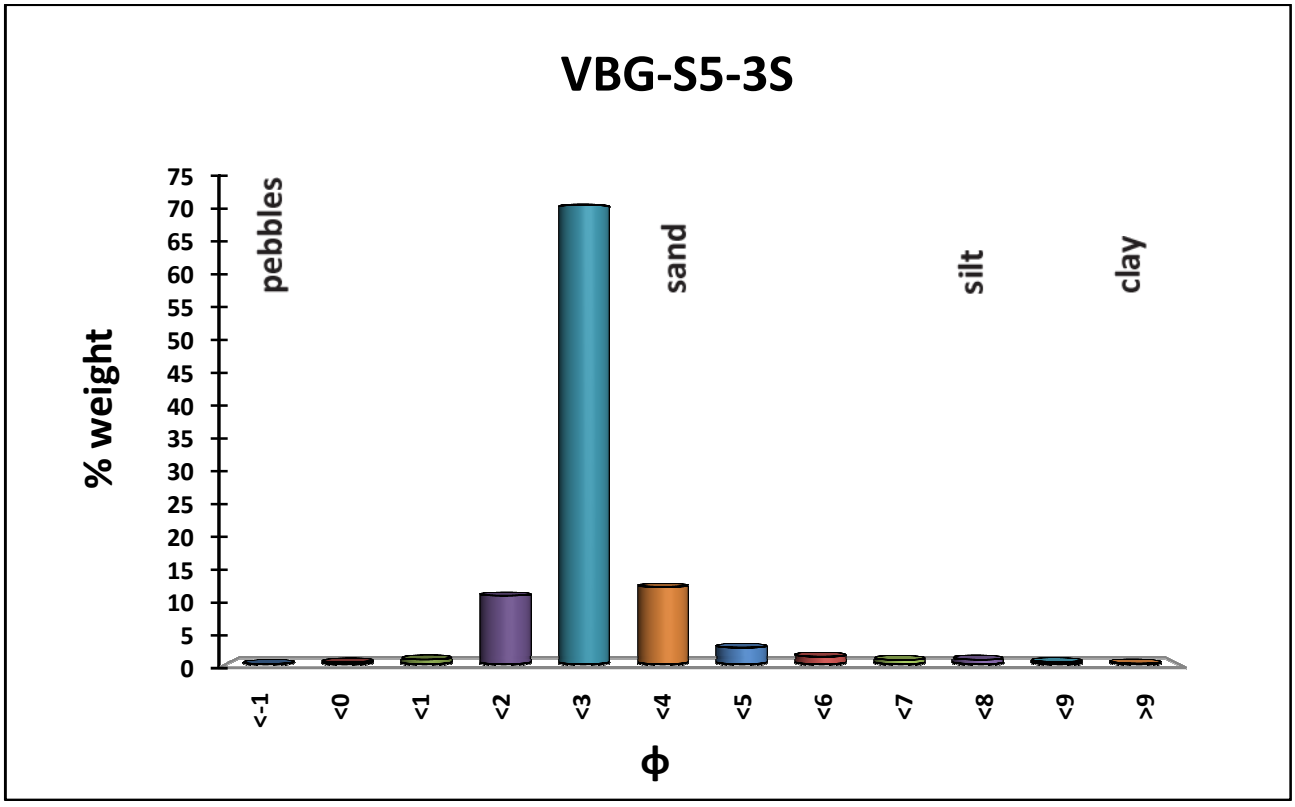

Total clay 0,41
Total silt 5,09%
Total sand 94,48%
Total pebbles 0,02%
The sample can be defined a fine sand

VBG-S5-4S (119-124 cm)

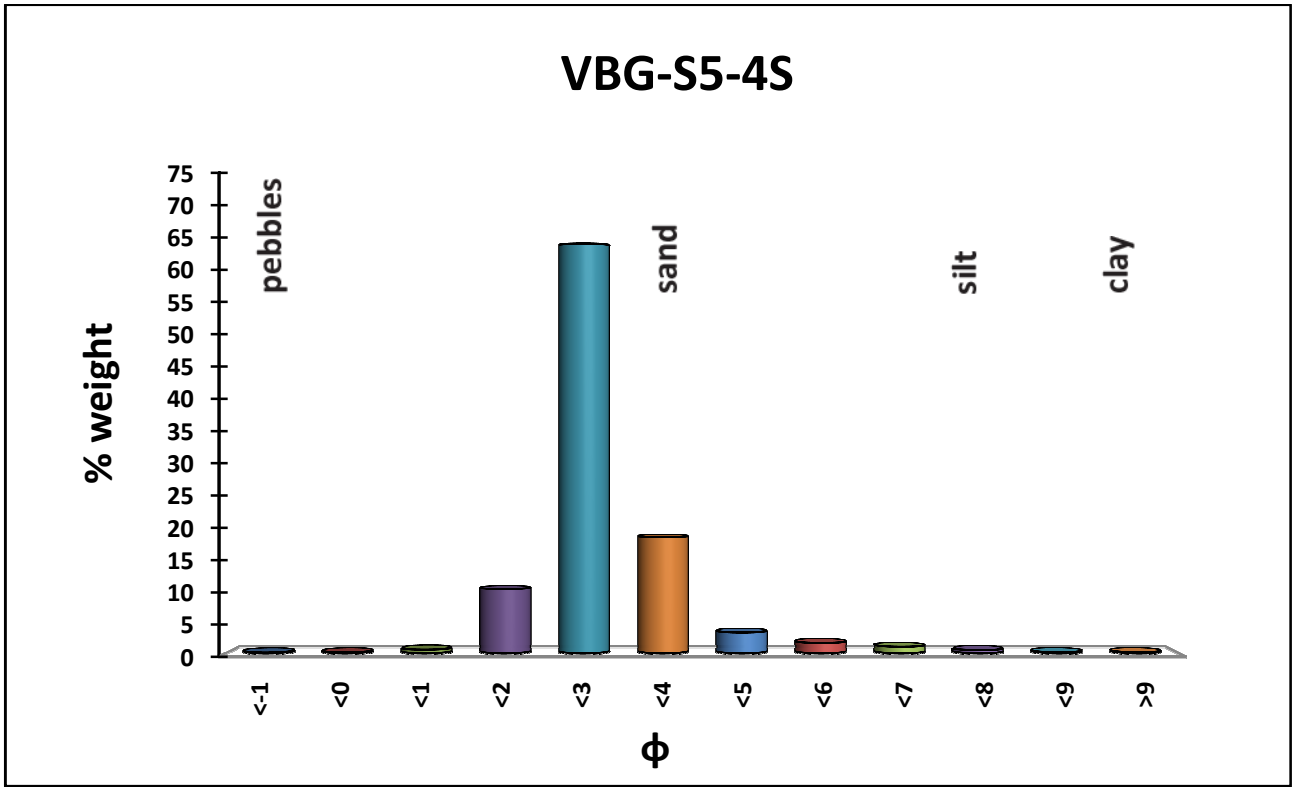

Total clay 0,30
Total silt 6,33%
Total sand 93,26%
Total pebbles 0,12%
The sample can be defined a fine sand

SSV-S2-1S (83-88 cm)

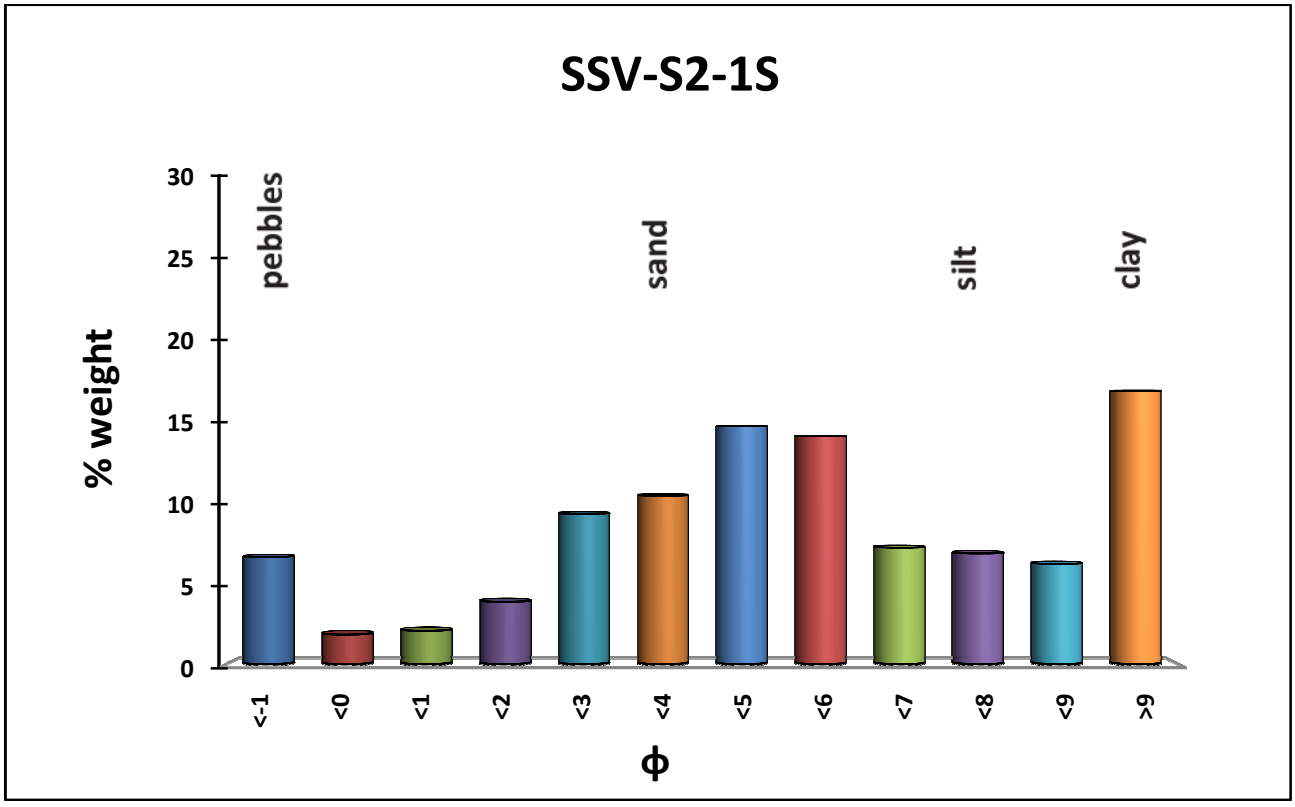

Total clay 23,08 %
Total silt 42,85%
Total sand 27,46%
Total pebbles 6,62%
The sample can be defined a sandy clayey silt with few pebble

SSV-S2-2S (192-197 cm)

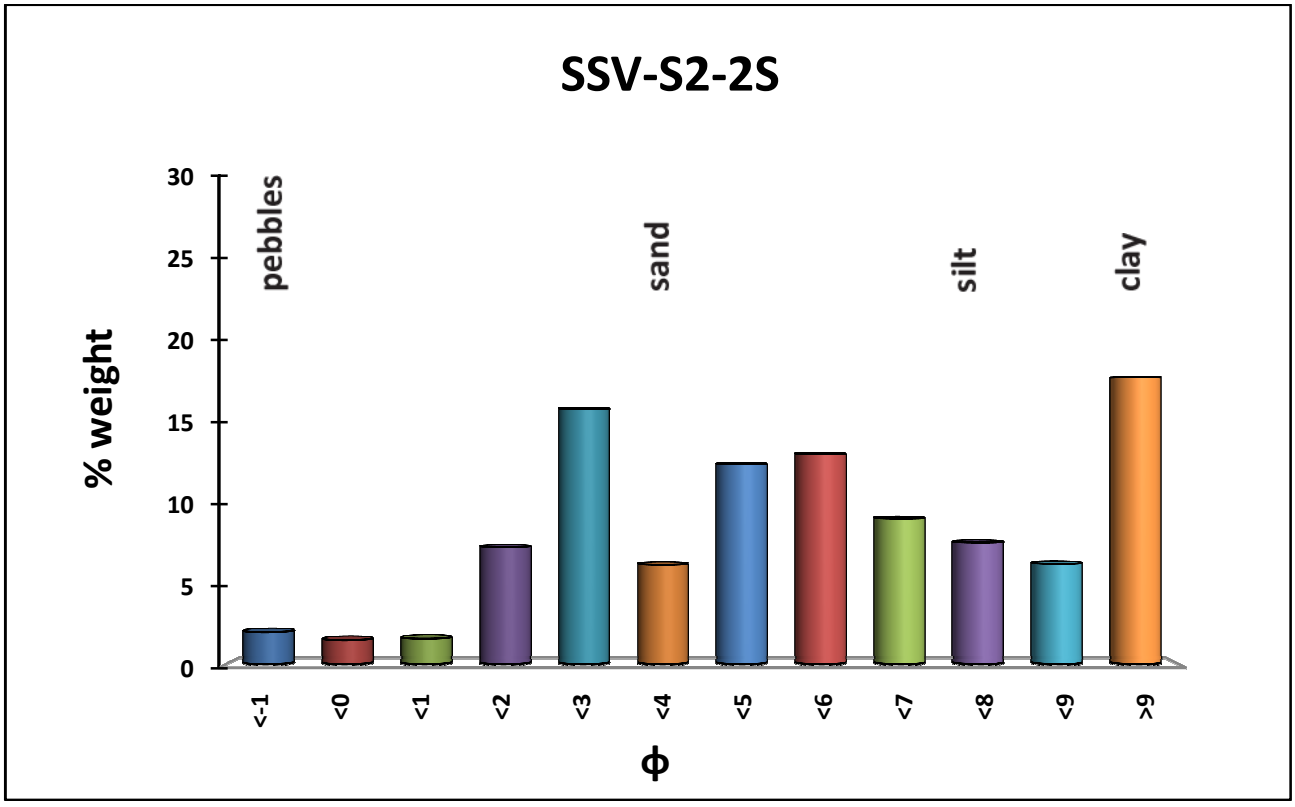

Total clay 23,92 %
Total silt 41,87%
Total sand 32,23%
The sample can be defined a sandy silt with clay

SSV-S2-3S (264-269 cm)

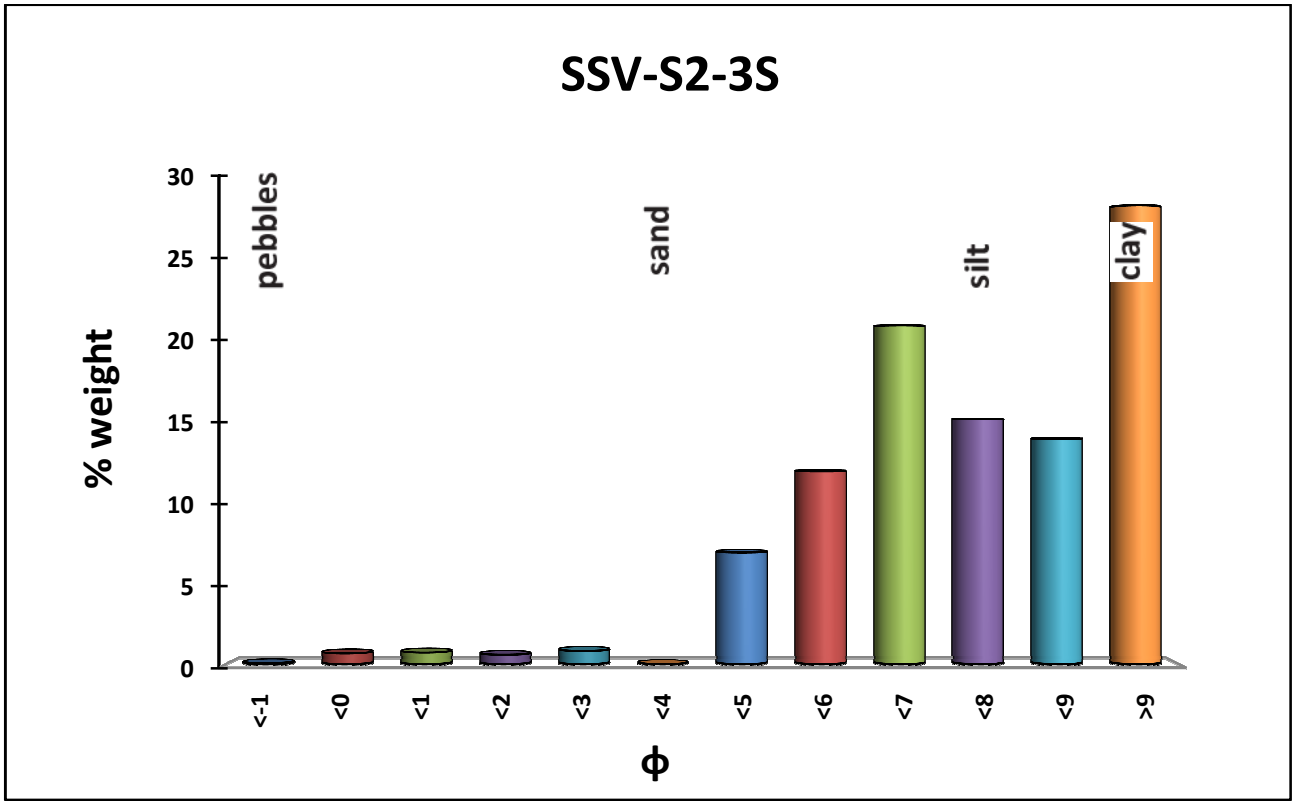

Total clay 42,26 %
Total silt 54,88%
Total sand 2,8%
The sample can be defined a clayey silt

SSV-S2-4S (332-337 cm)

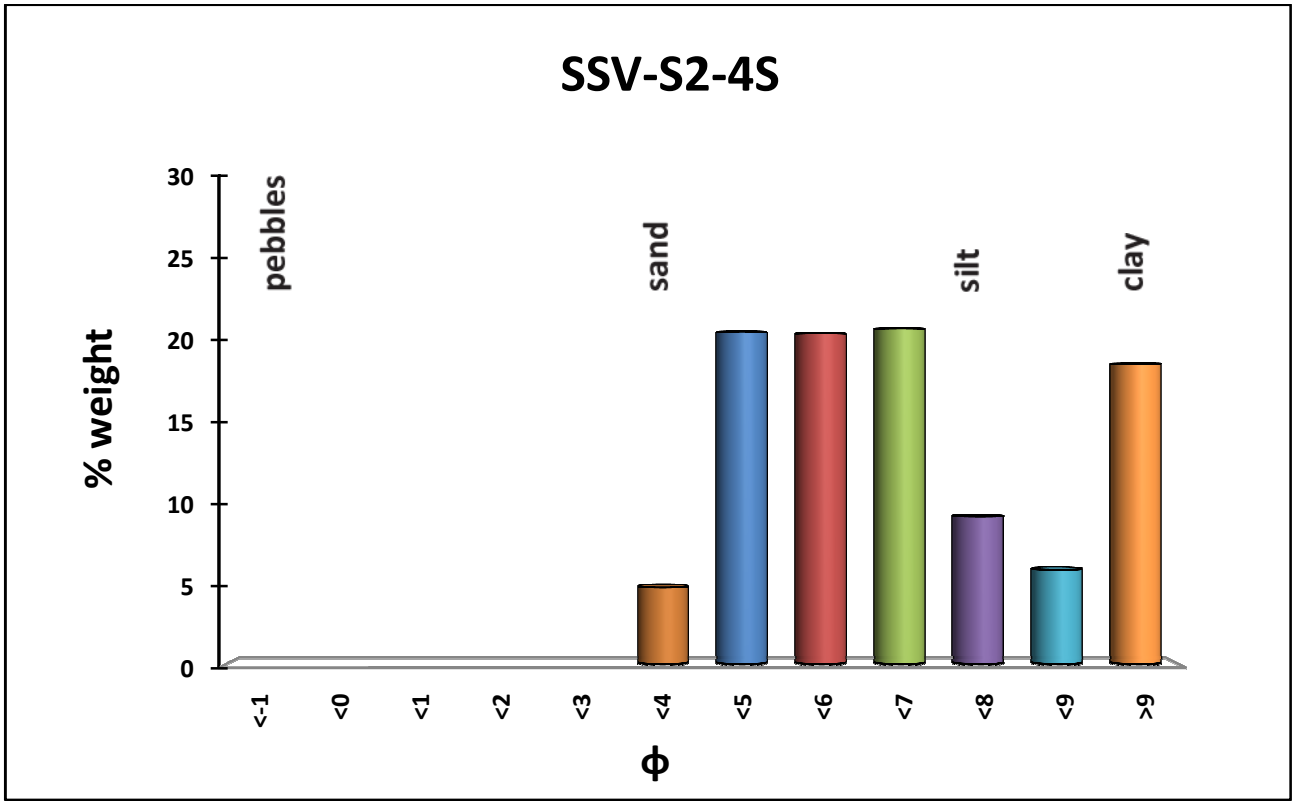

Total clay 24,4 %
Total silt 70,86%
Total sand 4,74%
The sample can be defined a clayey silt

SSV-S3-1S (390-395 cm)

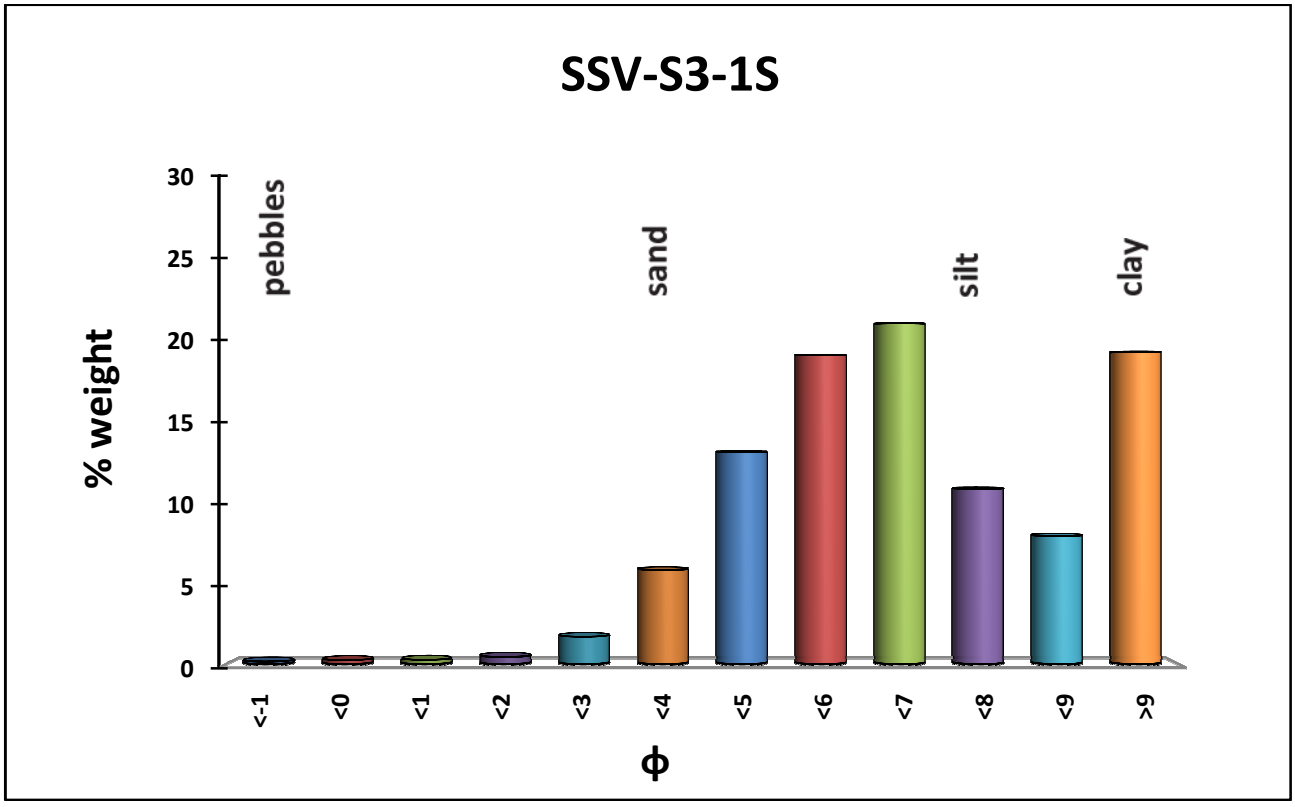

Total clay 27,22 %
Total silt 64,13%
Total fine sand 8,49%
The sample can be defined a clayey silt with few fine sand

SSV-S3-2S (505-510 cm)

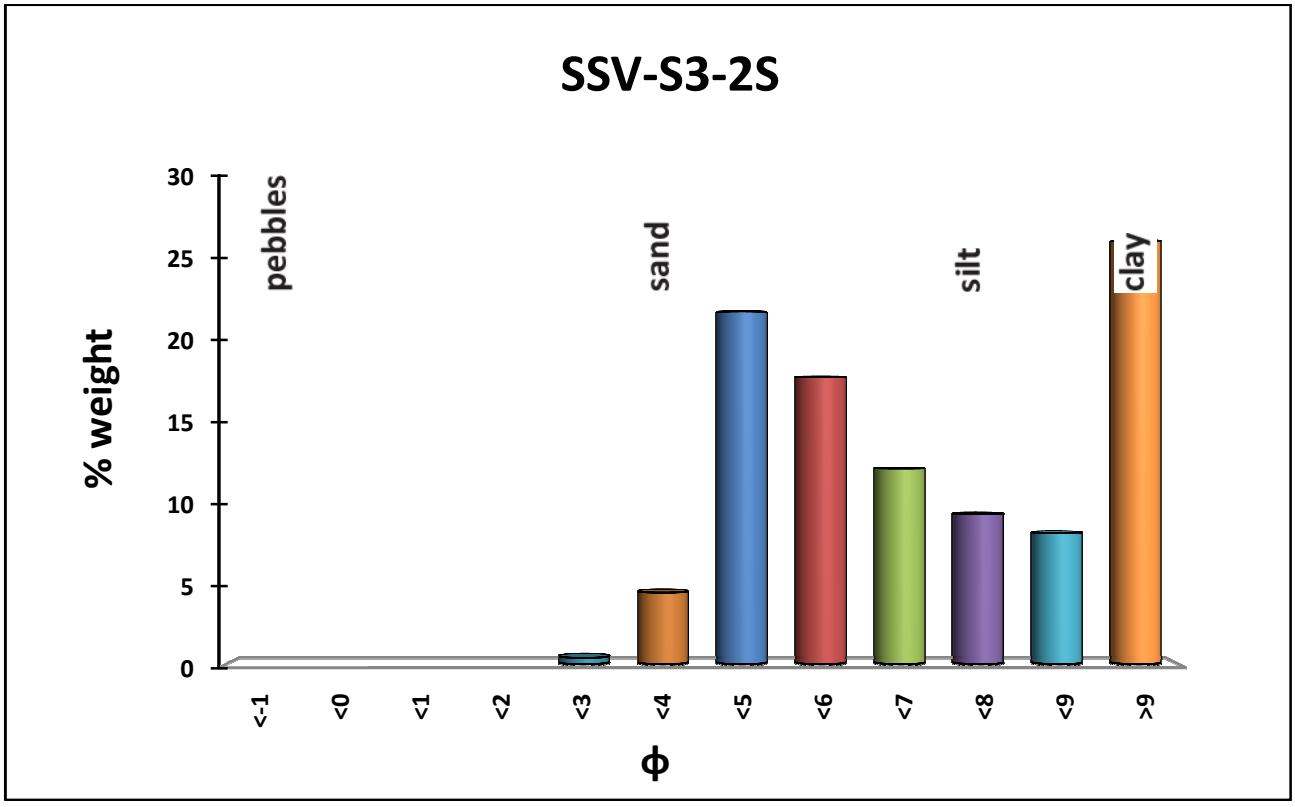

Total clay 34,28 %
Total silt 60,31%
Total fine sand 4,82%
The sample can be defined a clayey silt with few fine sand

The grain-size classification refers to the graph below by Wentworth , 1922.

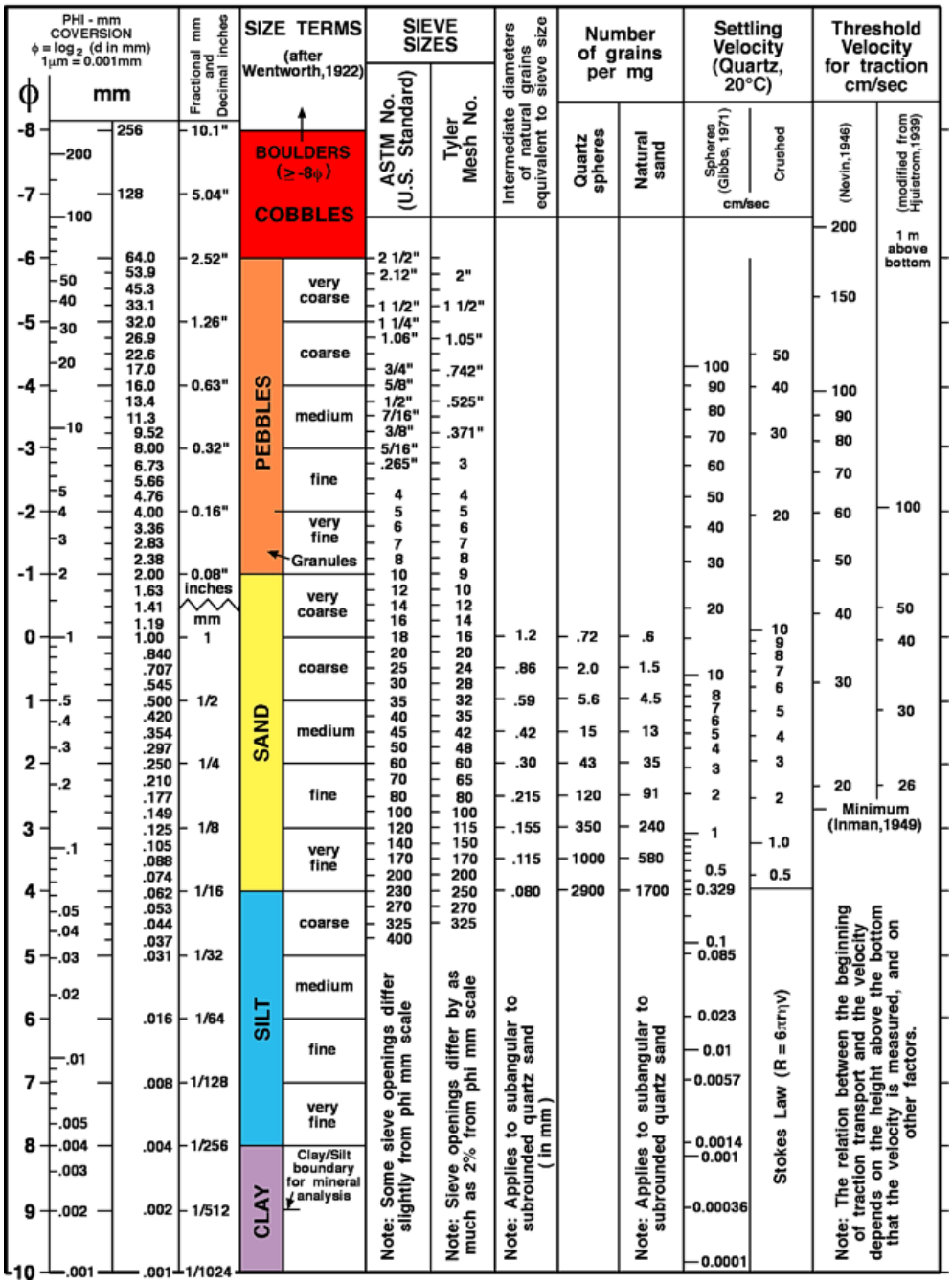

Chapter 3

Application Of The Amplification Factor Method In The Neam Region (North East Atlantic, Mediterranean And Its Connected Seas Region)

This work has been supported by the European Union's Seventh Framework Programme (FP7/2007-2013) under grant agreement 603839 (Project ASTARTE), and by the TSUMAPS NEAM Project, co-financed by the European Union Civil Protection Mechanism, Agreement Number: ECHO/SUB/2015/718568/PREV26.

The TSUMAPS-NEAM project (http://www.tsumaps-neam.eu/) produced the first region-wide long-term homogenous Probabilistic Tsunami Hazard Assessment (PTHA) map from earthquake sources for the coastlines of the North-East Atlantic, the Mediterranean, and connected Seas (NEAM) region. It represents a kind of spin-off of the ASTARTE project. EU project ASTARTE (www.astarte-project.eu) aimed at developing a higher level of tsunami hazard assessment in the North East Atlantic and Mediterranean (NEAM) region by a combination of field work, experimental work, numerical modeling and technical development.

1. Introduction

Tsunamis are low frequency high impact natural disasters. In the last two decades the destructive tsunami events of 2004 Indian Ocean and 2011 Tohoku caused loss and damages to both human coastal communities and related environments. At the same time, indirect consequences in terms of economic issues had global repercussions. Moreover, non-natural phenomena, like the Fukushima nuclear disaster, have determined a huge worsening of the tsunami consequences. These events highlighted the necessity to assess the tsunami inundations risk worldwide. Direct past tsunami observations are rare and scarce (Costa et al., 2016; De Martini et al., 2017). Geological and historical records of past tsunamis inundations are discontinuous in space and time and along most of the coastlines are totally absent due to a lack of specific investigation as well as complex geological processes and geomorphic settings preventing the preservation of such evidence. Nowadays the numerical simulations of these extreme events can provide a hazard assessment from a regional point of view as well as from a local point of view (Tonini et al., 2011; Løvholt et al., 2014).

2. Tsunami hazard assessment methods

Natural phenomena representing a hazard for the society have the necessity to be characterized in order to estimate a well-based risk assessment. The risk induced by natural phenomena is commonly based on the combination of three main factors: the probability that a certain event can occur (defined as the hazard), the value of the assets that may be affected by the event (defined as

the vulnerability) and the extent of damages that the event may induce in these assets (the value), (ASTARTE, DELIVERABLE D8.39).

A modeling approach is considered a viable procedure to estimate the hazard of a natural phenomena like a tsunami. Tsunami modeling, sometimes together with the spatial distribution of the geological evidence of past tsunamis (where available), can provide scenarios for the forecast of futures inundations. From a general point of view, tsunami modeling can be divided in three phases: generation, propagation and inundation. The generation phase includes the physical movement of the rock into the water, giving origin to the water displacement and exchange of energy between the rock and the water (Gisler, 2008). The propagation phase is characterized by a waves train, modeled in two dimension, travelling over a varying depth seafloor (Gisler, 2008). When the waves train approaches to the coast the inundation phase takes place. These three phases are often processed distinctly to each other. In tsunami simulations, approximations are usually used mainly in the propagation phase (e.g. the shallow water equations theory; Titov et al., 1997) as well as in the inundation phase.

The computationally-based hazard assessments are complex and characterized by a number of uncertainties that should be taken into account. Nowadays, in order to assess the hazard, several methods are adopted.

The Probabilistic Tsunami Hazard Analysis (PTHA, Geist and Parsons, 2006; Annaka et al., 2007; Thio et al., 2007) has the aim to determine the probability of exceedance of a given tsunami value (flow depth, run-up etc.) over a given exposure time for a selected coastal area, taking into account an uncertainty value. PTHA should take into account all earthquake sources that may cause a tsunami according to an earthquake probability model for a given region. For these sources, the parameters and the probability model describing the source recurrence in time, are defined (e.g. Geist & Lynett, 2014; Selva et al., 2016). Then, a hydrodynamic modeling for each source is computed. The final result is expressed by a hazard curve or by a family of hazard curves spanning the epistemic uncertainty. The hazard curve shows the probability that a given value of the chosen hazard intensity is exceeded. In the tsunami hazard context, this hazard intensity is often represented by run-up. The run-up is the (vertical) difference between the maximum topographic height reached inland and the reference sea level at the time of the tsunami. Another approach, called Empirical PTHA, takes as reference the effects of tsunamis recorded in the past, typically maximum run-ups for events occurred in the pre-instrumental era and tide-gauge and deep ocean sensor records for more recent events. These are treated statistically to retrieve tsunami activity rates and height-frequency relationships (ASTARTE, DELIVERABLE D8.39 - Quantifying and managing uncertainty in tsunami risk assessment methods: application to the ASTARTE test sites.

Contributors: J. Selva, S. Lorito, S. Orefice, B. Brizuela, S. Iqbal, F. Romano, M. Volpe, R. Tonini, R. Basili, M.M. Tiberti). Tsunami hazard analysis also follow a Scenario-Based Approach, SBTHA (Tinti and Armigliato, 2003; Løvholt et al., 2006; Lorito et al., 2008; Okal and Synolakis, 2008). The SBTHA method aims to estimate the credible – worst – scenarios for a specific site/coastal area. This procedure is articulated in two steps. The first one is the choice of the source areas for the target sites. This step is conducted thorough the analysis of catalogues of historical occurrences of a given tsunamigenic source type (in this method also landslides and volcanoes are considered), analysis of available databases/studies of potential/known tsunamigenic sources and analysis of the geomorphology and geodynamics of the selected geographical domain (ASTARTE, DELIVERABLE D8.39). The second step is based on the choice of the "credible worst case". For example for a seismogenic source the maximum credible value of magnitude is considered. Typical products of the SBTHA are aggregated fields of maximum water height (offshore and inland), flow depth onshore, particle velocities (offshore and onshore), maximum momentum flux (onshore), (ASTARTE, DELIVERABLE D8.39).

From a general point of view numerical simulations of tsunami inundation (to estimate tsunami run-up) can be computationally costly (Geist and Lynett, 2014). Several methods have been proposed to deal with this issue as far as local detailed PTHA is concerned (e.g. Lorito et al., 2015). In order to avoid costly inundation simulations when the scope of the assessment is regional, or for example in cases where very detailed topo - bathymetric data are not available, approximated methods to estimate run-up and inundation maps are often used. The amplification factor method is an approximated method, proposed and validated by Løvholt et al. (2012), to estimate run-up values and inundation distances along a stretch of coast. Moreover, the amplification factor method can be used in the context of PTHA, to provide regional tsunami hazard maps. Such an approach has been used for global PTHA (Davies et al., 2017).

An improved amplification factor procedure based on the use of the local bathymetric profiles instead of idealized profiles has been developed during the ASTARTE project (ASTARTE Deliverable D8.39). According to this procedure, in collaboration with TSUMAPS-NEAM partners, I performed the characterization of the coastal slopes of the NEAM region, to be used for amplification factors calculation. I also performed a comparison between the maximum water elevations, obtained from the factors method, and the results derived from conventional inundation models (e.g. ComMIT, COMmunity Model Tsunami Interface), thus contributing to uncertainty estimation of the amplification factors themselves.

3. The amplification factor procedure

This procedure consists in relating the water surface elevation at a given isobath, (from a tsunami simulation) with the maximum surface elevation during inundation past the shoreline using a set of amplification factors.

In previous works (Løvholt et al., 2012; Løvholt et al., 2014) the base of this procedure was made by a set of numerical plane wave simulations running on idealized two dimensions bathymetric transects (fig.1). The bi-dimensional idealized bathymetric profiles, for each observation point, were assigned manually, by inspecting the bathymetry visually. Parameters as the bathymetric profile, polarity of the wave (leading elevation or leading trough) and wave period (wave periods of 120, 200, 300, 600, 1000, 1800, 3600 seconds were used) were varied. From the plane wave simulations, amplification factors, relating the surface elevation at a given isobath to the maximum shoreline water level, were computed and stored in lookup tables (Løvholt et al., 2014). Therefore, to estimate the maximum shoreline water level from the offshore time series gauges in a tsunami simulation, the amplification factor was extracted from the lookup tables and in turn multiplied with the maximum surface elevation measured at the time series gauges (Løvholt et al., 2014).

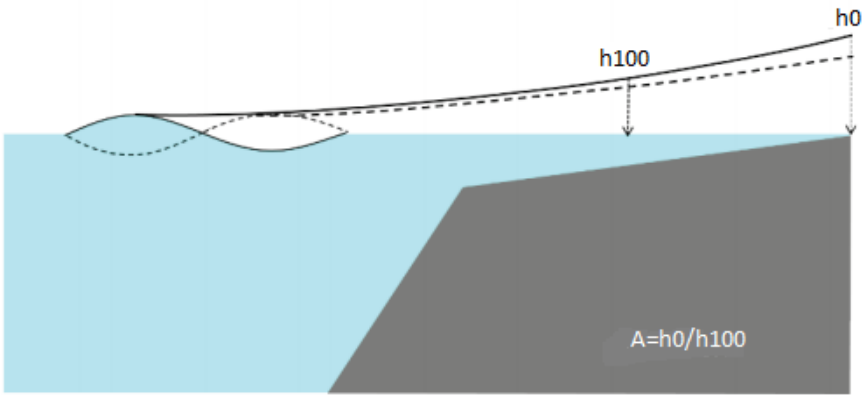

Fig.1 – An idealized bathymetric profile and the method of amplification factor. The amplification factor is defined as the ratio between the maximum water surface elevation at the shoreline h0 and the water surface elevation at a given isobaths (e.g. 100 m) (modified from UNISDR Global Assessment Report 2015 – GAR15).

In this study, it has been decided not to consider bathymetric profiles as 2D transects, but to evaluate the real bathymetry along a stretch of coast, computing the amplification factor on real local bathymetric profiles. The main idea adopted to trace profiles, was to sample the continental shelf, the slope and the abyssal plain in front of the studied shore, in order to better characterize the sea bottom morphologies, that play a fundamental role in the tsunami propagation. In fact, for example, Moode et al., (2016) found that the tsunami height on continental shelf is lower for steeper continental slope in comparison to flatter slope.

In this context, my contribution was mainly based on the bathymetric profiles acquisition, their processing, and the characterization of the locally representative profiles. For completeness of information I nevertheless describe here all the phases that were carried out to obtain the amplification factors and to estimate their uncertainty.

In the following, the procedure adopted to acquire the bathymetric profiles is described.

4. Bathymetric profiles acquisition and amplification factors

4.1 Investigated areas

This study has the aim to estimate the amplifications factors in three different areas: the Mediterranean Sea, the Black Sea and the North East Atlantic, practically the area known as NEAM, as this is the target of the TSUMAPS-NEAM project.

For each of these areas, bathymetric profiles were acquired using ArcGIS 10.2.1 and Python scripts. The base for the bathymetric profiles acquisition was a SRTM (Shuttle Radar Topography Mission) available at http://topex.ucsd.edu. In detail, for the Mediterranean Sea and for the Black Sea I used a SRTM with 15 arc seconds of resolution (cell size is about 450 meters) (fig. 2) while for the North East Atlantic a SRTM with 30 arc seconds of resolution was used (cell size is about 900 meters) (fig. 3). The shoreline was computed using the “generate contour” ArcGIS tool.

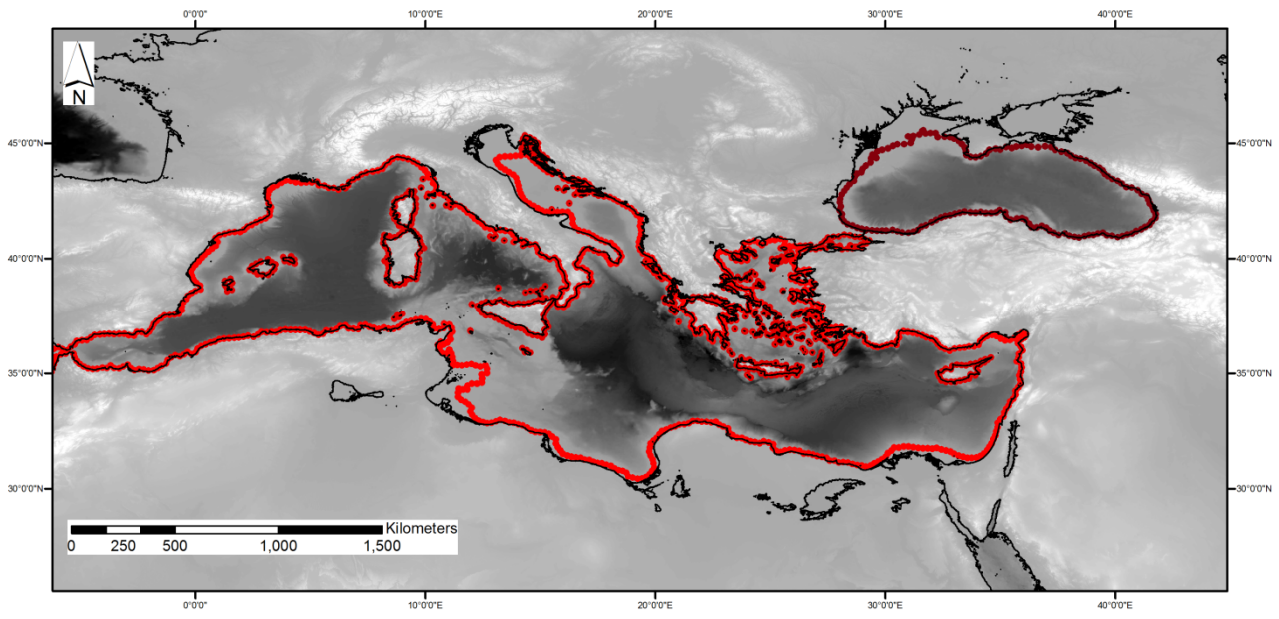

Fig. 2 – SRTM 15 (15 arc seconds of resolution)used for Mediterranean Sea and for the Black Sea. The analyzed coastlines are highlighted in red.

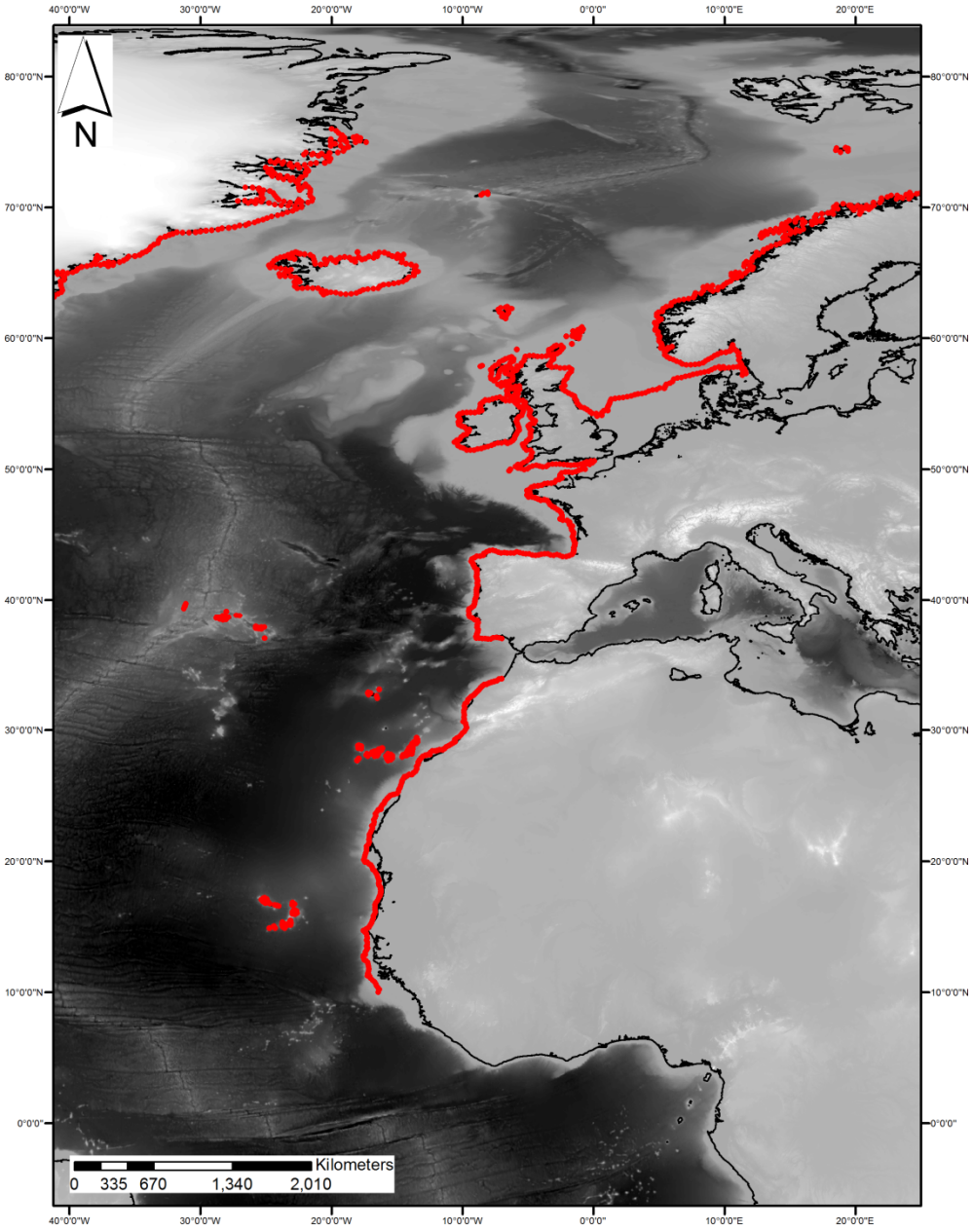

Fig. 3 - SRTM 30 (30 arc seconds of resolution) used for the North East Atlantic. The analyzed coastlines are highlighted in red.

4.2 Methodology

The starting point for the bathymetric profiles acquisition procedure considered the use of some offshore points located at -50 meters isobath. Each point is characterized by latitude, longitude and an ID index.

At the beginning, these points had a distance between them of about 2 kilometers. Subsequently they were down-sampled in order to obtain a larger distance of about 20 kilometers (fig. 4). This down-sampling was done in order to reduce the computational cost but saving the accuracy of the

results, being the aim a regional calculation instead of a local one for which denser sampling has to be preferred.

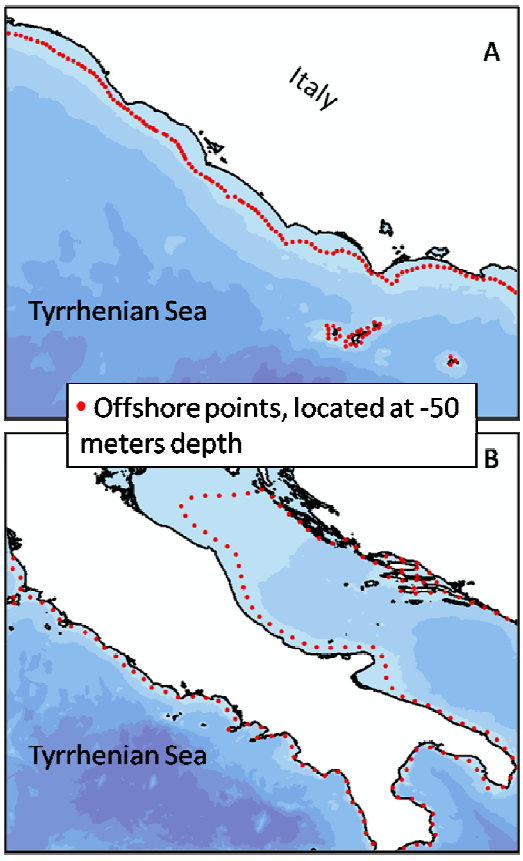

Fig. 4 –A) Hazard points located at -50 meters isobaths with a distance each from other of 2 km. B) New selection of hazard points with the new distance of about 20 km.

Once selected new offshore points, the nearest corresponding points along the coastline were found using the “near” ArcGIS tool. Nearest points on the shoreline preserve the ID index of the offshore hazard points.

Along the shoreline, from each point, an interpolation line passing through three points was created. From the shoreline, in correspondence to each interpolation line, a group of transects perpendicular to the line and characterized by a distance between them of 1 km, was traced (fig. 5). In this way, the bathymetric profiles traces were approximately perpendicular to the shoreline. All profiles that met islands were deleted in order to avoid positive values. Each group of transects was denominated with the ID index of the central shoreline point of the interpolation line, in order to have a group of profiles for each offshore control point.

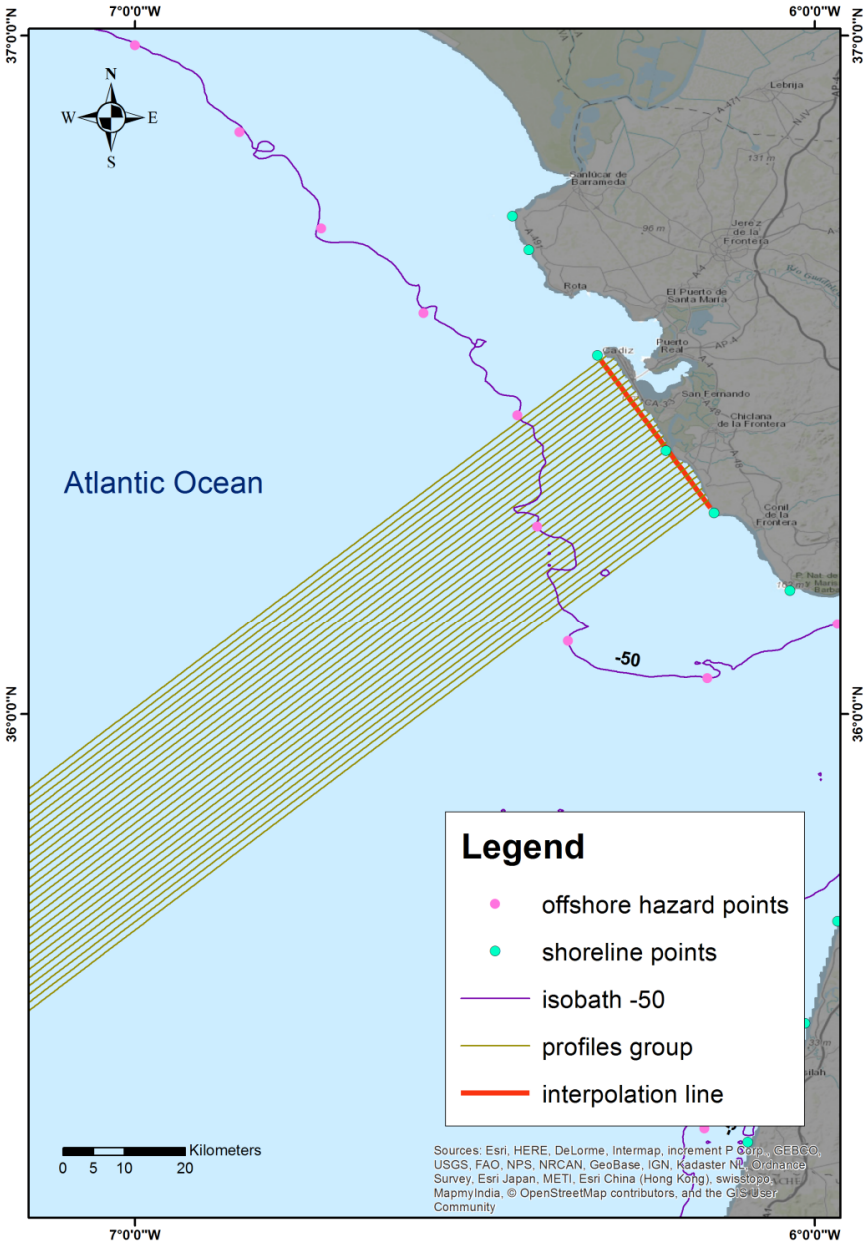

Fig. 5 – This figure shows the main features used to trace the transects. It is possible to note the two groups of interested points located at -50 meters and on the shoreline respectively, the interpolation line passing through three points on the shoreline, and a group of profiles perpendicular to the line and to the shoreline.

Sometimes the direction of profiles was changed because they need to go towards the deepest area in order to sample the continental shelf, the slope and the abyssal plain in front of the studied shore. In fact, the sea bottom morphologies play a fundamental role in the tsunami propagation. This happens because the trend of the coastline is often different from the trend of the -50 meters isobath. From a geological point of view the shape of the shoreline is the result of series of processes different from those that modeled the trend of the isobath. For this reason, sometimes, also the distance of the hazard points on the shoreline is not exactly 20 kilometers. From a general point of view, we can have a mutual distance of 20 km, on the shoreline, when the trend of the coastline is

quite linear. When the coastal morphology is quite tricky and articulated the distance between points on the shoreline may be variable.

This procedure was not applied in those areas characterized by a very articulated morphology as Aegean islands, deep and narrow bays (e.g. fjords) and Croatian islands. Therefore, in these areas, some hazard points were left out without transects in the automatic procedure. Here a new strategy was adopted. For the Aegean sea islands (fig. 6) only nine groups of transects, drawn manually, were acquired. For each group of profiles many offshore points were visually assigned.

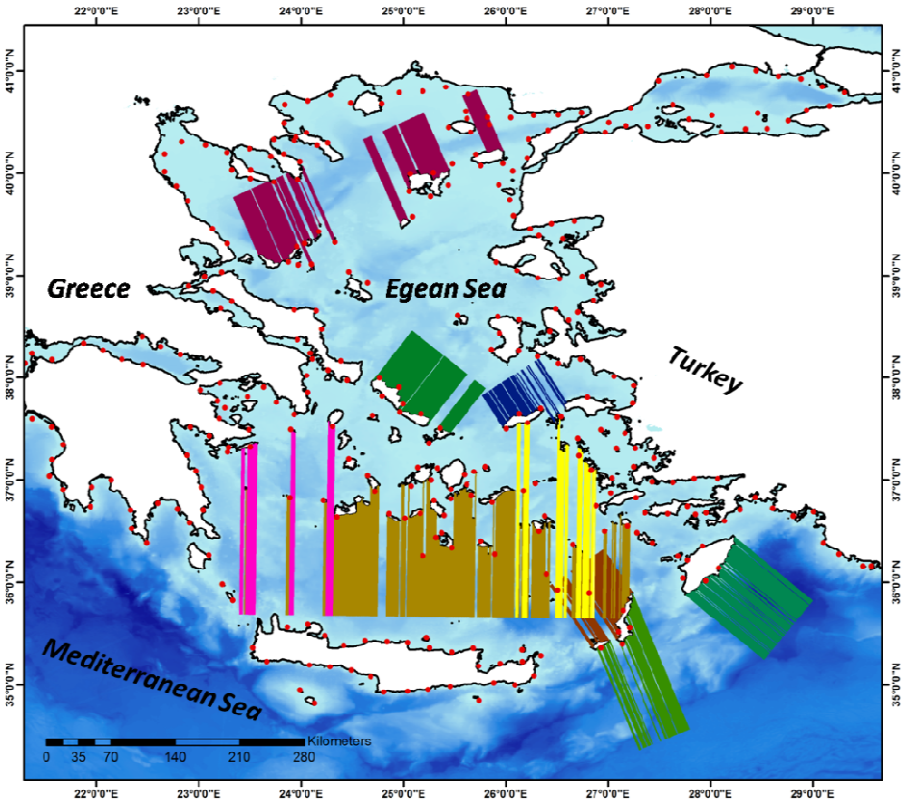

Fig. 6 – The map shows the 9 groups of transects chosen to characterized the Aegean islands bathymetry. Red points represent the hazard points located at -50 meters depth.

For the other particular cases, each point without transects was set equal to the closest neighboring factor (Fig. 7).

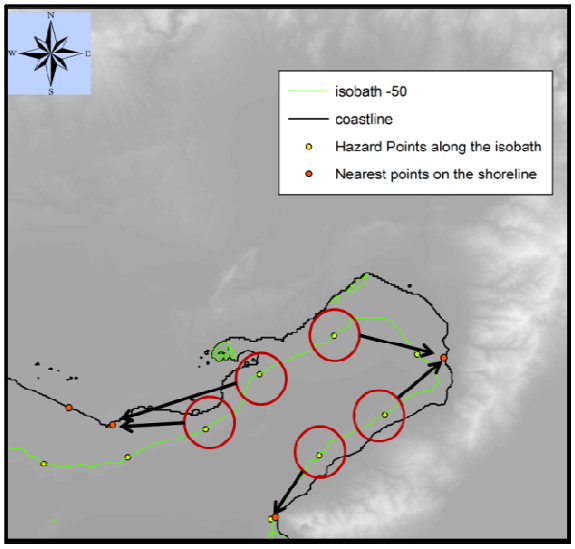

Fig. 7 – Example of a particular case. The figure shows a narrow and deep bay where profiles have been calculated only for the innermost point. Red circles represent the hazard points along the isobath without computed profiles. Orange points represent points with computed profiles. Black arrows indicate the points, with computed profiles, that can be related to points without any profile.

The drawing and the extraction of bathymetric profiles were performed in ArcGIS, using scripts written in Phyton language. In particular, transects extraction was computed using the "Stack profile" ArcGIS tool over the SRTM bathymetric maps. Output data were saved in a txt format. Each output file has the name of the hazard points index and arranges numeric values of a group of profiles, in two columns. The first column shows the distance from the shoreline in kilometers and the second column shows the depth in meters (fig.8). In total 149 profiles for the Black Sea, 935 profiles for the Mediterranean Sea (fig. 9) and 1158 profiles for the North East Atlantic region (fig. 10) were acquired.

1	0.000000	0.0097	NAN	0.000000	0.0545	NAN	0.000000	0.0119	NAN	0.000000
2	0.377403	-2.8638	NAN	0.376015	-3.7134	NAN	0.374653	-3.3422	NAN	0.367375
3	0.754806	-5.1106	NAN	0.752030	-5.4047	NAN	0.749306	-5.6041	NAN	0.734749
4	1.132210	-7.7326	NAN	1.128050	-7.4444	NAN	1.123960	-8.0121	NAN	1.102120
5	1.509610	-10.7276	NAN	1.504060	-9.8865	NAN	1.498610	-10.7232	NAN	1.469500
6	1.887020	-13.9341	NAN	1.880080	-12.6336	NAN	1.873270	-13.8466	NAN	1.836870
7	2.264420	-17.2856	NAN	2.256090	-15.5619	NAN	2.247920	-16.8954	NAN	2.204250
8	2.641820	-20.7486	NAN	2.632110	-18.4691	NAN	2.622570	-19.7789	NAN	2.571620
9	3.019220	-22.9364	NAN	3.008120	-21.2570	NAN	2.997230	-22.4521	NAN	2.939000
10	3.396630	-24.9527	NAN	3.384140	-23.9020	NAN	3.371880	-24.8125	NAN	3.306370
11	3.774030	-27.0294	NAN	3.760150	-26.3561	NAN	3.746530	-26.6604	NAN	3.673750
12	4.151430	-28.9363	NAN	4.136170	-28.4591	NAN	4.121190	-28.2634	NAN	4.041120
13	4.528840	-30.6650	NAN	4.512180	-30.1681	NAN	4.495840	-29.6382	NAN	4.408490
14	4.906240	-32.3160	NAN	4.888200	-31.6223	NAN	4.870490	-31.0126	NAN	4.775870
15	5.283640	-33.9772	NAN	5.264210	-33.0658	NAN	5.245140	-32.2279	NAN	5.143240
16	5.661050	-35.8904	NAN	5.640230	-34.5224	NAN	5.619800	-33.3775	NAN	5.510620
17	6.038450	-37.6513	NAN	6.016240	-35.8906	NAN	5.994450	-34.4543	NAN	5.877990
18	6.415850	-37.6953	NAN	6.392260	-36.9913	NAN	6.369100	-35.4451	NAN	6.245370
19	6.793260	-37.8890	NAN	6.768270	-37.9312	NAN	6.743760	-36.3533	NAN	6.612740
20	7.170660	-38.4847	NAN	7.144290	-38.7824	NAN	7.118410	-37.2081	NAN	6.980120
21	7.510470	-39.2367	NAN	7.485960	-39.6584	NAN	7.493060	-38.1056	NAN	7.347490
22	7.850280	-40.1173	NAN	7.827640	-40.6269	NAN	7.834690	-38.9016	NAN	7.714870
23	8.190090	-41.0989	NAN	8.169320	-41.6499	NAN	8.176320	-39.7836	NAN	8.056170
24	8.529910	-42.2257	NAN	8.511010	-42.7176	NAN	8.517950	-41.1495	NAN	8.397480
25	8.869730	-43.4360	NAN	8.852700	-43.8002	NAN	8.859580	-42.6749	NAN	8.738790
26	9.209560	-44.7332	NAN	9.194380	-44.8803	NAN	9.201220	-44.2135	NAN	9.080110
27	9.549390	-46.0313	NAN	9.536080	-45.9419	NAN	9.542860	-45.7772	NAN	9.421430
28	9.889220	-47.2171	NAN	9.877780	-46.9879	NAN	9.884510	-47.3009	NAN	9.762750
29	10.229000	-48.3118	NAN	10.219500	-48.0105	NAN	10.226200	-48.6483	NAN	10.104100
30	10.568900	-49.3374	NAN	10.561200	-48.9519	NAN	10.567800	-49.6934	NAN	10.445400
31	10.908700	-50.2662	NAN	10.902900	-49.8091	NAN	10.909500	-50.5580	NAN	10.786700
32	11.248600	-51.1080	NAN	11.244600	-50.5591	NAN	11.251100	-51.3058	NAN	11.128100
33	11.588400	-51.8118	NAN	11.586300	-51.2201	NAN	11.592800	-51.9597	NAN	11.469400

Fig. 8 – Output data of profiles where the first column on the left side shows the distance from the shoreline in kilometers and the second column on the right side shows the depth in meters. The "NAN" divides each single profile from the next one.

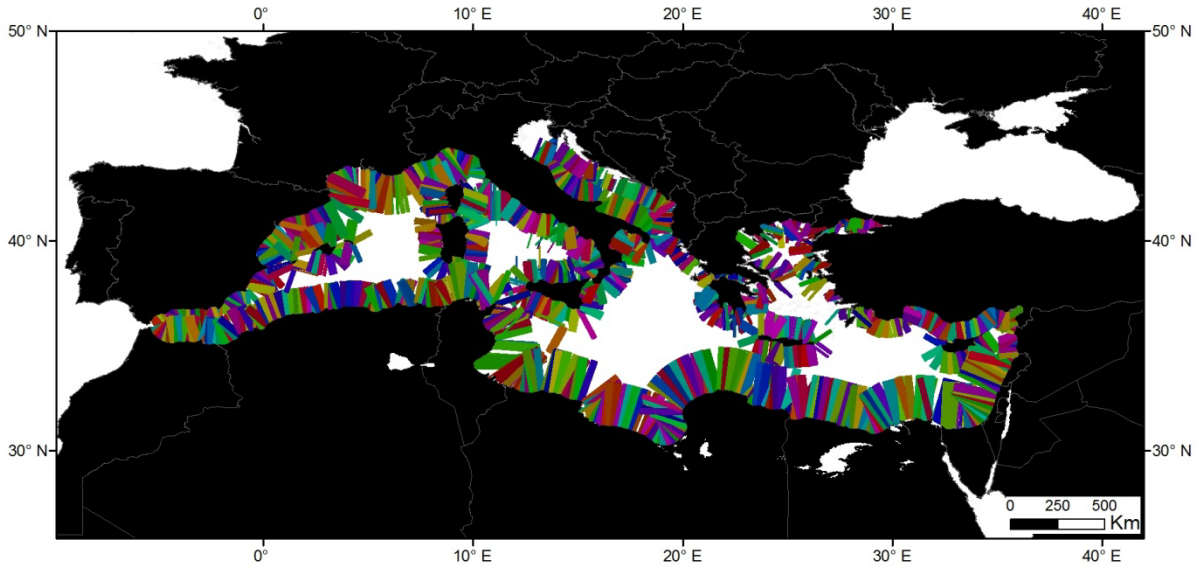

Fig. 9 – The map shows all Mediterranean profiles acquired.

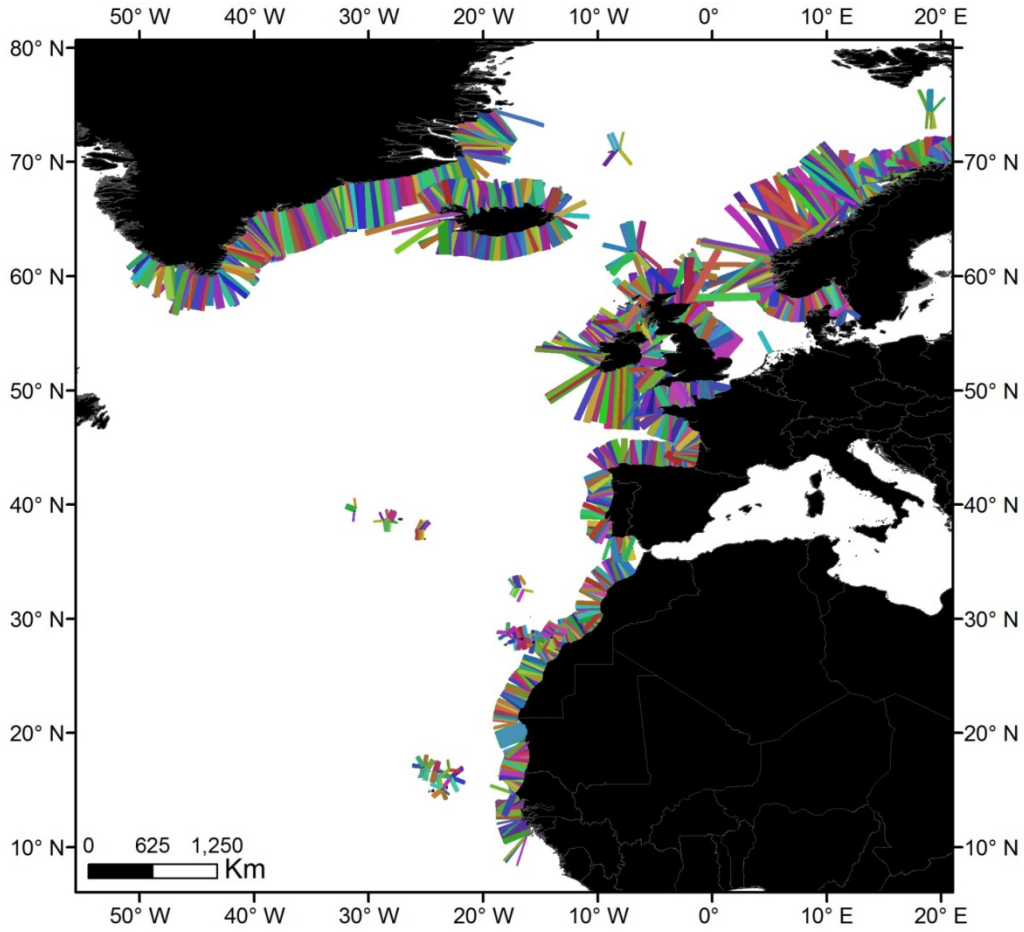

Fig. 10 – The map shows all NEA (North East Atlantic) profiles acquired.

Once the bathymetric profiles were extracted, for each group of profiles the amplification factors were computed along seven arbitrarily selected transects by using a 1HD linear shallow water wave model (LSW model). An initial wave of 1 m height in deep water, shaped as a single period

sinusoidal shaped wave (N-wave) is fed over the boundary of the model (ASTARTE Deliverable D8.39)

The wave amplification, from the offshore control point (located at about at -50 meters depth) to a point close to the shoreline, is computed varying the period and the polarity of the wave. In detail for each profile, the following parameters are varied (fig. 11):

• The polarity of the incident wave, i.e. either a leading trough or leading peak.

• The wave periods of 120, 200, 300, 600, 1000, 1800, 3600 seconds.

Finally, the ratio between wave height at the shoreline and the wave height at -50 meters depth represents the amplification factor for each profile.

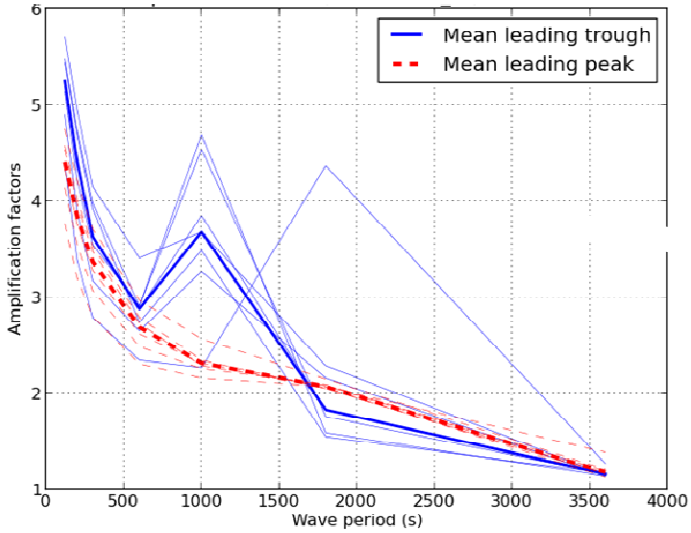

Fig.11– The figure shows the amplification factors for seven profiles taken from a group of transects of the Mediterranean Sea. The amplification factor are related to the different wave periods (seconds). The red and blue curves are the factors for leading peak (positive incident wave) and leading trough, (negative incident wave) respectively. The thin curves are the factors for the seven local profiles, while the thick lines are the median values for leading peak and leading trough. Figure from ASTARTE Deliverable D8.39.

4.3 Results

Amplification factors maps with a negative and a positive incident wave and wave periods of 120, 200, 300, 600, 1000, 1800, 3600 seconds respectively were produced (maps with amplification factors for a leading peak with a period of 120, 300, 1000 and 3600 seconds are presented in fig. 12). In addition, two versions of amplification factors were computed. The first set of factors provides the raw data values, while the second one is characterized by smoothed factors along the shoreline with a median filter, in order to avoid artificially short amplification fluctuations along the shoreline (fig. 13).

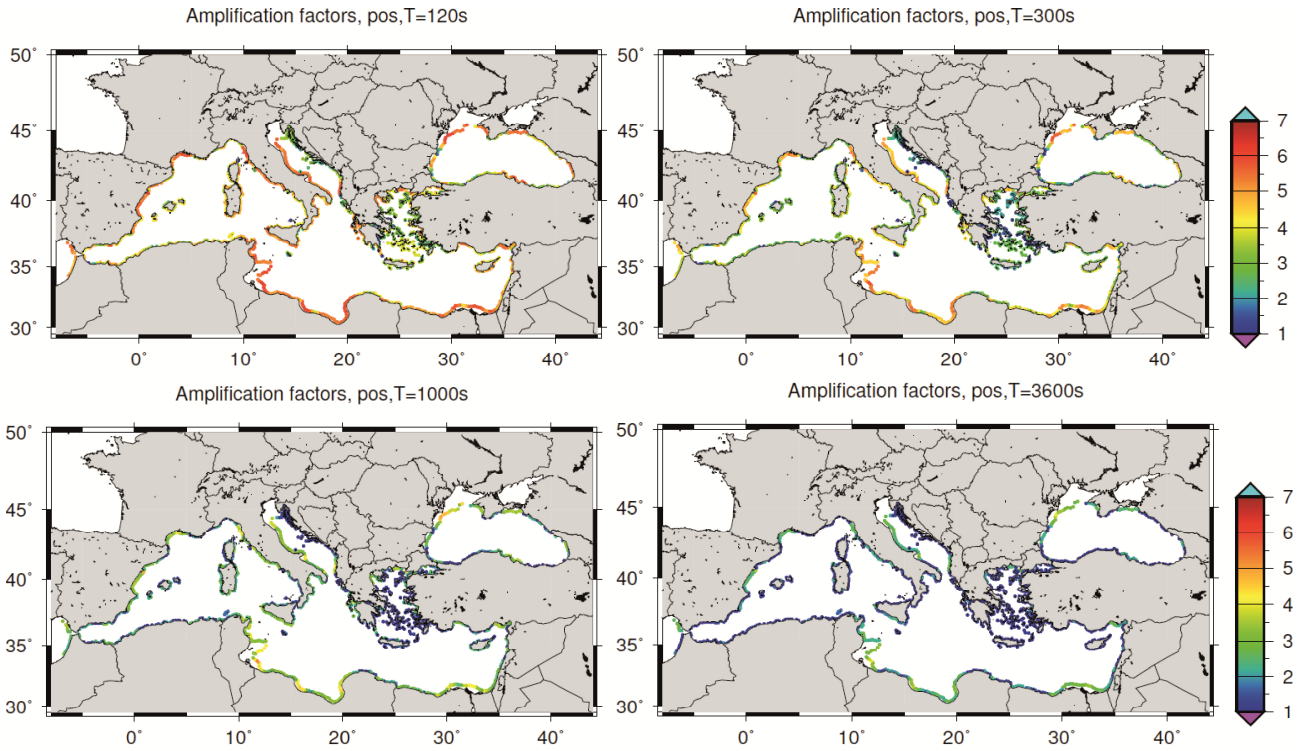

Fig.12 – The figure shows an example of 4 amplification factor maps for the Mediterranean and Black Sea. In detail the maps represent factors for a leading peak with a period of 120, 300, 1000 and 3600 seconds respectively. These factors are not smoothed.

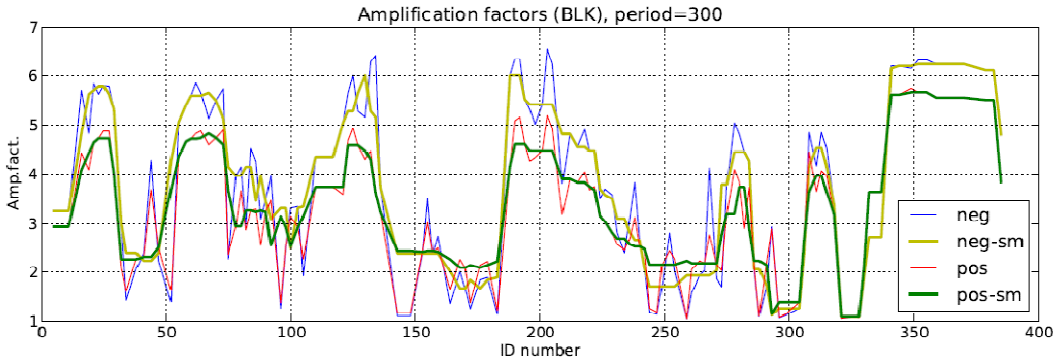

Fig. 13 – Example of amplification factors for the Black Sea computed with a wave period of 300 seconds. In particular the figure plots the amplification factors in function of the offshore hazard points (ID number). The set of factors smoothed using a filter ("sm" in the labels) is shown for negative (leading trough) and positive (leading peak) cases. The smoothed factors are then compared to those representing the raw data values.

From the amplification factor maps (fig. 12) it is possible to note that short waves (with a low period) give more amplification than a long wave as suggested by Tadepalli and Synolakis, (1996). In addition, a leading negative polarity gives more amplification than a leading positive polarity (fig. 14).

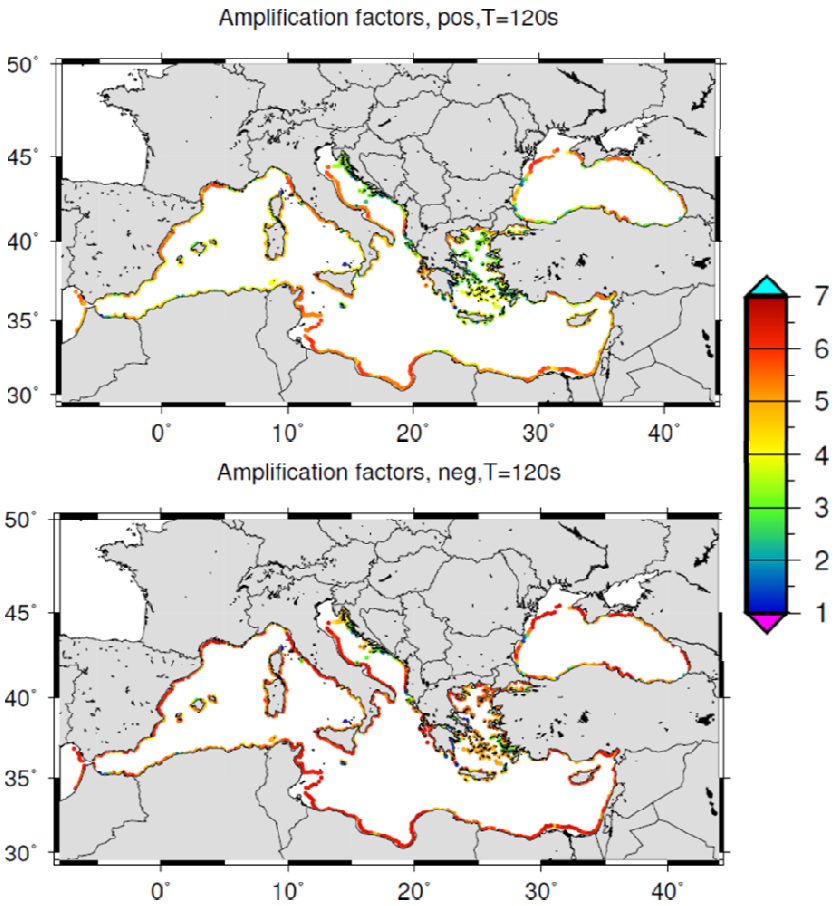

Fig. 14 - Amplification factor maps for the Mediterranean and Black sea with a leading positive polarity and a leading negative polarity respectively. The period of the wave is 120 seconds. It is possible to note that waves with a leading negative polarity, equal to the period, give more amplification.

In detail, the amplification factor depends mostly from the distance between the offshore control point and the shoreline. Løvholt et al. (2012) found that waves shorter than the distance between the shoreline and the offshore point give factor values up to 6. On the other hand, if the waves are long (compared to the distance between the shoreline and the offshore point), the wave height at the shoreline and at the hazard point will be more or less the same, with factors down to 1.

However this procedure is considered a deterministic method. Therefore, in the ASTARTE project it was decided to compare the results obtained with local inundation models in order to estimate and to quantify the amplification factor bias and uncertainty.

5. Tsunami Simulations

The comparison between the amplification factors and local inundation models was performed at three ASTARTE test sites: Sines (Portugal), Colonia Sant Jordi (Spain), and Heraklion (Greece). For each site, 3 earthquake sources with varying magnitude (Mw7.0, Mw7.5, and Mw8.0) were used. Only for Sines and Heraklion a fourth source with magnitude 8.5 and 9.0 was adopted. Different inundation models (non-linear shallow water models – NLSW) were used for the different

locations. For Sines, the tsunami propagation and local inundation simulations are modelled with the NSWING model (e.g. Wronna et al., 2015). For Colonia Sant Jordi and Heraklion the HySEA model and a combination of the GloBouss and ComMIT model were used (Titov and Gonzalez, 1997; Pedersen and Løvholt, 2008). The GloBouss model is used to produce the input propagation files for the inundation model ComMIT (Løvholt et al., 2010). All offshore tsunami simulations are conducted on grids with 30 arc seconds of resolution while the resolution of the finest grids (to simulate the inundation) is about 10 meters at all locations. The Manning-friction coefficient (n) is in all simulations set by default to n=0.03.

In this context, I performed three tsunami simulations on Colonia Saint Jordi (Palma de Mallorca, Baleares Islands, Spain), using the ComMIT (COMmunity Model Tsunami Interface) model. In particular, I used three different sources with different magnitude of Mw7.0, Mw7.5, and Mw8.0 (one example of source is shown in fig. 15), in order to produce three different inundation scenarios. The figure 16 shows an example of inundation related to the Mw8.0 earthquake source scenario. Parameters that describe the sources are reported in the table 1 where it is possible to note that the Mw7.0 scenario is tested with a normal fault (rake angle of -90 degrees and dip angle of 70 degrees) while the other two scenarios (Mw7.5, and Mw8.0) take into account a reverse fault with two different dip angles (30 and 10 degrees). More in detail, the source parameters have been chosen taking into account the Algerian thrust, in order to obtain a tsunami waves variability in terms of periods and wavelengths at studied site (ASTARTE [603839] – Deliverable 8.39).

Magnitude	Length (km)	Width (km)	Slip(m)	Strike	Dip	Rake	Depth_Center(km)
7.0737	54.1	17.9	1.77	67.5	70	-90	9.4
7.5435	102.5	25.3	3.34	67.5	30	90	7.3
8.09	216.3	38	7	67.5	10	90	4.3

Table 1: Parameters of the three sources used in the Saint Jordi tsunami simulations.

Once obtained all local inundation scenarios, for each site, the comparison between the amplification factors and the local inundation models was performed. Below is a brief description of the comparison procedure.

In the local tsunami simulation for each site and for each scenario, the maximum water elevation and the wave period were extracted at the offshore hazard point (the same points used in the amplification factor method) by an automatic procedure. The period of the wave is then used to determine the appropriate amplification factor, because we know that the factors are related to the period and polarity of the wave.

For each site and for each scenario the deterministic maximum inundation height was estimated taking into account the new amplification factors (fig. 17). The maximum inundation height is obtained multiplying the maximum surface elevation (obtained from local inundation model

simulations) at the offshore points, (located at -50 meters depth, in front of the studied locations), for the more appropriate amplification factor. This value is considered the median tsunami maximum inundation height MIH (ASTARTE Deliverable D8.39).

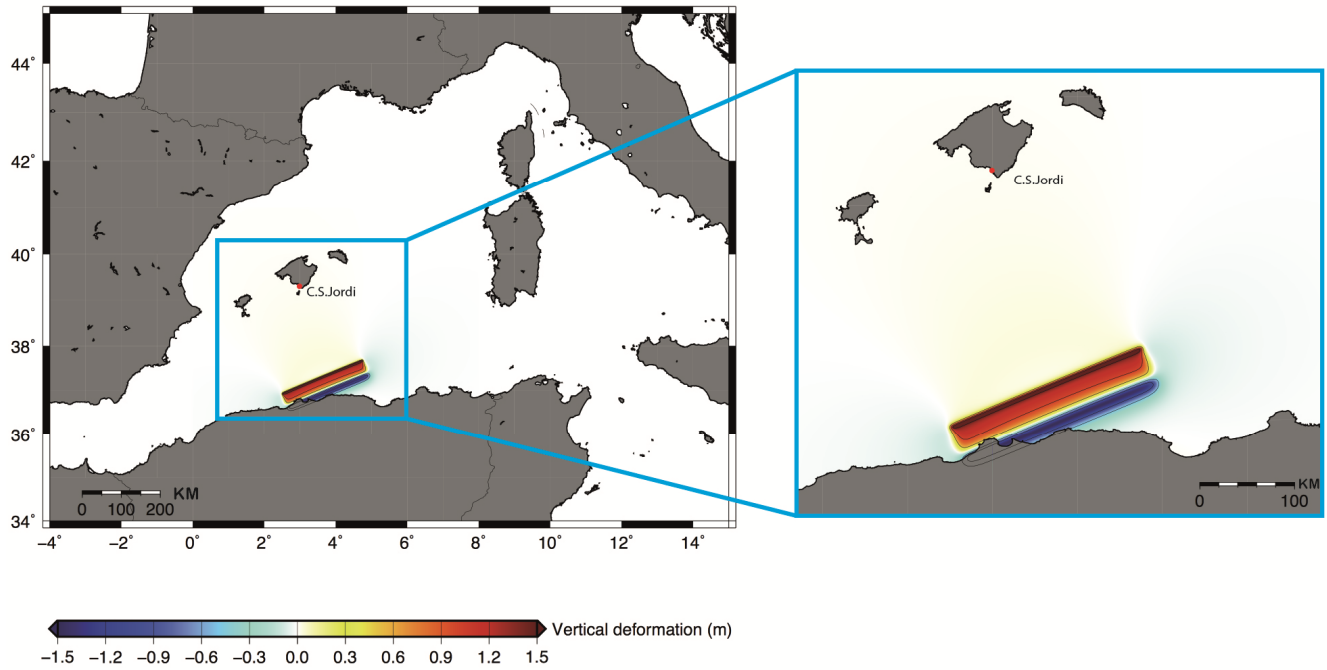

Fig. 15 – The figure shows the Mw8.0 earthquake source (dip angle of 10 degrees) used for C.S. Jordi site (Palma de Mallorca, Baleares Islands). In detail, It is possible to note the initial fields set in the simulation (vertical deformation). Note that the contour lines have an interval of 0.5 meters.

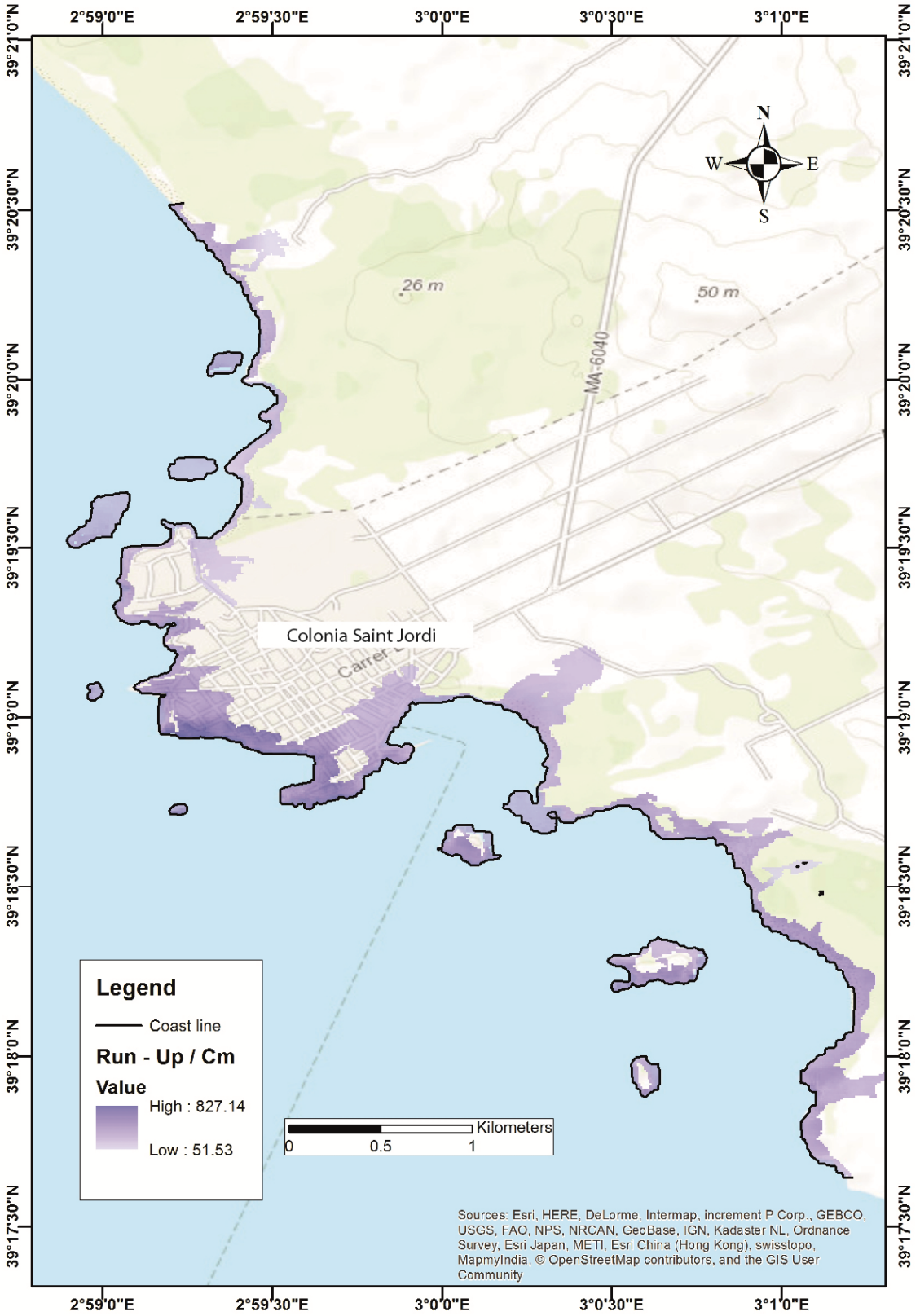

Fig. 16 – The map shows the maximum waves amplitude (expressed in cm) obtained for Colonia Saint Jordi site, using the ComMIT inundation model. This scenario derives from the Mw8.0 earthquake source. It is possible to note a maximum run-up value of about 8 meters and a maximum inundation distance of about 500-600 meters from the shoreline.

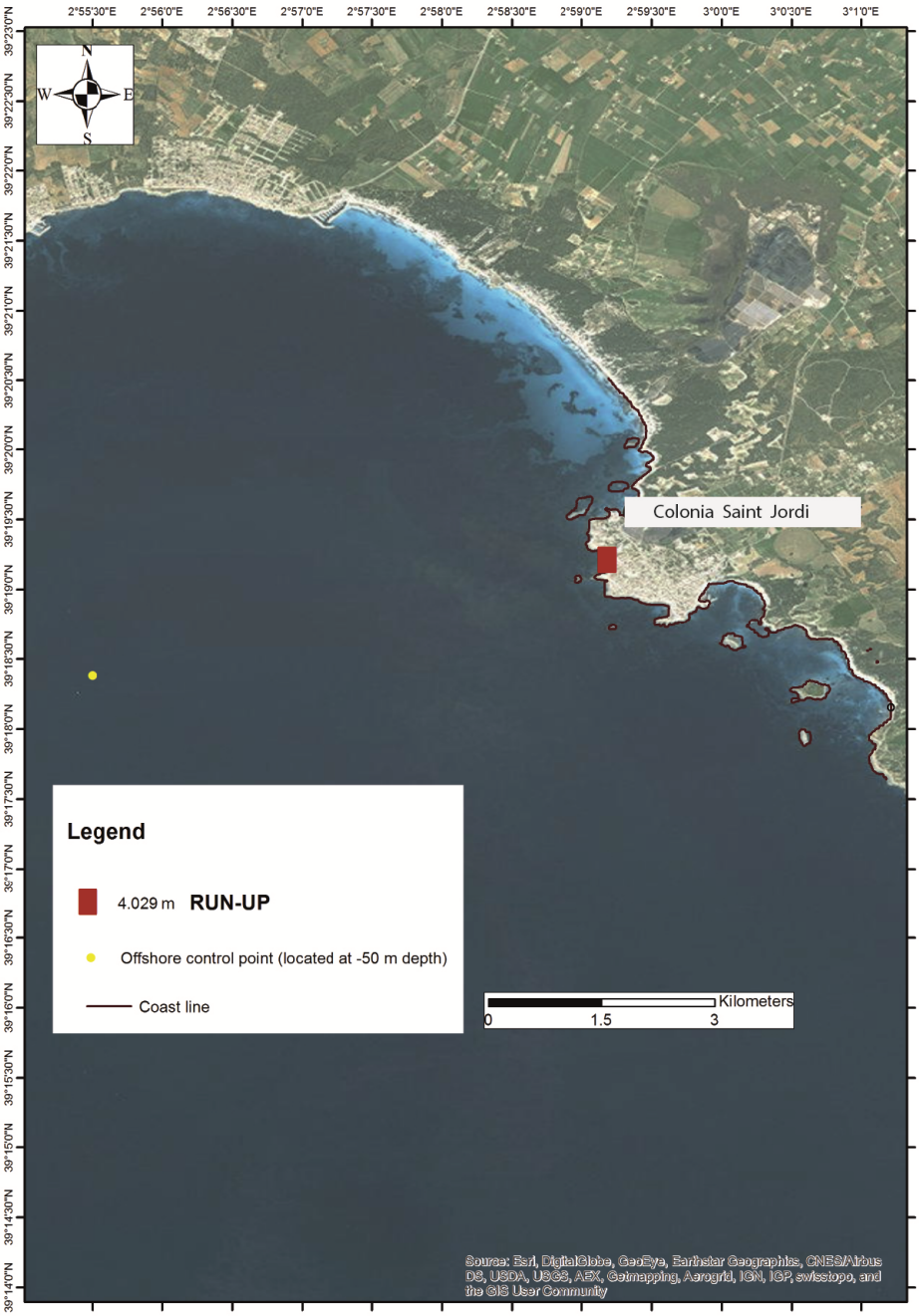

Fig. 17 – The water elevation at the shoreline for Saint Jordi (run-up) obtained multiplying the maximum surface elevation at the offshore point (obtained from the ComMIT inundation model, with a scenario of Mw8.0) for the amplification factor. The correct amplification factor was chosen after extracting the waves period from the ComMIT simulation.

6. Maximum inundation height uncertainty

For each scenario, the maximum inundation height uncertainty was estimated using statistical methods. The procedure reported in the ASTARTE Deliverable D8.39 can be summarized as follow:

For each scenario, the maximum inundation height (MIH) was extracted from the local inundation simulations using the finest grid. The MIH distributions were extracted in N-S or E-W directions depending on the coastal strike. When the shoreline was too high to be inundated, only small values (at least one cell) of maximum surface elevation were considered.

The MIH probability density for each simulation was obtained. Then the MIH probability density was fitted to a lognormal probability density function (PDF) using standard PDF fitting procedures in Matlab. The lognormal distribution of the MIH is:

$$p(MIH) = \frac{1}{\sqrt{2\pi} \cdot MIH \cdot \sigma} e^{-\frac{(ln(MIH)-\mu)^2}{2\sigma^2}}$$

The MIH median and mean values for the local probability distributions are e^{μ} and $e^{\mu+\sigma^2/2}$. The fitted mean and median MIH's were both compared with the results obtained from the amplification factors, in order to quantify biases for all single simulations. The biases were estimated using two different expressions: the first one is a direct comparison between the logarithms of the MIH from the amplification factor with the normal mean from the fitted distribution

$$\epsilon_1 = \ln(MIH) - \mu$$

and the second one is a normalized error measure

$$\epsilon_2 = \frac{e^{\mu} - MIH}{e^{\mu}}$$

The results obtained from this procedure show that for the Heraklion test site (logarithmic bias $\epsilon 1$ ~ 0.2) the amplification factor method seems to overestimate the run-up, except for the subduction zone event (this source is placed in the opposite side of the island with respect to the site location). Colonia Sant Jordy shows the largest biases compared to the ComMIT model (example shown in figure 18), while HySEA provides MIH's close to or slightly smaller than the amplification factor method. For the largest magnitudes, the biases are relatively small, $\epsilon 1$ ranging from -0.09 to 0.23. Finally, Sines shows that the amplification factors underestimate the inundation simulations results.

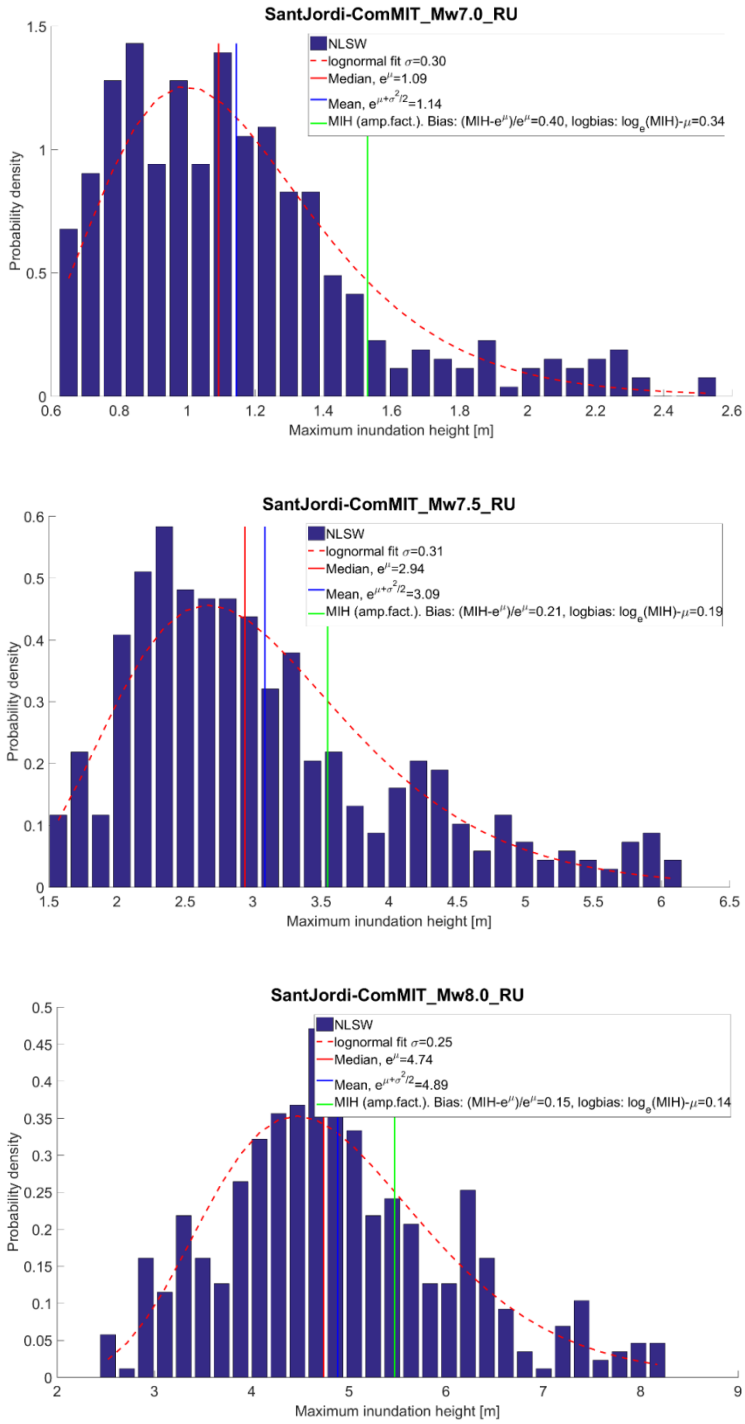

Fig. 18 - Distribution of MIH and fitted lognormal distribution for the Colonia Sant Jordi test site using the ComMIT model. Upper panel, Mw7 scenario; mid panel, Mw7.5 scenario; lower panel, Mw8.0 scenario. V (from ASTARTE PROJECT - DELIVERABLE D8.39).

7. Conclusions

Local bathymetric profiles were acquired by using Phyton scripts run in ArcGIS environemnt. In total 149 profiles for the Black Sea, 935 profiles for the Mediterranean Sea and 1158 profiles for the North East Atlantic region were acquired. Although the NEAM coasts were characterized by local bathymetries, amplification factor method gives only an overview of the wave amplification and therefore it cannot be used for local hazard assessment.

Amplification factor maps for different periods (120, 200, 300, 600, 1000, 1800, 3600 seconds) and wave polarity (positive and negative leading wave) were produced on local bathymetric transects. In particular, it was observed that the wave amplification depends on the wave's period in relation of the distance between the offshore control point (the depth from which the wave is amplified) and the shoreline:

• Waves shorter than this distance (with a low period) give factors up to 6

• Waves longer than this distance (with a high period) give factors down to 1

This may mean that coastal areas, where the depth remains low for a long distance towards the sea, tend to give more amplification. Similarly, Moode et al. (2016) found that the tsunami height on continental shelf is higher for flatter continental slope in comparison to steeper slope. This means that while the continental slope becomes flatter, more energy is transmitted to the shelf and higher tsunami height is observed.

Løvholt, together with his research team, found that the comparison between the factors and the local inundation models gave a mean bias close to 0. At the same time, it should be noted that the comparison between the amplification factors and the local inundation model is performed only on few sites. The test should be carried out on more localities. But, on the base of this investigation, it seems that there is not the necessity to correct the amplification factor method; the associated uncertainty should be propagated to PTHA results.

It is possible to conclude that the amplification factor method is a viable procedure to produce and compute run ups as well inundation distances in front of an examined stretch of coast. The improved method, that takes into account the local bathymetries, provides more accurate results than the previous one. These results may nevertheless be used to have an overview of the regional tsunami hazard for a certain region and not for local hazard studies.

References

Annaka T., Satake K., Sakakiyama T., Yanagisawa K., Shuto N., (2007). Logic-tree approach for probabilistic tsunami hazard analysis and its applications to the Japanese coast. Pure and applied Geophysics 164, 577-592.

ASTARTE PROJECT - DELIVERABLE D8.39 - Quantifying and managing uncertainty in tsunami risk assessment methods: application to the ASTARTE test sites.

Costa P.J.M., Dawson S., Quintela M., Andrade C., Milne F., Dourado F. and Dawson A. (2016). Tsunami Deposits Database – Retrieved from http://tsunami.campus.ciencias.ulisboa.pt/.

Davies G., Griffin J., Løvholt F., Glimsdal S., Harbitz C., Thio H.K., Lorito S., Basili R., Selva J., Geist E., Baptista A.M. (2017). A global probabilistic tsunami hazard assessment from earthquake sources, in Tsunamis: Geology, Hazards and Risks, edited by E. M. Scourse, N. A. Chapman, D. R. Tappin and S. R. Wallis, Geological Society of London Spec. Pub. 456, London, doi:10.1144/SP1456.1146 .

De Martini P.M., Patera A., Orefice S., Paris R., Volker D., Lastras G., Terrinha P., Noiva J., Smedile A., Pantosti D., Hunt J., Gutscher M.A., Migeon S., Papadopoulos G., Triantafyllou I., Yalciner A.C., (2017). The ASTARTE Paleotsunami and Mass Transport Deposits databases – web-based references for tsunami and submarine landslide research around Europe. Geophysical Research Abstracts, Vol. 19, EGU 2017-15055, 2017, EGU General Assembly 2017.

Geist E.L. and Lynett, P.J., (2014). Source Processes for the Probabilistic Assessment of Tsunami Hazard. Oceanography, Special Issue on Undersea Natural Hazards.

Geist E., & Parsons T., (2006). Probabilistic Analysis of Tsunami Hazards. Natural Hazards, 37, 277-314, 10.1007/s11069-005-4646-z.

Gisler G. R., (2008). Tsunami Simulations. Annu. Rev. Fluid Mech. 40, 71–90. Doi: 10.1146/annurev.fluid.40.111406.102208

Lorito, S., Selva, J., Basili, R., Romano, F., Tiberti, M.M. & Piatanesi, A., (2015). Probabilistic hazard for seismically induced tsunamis: accuracy and feasibility of inundation maps. Geophys. J. Int., 200, 574–588.

Lorito S., Tiberti M. M., Basili R., Piatanesi A., & Valensise, G., (2008). Earthquake-generated tsunamis in the Mediterranean Sea: Scenarios of potential threats to Southern Italy. J. Geophys. Res., 113, B01301, 10.1029/2007JB004943.

Løvholt F., Glimsdal S., Harbitz Carl B., Horspool N., Smebye H., De Bono A., Nadim F., (2014). Global tsunami hazard and exposure due to large co-seismic slip. International Journal of Disaster Risk Reduction.

Løvholt F., Glimsdal S., Harbitz Carl B., Zamora N., Nadim F., Peduzzi P., Dao H., Smebye H., (2012). Tsunami hazard and exposure on the global scale. Earth-Science Reviews, Volume 110, Issues 1–4, Pages 58-73.

Løvholt F., Bungum H., Harbitz C. B., Glimsdal S., Lindholm C.D., Pedersen G., (2006). Earthquake related tsunami hazard along the western coast of Thailand. Natural Hazard and Earth System Sciences 6, 1-19-

Løvholt, F., G. Pedersen, and S. Glimsdal, (2010). Coupling of dispersive tsunami propagation and shallow water coastal response. Open Oceanography Journal, Caribbean Waves Special Issue, 4, 71-82.

Moode S., Behera M.R., (2016). Effect of continental slope on N-wave type tsunami run-up. International Journal of Ocean and Climate Systems, 27, 2, 47 – 54. DOI: 10.1177/1759313116656865

Okal E., Synolakis C.E., (2008). Far field tsunami hazard from mega thrust earthquakes in the Indian Ocean. Geophysical Journal International 172, 995-1015.

Pedersen, G. and Løvholt, F., (2008). Documentation of a global Boussinesq solver, Preprint Series in Applied Mathematics 1, Dept. of Mathematics, University of Oslo, Norway.

Selva J., R. Tonini, I. Molinari, M. M. Tiberti, F. Romano, A. Grezio, D. Melini, A. Piatanesi, R. Basili, and S. Lorito (2016) Quantification Of Source Uncertainties in Seismic Probabilistic Tsunami Hazard Analysis (SPTHA), Geophys. J. Int. 205, 1780-1803, doi: 10.1093/gji/ggw107.

Tadepalli S., Synolakis C.E., (1996). Model for Leading Waves of Tsunamis.Phisical Review Letters, 77, 10, 2141 – 2144.

Thio H.K., Sommerville P., Ichinose G., (2007). Probabilistic analysis of strong ground motion and tsunami hazard in Southest Asia. Proc. From 2007 NUS-TMSI Work shop. National University of Singapore, Singapore (7-9 March).

Tinti S., Armigliato A., (2003). The use of scenarios to evaluate the tsunami impact in southern Italy. Marine Geology 199 (3-4), 221, 243.

Titov V.V., and F.I. Gonzalez (1997). Implementation and testing of the Method of Splitting Tsunami (MOST) model. NOAA. Technical Memorandum ERL PMEL-112, 11 pp.

Tonini, R., Armigliato, A., Pagnoni, G., Zaniboni, F. & Tinti, S., (2011). Tsunami hazard for the city of Catania, eastern Sicily, Italy, assessed by means of Worst-case Credible Tsunami Scenario Analysis (WCTSA). Nat. Hazards Earth Syst. Sci., 11, 1217–1232.

Wronna M., Omira R., and Baptista M. A., (2015.). Deterministic approach for multiple-source tsunami hazard assessment for Sines, Portugal, Nat. Hazards Earth Syst. Sci., 15, 2557-2568, doi:10.5194/nhess-15-2557-2015.

Chapter 4

Final discussion and conclusions

1. General discussion and conclusions

The research activity carried out within my PhD highlighted the importance of a multidisciplinary approach in order to have a better knowledge of a given phenomenom. The tsunami topic was analyzed from three different points of view, trying to add new scientific knowledge on the subject.

The Astarte Paleotsunami deposits database – NEAM region (De Martini et al., 2017) provides a very detailed dataset about past geological evidence of tsunami in the NEAM (North-Eastern Atlantic, Mediterranean and connected seas) region. The database was designed to be constantly updated (once per year) in order to be the future reference source for this kind of research in the NEAM region.

The database has allowed to know and to identify portions of coast affected by tsunami in the past within the NEAM region. Moreover, it is possible to derive data about run-up heights and inundation distances, relevant in terms of hazard estimation. Both these data should be considered as minimum values, considering that during the Holocene the sea level was never higher than today (Fleming et al., 1998) and taking into account that a tsunami wave can reach sites located far inland but without leaving a ”signature” able to be preserved for long time. In fact, the Tohoku tsunami deposit, in the Sendai plain, was found up to 4 km inland but the tsunami wave reached 6 km inland (Goto et al., 2014). This kind of data could be used as a benchmark: a) to make a comparison between the geological data (heights and distances obtained from deposits) and modeled inundations from tsunami simulations (e.g. Sawai et al., 2012) or b) to have a minimum constraint on the tsunami effects to be integrated into the inundation models (e.g. Jaffe et al., 2012).

From a general point of view, it is possible to note that in the NEAM database tsunami evidence is represented by 76 % of sediment, 18 % of transported blocks and only 6% of geomorphological signatures. Moreover, the geological evidence of a paleotsunami is directly related to the geomorphic setting of a site. This means that most of sites recorded in the database show coastal settings suitable for the deposition and preservation of a tsunami layer (e.g. lowlands, marshes, coastal lakes or lagoon but also abandoned fluvial plains or estuaries where the sedimentation is mainly related to low energy environments in the Holocene). Otherwise, all rocky coastal settings (e.g. a rocky platform) have the potential to be suitable for the deposition of transported blocks. Today, it is still difficult to estimate if the emplacement of a rocky block may be attributed to a storm or to a tsunami wave (Barbano et al., 2010). In addition, a coastal site able to preserve transported blocks, should have a particular bedding of the bedrock that may favor the boulders displacement (Scicchitano et al., 2007). Conversely, geomorphological evidence of paleotsunami is very rare (only 6%). This could be attributed to the fact that it is particularly difficult to recognize a

morphological signatures left by a tsunami, especially because coastal areas may be characterized by high energy environments potentially able to erase any geomorphological signatures, including those related to tsunami inundations of the past.

As previously mentioned, the heights above the sea level and the distance from the present shoreline of the sites can provide minimum run-up height and inundation distance value. From the analysis of the elevation and distance fields (sites table) it emerges that about 50 % of the analyzed sites has an elevation (run-up) above the present sea level within 5 meters (somehow expected) while up to 23% of the sites has an elevation above 10 meters. At the same time, about half of the analyzed sites present a distance from the present shoreline (inundation limit) <= 200 meters (the storms inundation limit, Morton et al., 2007) while up to 14% of the sites overcomes the value of 1000 meters. Even these two values (height and distance) have a direct relation with respect to the geomorphic setting of a coastal site and thus should be considered site-dependent. From a general point of view, sites characterized by geomorphic settings able to preserve tsunami layers show variables inundation distances that can reach peaks of 1000/1500 meters from the shoreline and heights of 10 meters a.s.l. Instead, sites able to guest transported blocks show distances of maximum 70/100 meters (with some exceptions) from the shoreline and heights that difficulty overcome 10 meters a.s.l.. Most of the sites exceeding an elevation of 10 meters a.s.l. is located along the coast of Norway where the main historical tsunami event is attributed to the Storegga tsunami (dated about 8150 BP, Bondevik et al., 2012). Therefore, these elevation values cannot be considered “real” since the relative sea level was higher than today (Bondevik et al., 1997) and the isostatic rebound modified the earth elevation at these localities making the evaluation of the run-up very difficult.

At National level, all paleotsunami deposits are concentrated in the southern Italy. In detail, the regions of Apulia and Sicily host 25 sites with a total of 57 geological evidence of tsunami inundations. Actually, in the other Italian regions, it was not recorded any tsunami deposit, maybe because several portions of coasts have not yet been investigated and most of known historical events occurred in the Ionian and southern Adriatic sea. The database shows that most of paleotsunami deposits, found along the coast of Italy, are represented by sediment layers (70 %), followed by 23 % of transported blocks and by 7% of geomorphological evidence. Even in this case, a solid relation between the type of evidence and the geomorphic setting exists. Taking into account that each site may have one or more geomorphic setting it is possible to note that coastal settings like marsh, lakes, fluvial plain, estuaries and back dune environment are suitable for the deposition, conservation and investigation of tsunami deposit represented by sediment and also by

geomorphic features. Differently rocky coast is the most favorite setting for the detachment, transport and deposition of large boulders.

Finally, from a general point of view the most relevant data, extrapolated from the database, can be summarize as follow:

Data from the whole database (NEAM region):

- ✓ The Astarte paleotsunami geodatabase contains 151 sites and 220 geological evidence of tsunamis.
- ✓ The tsunami evidence is characterized by a predominance of sediment layers (76%), followed by transported blocks (18%) and geomorphological signatures (6%).
- ✓ Actually, in the geodatabase, 50% of the sites have an elevation above sea level within 5 meters while 23 % of sites exceeds the value of 10 meters. In addition, about half of the analyzed sites have a distance from the present shoreline <=200 meters and 14% of the sites overcome peaks of 1000 meters. Moreover, there are several sites, with an elevation > 10 meters, located in Norway where the main tsunami event was attributed to the Storegga tsunami (dated about 8150 BP, Bondevik et al., 2012) and the isostathic rebound played an important role clearly uplifting the local ground surface.
- ✓ From a scientific point of view, environmental, paleontological and sedimentological analyses seem to be the most resolute and used approaches in order to identify and characterize a tsunami deposit.

Data from Italy:

- ✓ At national level, all sites, where geological evidence of tsunami were found, are located along the coasts of Sicily and Apulia regions (Southern Italy).
- ✓ The southern Italy presents 25 sites and 57 events, where 70 % of tsunami deposits is represented by sediment layers
- ✓ Most of derived minimum run-up values (from the elevation of paleotsunami deposits) are within 5 meters above sea level. Interestingly, 5% of the sites have an elevation > 10 meters.
- ✓ 55% of derived inundation distances are within 200 meters while 27% overcomes values of 500 meters from the present shoreline. Very flat coastal morphologies (e.g. the Pantano Morghella site located in south eastern Sicily) may favor long inundation distances even longer than 1 km.

The research of paleotsunami deposits inland (Orefice et al., 2016), along the coasts of eastern Sicily, did not give the expected results. It was not found a typical tsunami layer but interesting interpretations in terms of short lasting high energy events were carried out.

This investigation allowed identifying a potential tsunami evidence based on an environmental change recognized in the cores stratigraphy of the Vendicari lagoon area. An extreme event, potentially related to a tsunami or to a local earthquake, could have caused the modification of the coastal morphology by rupturing the sandy barrier that divides the lagoon from the Ionian Sea, thus causing a direct connection between the lagoon and the sea as well as environmental change from lagoonal/alluvial to marine environment. The available literature potentially supports this kind of interpretation. In fact, Amore et al. (1994) studied the sediments of this protected area (by means of 1 m long cores on very recent deposits) and evidenced a similar environmental change but unlikely nothing is available in terms of time constraint. In addition, it is known that large tsunami waves are able to drastically modify coastal morphologies. Today many authors described coastal morphological changes caused by the 2004 Indian Ocean Tsunami (Umitsu et al., 2007; Paris et al., 2009). Moreover, Koiwa et al. (2017) observed the recovery of the barrier spit of Pakarang Cape (southern Thailand) after the erosion caused by the 2004 Indian Ocean tsunami. In terms of timing of this hypothesized strong event, that affected the Vendicari area, both cores got a radiocarbon constrained average sedimentation rate, very similar and stable, of about 0.5 mm/yr. Applying this sedimentation rate to the lagoonal/alluvial deposits overlaid by the beach sands, it is possible to derive a maximum age of the sand bottom ranged between BC 280 – 230 AD. This age is defined as maximum value because, taking into account the presence of a clear erosive contact between the beach sand and the deposits below, some cm of sediments could have been missed. Interestingly, this age is well comparable with the ages of some tsunami deposits found in the nearby sites (De Martini et al., 2012), in particular with respect to the Ex event (from offshore data in the Augusta Bay, Smedile et al., 2011), PR-02 event (from Priolo Reserve site, De Martini et al., 2010), and MOR-T2 event (from Pantano Morghella site, Gerardi et al., 2012) that were all tentatively related to the 365 AD Crete tsunami by the above mentioned authors. Finally, this event, based on its chronostratigraphical constraints together with tsunami inundations recorded in the nearby areas, could be tentatively related to the Crete 365 AD event.

In the area of the Sircausa salt pans, instead, the cores stratigraphy presented a peculiar bioclastic calcarenite layer interpreted as a high energy event and dated about 750 BC. The age of this layer is comparable with the age of two tsunami deposits found in the Augusta Bay and dated between 975-800 BC and 700-500 BC (De Martini et al., 2010; Smedile et al., 2011). This deposit should provide

a new minimum run-up value of about 2 meters a.s.l. and a minimum inundation distance of about 470 meters. Moreover, the potentially tsunamigenic deposit found in Siracusa area, may confirm the occurrence of a local unknown tsunami that hit the coastline for about 23 km from the Augusta Bay to Siracusa area during the first millennium BC (975 – 500 BC) (fig. 1). Differently, De Martini et al., 2012 showed that the historically known regional and local events (large earthquakes occurred in 1908, 1693, 1169, 365 AD), on the base of their geological evidence, have the potential to hit up to 70% of the entire coast of eastern Sicily (fig. 1).

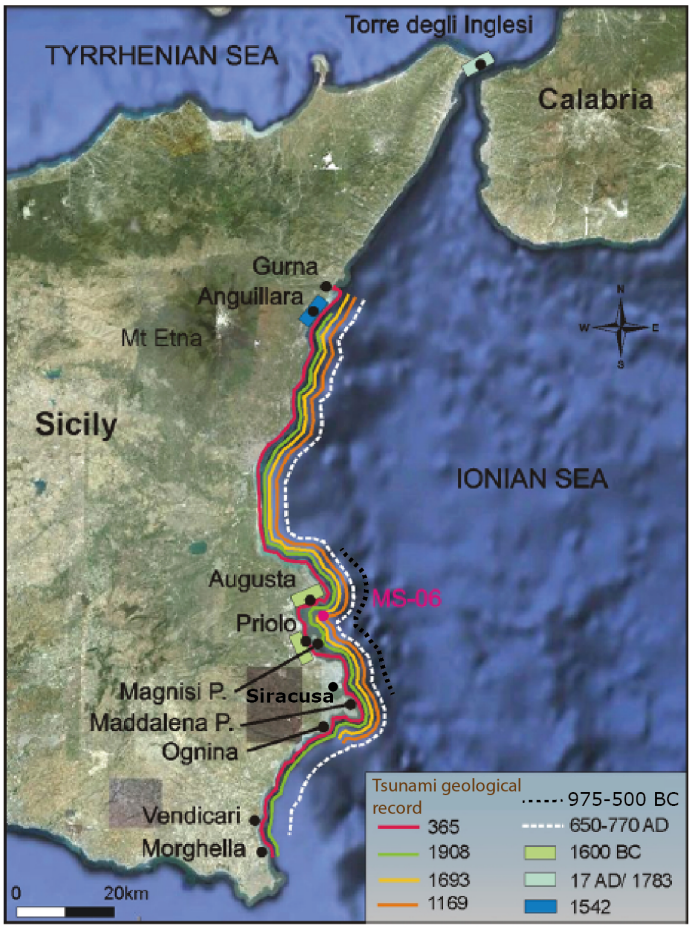

Fig. 1 -Tsunamis geological record. Google Earth map of eastern Sicily synthesizing the portion of the coast hit by different tsunamis as colored full lines, whereas the dashed line marks the coast inundated by the largest unknown tsunami. Rectangles indicate the portions of coast inundated by local events (see legend for age correlation). Modified from De Martini et al., 2012.

The amplification factor method, gave a general overview of how a tsunami wave amplifies from -50 meters of depth to the shoreline. Amplification factor maps for different periods and wave polarity (positive and negative leading wave) were produced. In particular, it was observed that the wave amplification depends on the wave's period in relation of the distance between the offshore control point (the depth from which the wave is amplified) and the shoreline:

• Waves shorter than this distance (with a low period) give amplification factors up to 6
• Waves longer than this distance (with a high period) give amplification factors close to 1

This means that coastal areas, where the depth remains low for a long distance towards the sea, tend to give more amplification. This important consideration is shown in figure 2 and 3 where, the amplification is quite high notwithstanding the high period of the wave applied. This is due to the distance between the offshore control point (located at -50 meters of depth) and the shoreline that is more than the wave's length.

Moreover, some areas displaying high amplification despite high wave periods applied are known to host paleotsunami deposits. It is possible to note this relation in the Manfredonia Gulf (Apulia, Italy fig. 2), where tsunami deposits of the 1627 event (local tsunami that struck the Adriatic Apulia coast) and probably of the 365 A.D. event were found (De Martini et al., 2003). This kind of relation is also well appreciable at Al Alamein site (Egypt, fig. 3), where tsunami deposits of 1870, 1303 and 365 AD events were recognized and characterized (Meghraoui M., 2017). The figure 3 clearly shows amplification factor values higher than surrounding areas just in front of El Alamein site.

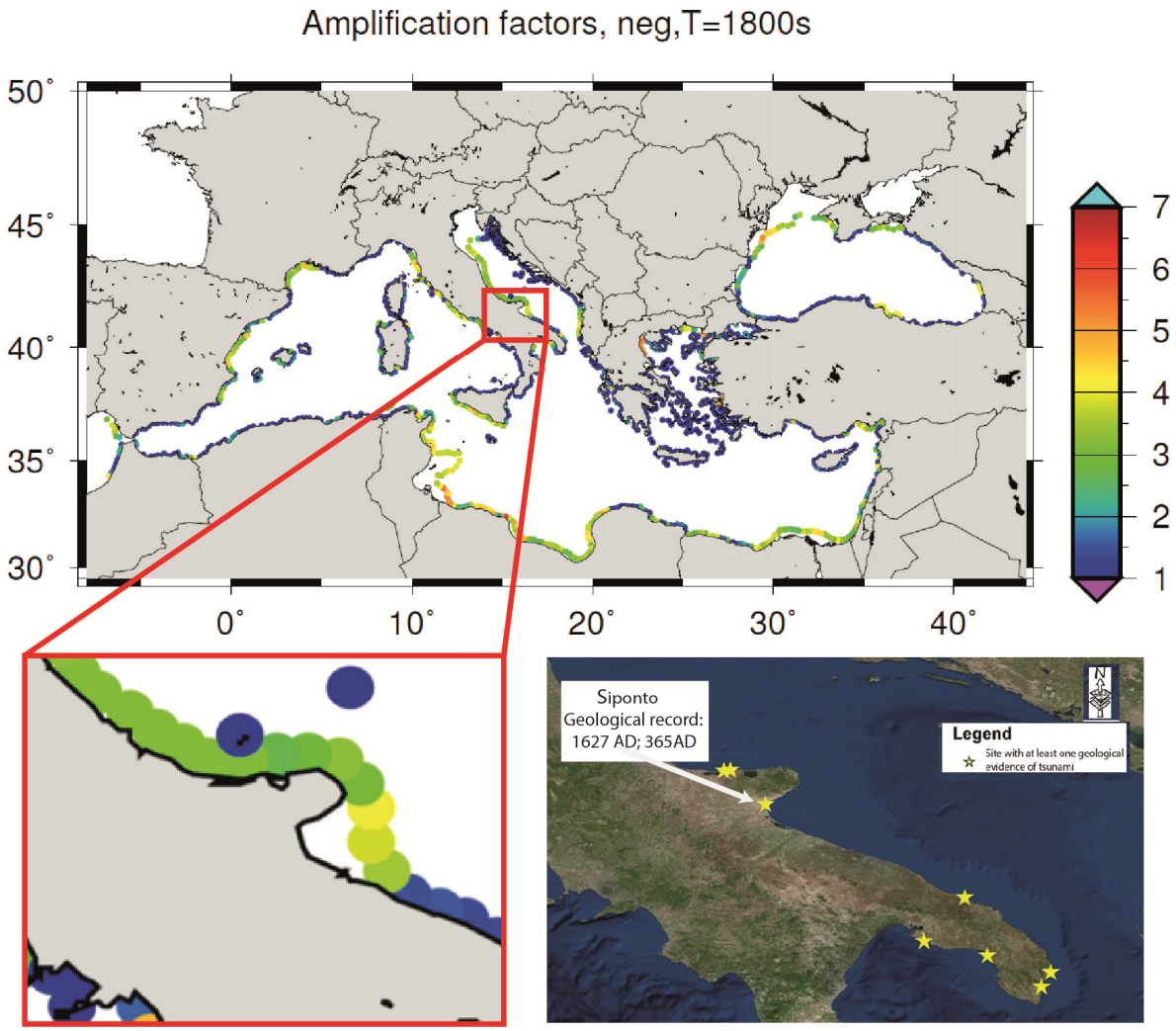

Fig. 2 – The upper image shows amplification factors for negative leading waves with a period of 1800 s. In the lower left panel it is possible to note a zoom of the Manfredonia Gulf (Gargano, Apulia region, Italy), where the amplification is higher than the surrounding areas. Amplification factors symbols (colored circle) are located along the – 50 meters depth isobath, in the exact location of the offshore control points. The lower right panel shows the Apulia region sites with at least one paleotsunami deposit, with a particular attention for the Manfredonia Gulf.

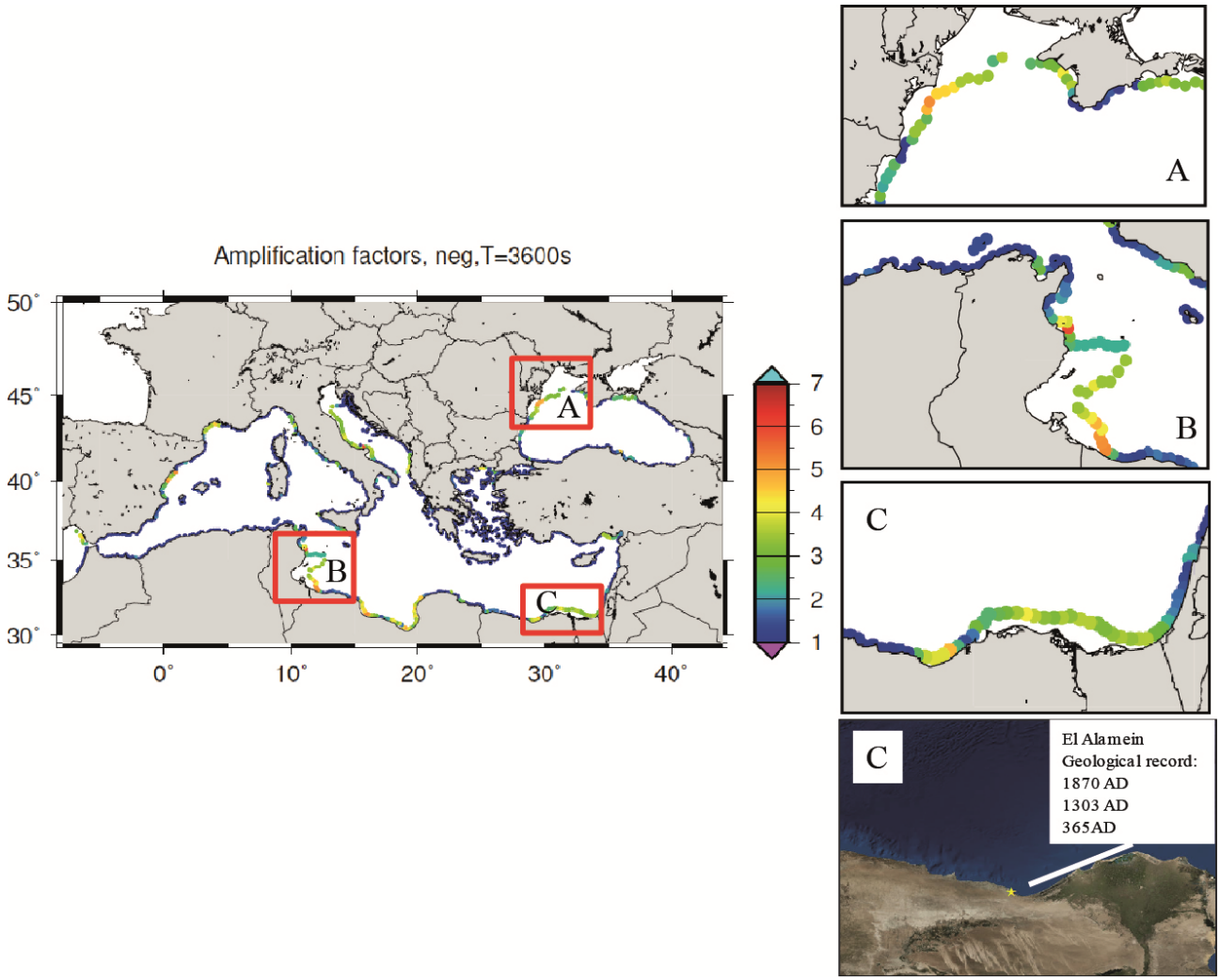

Fig. 3 – The picture on the left side shows amplification factors for a negative leading wave with a period of 3600 seconds. Amplification factors symbols (colored circle) are located along the – 50 meters depth isobath, in the exact location of the offshore control points. On the right side three examples (A, B and C) of high amplification values are displayed. In addition the example C (El Alamein site in the Astarte paleotsunami database) shows a relation between the high amplification and the presence of 3 tsunami deposits related to the 1870, 1303, and 365 AD events (Meghraoui M., 2017).

The amplification factor procedure is considered a deterministic method. For this reason it was compared with some conventional inundation models. Bias derived from this comparison were close to 0, making this method a viable procedure to estimate run-up heights and inundation distances. The future application of this procedure will be based on the estimation of run-ups and inundation distances for the NEAM region. In fact, the amplification factors will be used to produce regional tsunami hazard maps, for example in the context of PTHA (Probabilistic Tsunami Hazard Assessment).

2. Future Directions

The Astarte Paleotsunami deposits database has been implemented with the purpose to be the future information repository for tsunami research in the NEAM region, integrating the existing official scientific reports and peer reviewed papers on these topics. Therefore, the database will be updated every 12 months by extending the collaboration to institutes and/or universities that were not included in the Astarte project and through further field surveys. Moreover, the current version of the database will be presented in a paper to be submitted to Marine Geology:

The ASTARTE Paleotsunami Deposits data base –web-based references for tsunami research in the NEAM region (Paolo Marco De Martini, Simone Orefice, Alessandra Smedile, Antonio Patera, Raphael Paris, Pedro Terrinha, James Hunt, Gerassimos Papadopoulos, Daniela Pantosti, João Noiva, Ioanna Triantafyllou and Ahmet C. Yalciner).

In addition, tsunami deposits data (derived run-up and inundation distance) will be used to make a direct comparison with local inundation scenarios along the coast of eastern Sicily (Tonini et al., 2017). In fact, tsunami data available for this area are particularly rich with respect to the scarce and heterogeneous data-sets usually available elsewhere. Therefore, tsunami deposits data can represent valuable benchmarks for testing and strengthening the results of such kind of studies.

The results obtained in the research of potential paleotsunami deposits along the coast of eastern Sicily, will be presented in a paper to be submitted to Annals of Geophysics:

High energy events in the Holocene stratigraphy: the Astarte EU Project Siracusa test site case study, SE Sicily, Italy (Simone Orefice, Alessandra Smedile, Stefania Pinzi and Paolo Marco De Martini).

Amplification factors will be used in the context of the Probabilistic Tsunami Hazard Assessment (PTHA) in order to produce regional tsunami hazard maps. Results obtained so far and from the regional tsunami hazard maps will be present in a future paper.

References

Barbano M.S., Pirrotta C., Gerardi F., (2010). Large boulders along the south-eastern Ionian coast of Sicily: Storm or tsunami deposits?. Marine Geology, 275, 140 – 154.

Bondevik S., Stormo S.K. & Skjerdal G.(2012). Green mosses date the Storegga tsunami to the chilliest decades of the 8.2 ka cold event. Quaternary Science Reviews, 45, 1–6.

Bondevik S., Svendsen J.I., Johnsen G., Mangerud J. & Kaland P.E. (1997). The Storegga tsunami along the Norwegian coast, its age and run-up. Boreas, 26, 29–53.

De Martini P.M., Barbano M.S., Pantosti D., Smedile A., Pirrotta C., Del Carlo P., and Pinzi S. (2012). Geological evidence for past-tsunamis along eastern Sicily (Italy): an overview, Nat. Hazards Earth Syst. Sci., 12, 2569-2580, doi:10.5194/nhess-12-1-2012.

De Martini P.M., Barbano M.S., Smedile A., Gerardi F., Pantosti D., Del Carlo P., Pirrotta C., (2010). A unique 4000 year long geological record of multiple tsunami inundations in the Augusta Bay (eastern Sicily, Italy). Marine Geology, 276, 42-57, doi: 10.1016/j.margeo.2010.07.005

De Martini P.M., Burrato P., Pantosti D., Maramai A., Graziani L., Abramson H., (2003) Identification of tsunami deposits and liquefaction features in the Gargano area (Italy): paleoseismological implication. ANNALS OF GEOPHYSICS, VOL. 46, N. 5.

De Martini P.M., Patera A., Orefice S., Paris R., Volker D., Lastras G., Terrinha P., Noiva J., Smedile A., Pantosti D., Hunt J., Gutscher M.A., Migeon S., Papadopoulos G., Triantafyllou I., Yalciner A.C., (2017). The ASTARTE Paleotsunami and Mass Transport Deposits databases – web-based references for tsunami and submarine landslide research around Europe. Geophysical Research Abstracts, Vol. 19, EGU2017-15055, 2017, EGU General Assembly 2017.

Fleming K., Johnston P., Zwartz D., Yokoyama Y., Lambeck K., Chappel J., (1998). Refining the eustatic sea-level curve since the Last Glacial Maximum using far and intermediate-fields sites. Earth and Planetary Science Letters 163, 327-342.

Gerardi F., Smedile A., Pirrotta C., Barbano M. S., De Martini P. M. ,Pinzi S. , Gueli A. M., Ristuccia G. M., Stella G., and Troja S. O., (2012). Geological record of tsunami inundations in Pantano Morghella (south-eastern Sicily) both from near and far-field sources. Nat. Hazards Earth Syst. Sci., 12, 1185–1200. doi: 10.5194/nhess-12-1185-2012.

Goto K., Hashimoto K., Sugawara D., Yanagisawa H., Abe T., (2014). Spatial thickness variability of the 2011 Tohoku-oki tsunami deposits along the coastline of Senday Bay. Marine Geology, 358, 38 – 48.

Jaffe B.E., Goto K., Sugawara D., Richmond B.M., Fujino S., Nishimura Y., (2012). Flow speed estimated by inverse modeling of sandy tsunami deposits: results from the 11 March 2011 tsunami on the coastal plain near the Sendai Airport, Honshu, Japan Sedimentary Geology 282, 90–109

Koiwa N., Takahashi M., Sugisawa S., Ito A., Matsumoto H., Tanavud C., Goto K., (2017). Barrier spit recovery following the 2004 Indian Ocean tsunami at Pakarang Cape, southwest Thailand. Geomorphology (Accepted Manuscript), doi: 10.1016/j.geomorph.2017.05.003.

Meghraoui M., (2017). Onshore tsunami deposits, contribution of CNR-IPG Strasbourg. ASTARTE project (Assessment, Strategy And Risk Reduction for Tsunamis in Europe - FP7-ENV2013 6.4-3, Grant 603839; Nov. 2013 – April 2017): scientific periodic report task 2.3 : onshore tsunami deposits.

Orefice S., De Martini P.M., Smedile A., Pinzi S., (2016). INGV Report on tsunami deposits research on land (Siracusa test Site Area, ITALY) performed within WP2 of Astarte Project (Assessment, Strategy And Risk Reduction for Tsunamis in Europe - FP7-ENV2013 6.4-3, Grant 603839; Nov. 2013 – April 2017). Task 2.3: Onshore Tsunami deposits.

Paris R., Wassmer P., Sartohadi J., Lavigne F., Barthomeuf B., Desgages E., Grancher D., Baumert, P., Vautier F., Brunstein D., Gomez C., (2009). Tsunamis as geomorphic crises: Lessons from the December 26, 2004 tsunami in Lhok Nga, West Banda Aceh (Sumatra, Indonesia). Geomorphology 104(1–2), 59-72.

Sawai Y., Namegaya Y., Okamura Y., Satake K., Shishikura M., (2012). Challenges of anticipating the 2011 Tohoku earthquake and tsunami using coastal geology. GEOPHYSICAL RESEARCH LETTERS, VOL. 39, L21309, doi:10.1029/2012GL053692.

Smedile A., De Martini P. M., Pantosti D., Bellucci L., Del Carlo P., Gasperini L., Pirrotta C., Polonia A., and Boschi E., (2011). Possible tsunamis signatures from an integrated study in the Augusta Bay offshore (Eastern Sicily–Italy). Mar. Geol., 281,1–13.

Tonini R., Volpe M., Lorito S., Selva J., Orefice S., Graziani L., Brizuela B., Smedile A., Romano F., De Martini P.M., Maramai A., Piatanesi A. and Pantosti D., (2017). Site-specific seismic probabilistic tsunami hazard analysis: performances and potential applications. Geophysical Research Abstracts Vol. 19, EGU2017-15309, 2017 EGU General Assembly 2017.

Umitsu, M., Tanavud, C., Patanakanog, B., (2007). Effects of landforms on tsunami flow in the plains of Banda Aceh, Indonesia, and Nam Khem, Thailand. Marine Geology 242, 141-153.

Acknowledgments

The research activity carried out in this thesis was founded by the European Union's Seventh Framework Programme (FP7/2007-2013) under grant agreement 603839 (Project ASTARTE), and by the TSUMAPS NEAM Project (www.tsumaps-neam.eu), co-financed by the European Union Civil Protection Mechanism, Agreement Number: ECHO/SUB/2015/718568/PREV26.

The results obtained in this thesis came from of a collaboration of many researchers. For this reason, I really want to thank Paolo Marco De Martini and Antonio Patera (from Istituto Nazionale di Geofisica e Vulcanologia –INGV, Rome, Italy) for the scientific and technical support provided for the Astarte Paleotsunami deposits database.

At the same time, I want to thank Alessandra Smedile and Stefania Pinzi (from Istituto Nazionale di Geofisica e Vulcanologia – INGV, Rome, Italy) for the micropaleontological and sedimentological analysis performed on the cores collected for the research of paleotsunami deposits onland.

Many thanks also to Stefano Lorito and Fabrizio Romano from Istituto Nazionale di Geofisica e Vulcanologia of Rome, and to Finn Løvholt, and Sylfest Glimsdal (from Norvegian Geotechnical Institute – NGI, Oslo, Norway) for the scientific support provided in the application of the Amplification factor method and for the opportunity to live two months at NGI (Norvegian Geotechnical Institute, Oslo, Norway) in order to give a direct contribution in the Amplification factor procedure. Another thank to Beatriz Brizuela (from Istituto Nazionale di Geofisica e Vulcanologia –INGV, Rome, Italy) for the fundamental help provided in the realization of Python scripts for the bathymetric profiles acquisition (in the Amplification factor method).

Finally, a special thank to Paolo Marco De Martini for the scientific support provided in the entire thesis and to Francesca Funiciello (from Roma Tre University) for the assistance performed at Roma Tre University.